NOVA SCHOOL OF SCIENCE & TECHNOLOGY

DEPARTAMENT OF CIVIL ENGINEERING

TIAGO LETRAS RIBEIRO

BSc in Sciences of Civil Engineering

STUDY OF ASPHALT SELF-HEALING WITH COLORLESS BINDER AND PIGMENTED OIL

MASTER IN CIVIL ENGINEERING

NOVA University Lisbon

November, 2022

DEPARTAMENT OF
CIVIL ENGINEERING

STUDY OF ASPHALT SELF-HEALING WITH COLOR-LESS BINDER AND PIGMENTED OIL

TIAGO LETRAS RIBEIRO

BSc in Sciences of Civil Engineering

Adviser: Doctor Rui Alexandre Lopes Baltazar Micaelo
Associate Professor, NOVA University Lisbon

Co-adviser: Doctor Ana Cristina Ferreira de Oliveira Rosado Freire
Assistant Researcher, Laboratório Nacional de Engenharia Civil

Examination Committee:

Chair: Doctor José Nuno Varandas Ferreira,
Assistant Professor, NOVA University Lisbon

Rapporteurs: Doctor Vítor Filipe Silva Antunes,
Assistant Professor, Universidade Lusófona

Adviser: Doctor Rui Alexandre Lopes Baltazar Micaelo,
Associate Professor, NOVA University Lisbon

MASTER IN CIVIL ENGINEERING

NOVA University Lisbon
November, 2022

STUDY OF ASPHALT SELF-HEALING WITH COLORLESS BINDER AND PIGMENTED OIL

Acknowledgments

I would like to extend my gratitude to my adviser, Professor Rui Micaelo, for his invaluable expertise and guidance. His willingness to help, creativity, and constant availability were key in overcoming the challenges faced during this dissertation.

I would also like to thank Doctor Ana Cristina Freire, my co-adviser, for her incisive and insightful feedback that always pushed me in the right direction.

I would like to thank everyone at LNEC's Transportation Department for welcoming me with open arms. I would like to especially acknowledge Mr. João Costa, who was a pleasure to be around and greatly helped me with most experiments and tests.

Thank you to everyone from LNEC's Materials Department who kindly lent me their time and equipment.

I must thank Hélio Nunes from Repsol, Daniela Augusto from Ravago Chemicals, and Alves Ribeiro for providing me with essential materials.

I must also thank Doctor João Canejo and Doctor João Paulo Borges for enabling and aiding the production of calcium alginate capsules at NOVA University Lisbon's Department of Materials Science.

Finally, I would like to express my gratitude to my family and friends who always made an effort to understand my struggles and continually motivated me to overcome them. A special thank you to Ana.

Abstract

Encapsulated rejuvenators are an innovative solution to improving the durability of asphalt pavements, which can result in roads that are cheaper to maintain and have a small environmental footprint. One technique for creating these encapsulated rejuvenators uses sodium alginate, that can be produced from seaweed, sunflower seed oil, and a simple laboratory process to form calcium alginate capsules with pockets of oil, the rejuvenator, inside.

One of the ways that more can be learned about this technology is by studying its working mechanism, which is typically done with complex techniques, such as computed tomography scans or infrared spectroscopy. They are then combined with mechanical testing. While extremely useful, such techniques require expensive equipment and are typically limited to smaller samples.

This work aimed to find an alternative method for observing the encapsulated rejuvenator's behavior in asphalt. By combining light-colored asphalt made with a synthetic binder and pigmented oil capsules, the rejuvenator's propagation was studied visually.

To achieve this, a suitable pigment had to be found and calcium alginate capsules containing colored oil had to be produced, along with light-colored asphalt. These materials had to be tested and understood before a set of tests was devised to study the rejuvenator's behavior in asphalt.

Overall, findings showed that oil and pigment release was limited and lacked uniformity. The solubility of vegetable oil in synthetic binder was also limited when compared to bitumen. Asphalt concrete mixtures with capsules showed more instances of pigment/oil release than comparable stone mastic asphalt mixtures.

Keywords: Encapsulated rejuvenator; Asphalt self-healing; Pigmented oil; Calcium alginate capsules.

Resumo

Os rejuvenescedores encapsulados são uma solução inovadora para melhorar a durabilidade dos pavimentos rodoviários, que pode resultar em pavimentos mais duráveis e com uma menor pegada ambiental. Uma das várias técnicas de produção de rejuvenescedores encapsulados utiliza alginato de sódio, que pode ser produzido a partir de algas marinhas, óleo de sementes de girassol, e um processo de laboratório simples para formar cápsulas de alginato de cálcio com bolsas de óleo, que actua como rejuvenescedor, no seu interior.

Uma forma de saber mais sobre esta tecnologia é estudar o seu mecanismo de funcionamento recorrendo a técnicas complexas, tais como a tomografia computorizada ou espectroscopia de infravermelho, em conjunto com ensaios mecânicos. Embora extremamente úteis, tais técnicas requerem equipamento dispendioso e são tipicamente limitadas a amostras pequenas.

Este trabalho analisou um método alternativo para observar o comportamento dos rejuvenescedores encapsulados em misturas betuminosas. A hipótese subjacente ao método é que será possível estudar visualmente a propagação do rejuvenescedor através da combinação de uma mistura betuminosa de cor clara, feita com um ligante sintético, e cápsulas com óleo pigmentado. Foi necessário encontrar um pigmento adequado e produzir cápsulas de alginato de cálcio contendo óleo colorido, juntamente com a mistura betuminosa já referida. Estes materiais foram testados antes de ser concebido um plano experimental para estudar o comportamento do rejuvenescedor na mistura betuminosa.

Os resultados mostraram que a libertação de óleo e pigmento foi limitada e pouco uniforme. A solubilidade do óleo vegetal no ligante sintético mostrou-se também limitada quando comparada com betume. As misturas asphalt concrete com cápsulas mostraram mais ocorrências de libertação de pigmento/óleo que misturas comparáveis stone mastic asphalt.

Palavras chave: Rejuvenescedor encapsulado; Autorreparação de misturas betuminosas; Óleo pigmentado; Cápsulas de alginato de cálcio.

CONTENTS

List of Figures

List of Tables

ACRONYMS

3 PBT	Three Point Bending Test.
4 PBT	Four Point Bending Test.
AC	Asphalt Concrete.
CT	Computed Tomography.
FTIR	Fourier Transform Infrared.
GDP	Gross Domestic Product.
MMF	Melamine-Formaldehyde modified by Methanol.
O/Alg	Oil to sodium Alginate ratio.
O/W	Oil to Water ratio.
PEMA	Poly(Ethylene-alt-Maleic Anhydride).
SMA	Stone Mastic Asphalt.
SPA	Saturated Porous Aggregate.

1

INTRODUCTION

1.1 Background

Transportation is extremely important for any society. Increases in travel speed and capacity have historically been responsible for great economic and social developments. Advancements such as the extensive road network we now find in Europe have brought various regions closer together and enabled efficient trade between them. Maintaining this infrastructure is critical to ensure its safe and efficient operation, though this comes at a cost. In 2016, operational and maintenance expenditures with roads in Portugal were close to € 400 million, about 0.3% of gross domestic product (GDP) (Euros expressed in price level 2016 and adjusted for purchasing power) [1]. Portugal's maintenance expenditure is not high compared to the European Union's average, in part because its road network does not have a very high density of tunnels and bridges, and winter maintenance is not very significant. Despite this, there clearly is room for savings, which could be achieved with more durable paving materials, for example.

Most of the roadways found in Europe use flexible pavements [2], made with bituminous materials. These roads are designed to have a service life of ten to thirty years, but repaving is needed about every eight years [3], [4]. Bitumen, one of the key components in this type of material, is an organic substance, and so it is affected by the presence of oxygen, ultraviolet radiation, and by changes in temperature, which cause it to harden over time [5]. This effect may be beneficial for the pavement structure due to increased stiffness, but in the surface layer it increases the likelihood of fretting and cracking (non-fatigue related). Damage in asphalt is generally thought to begin with microcracks, which grow over time, facilitating the access of water and oxygen into the mixture, further exacerbating damage [6].

Asphalt's ability to self-heal was first reported in 1967 [7], with healing being found to relate to temperature. Since then, other factors have been found to influence this property, like the binder's viscosity, chemical composition, and the density of aggregates in the mixture [8]. Various mechanisms have been proposed to explain this phenomenon at various scales.

One of the main reasons why asphalt's own self-healing does not significantly extend pavement life is that it requires considerable rest periods to materialize (multiple days [9]), which is incompatible with regular traffic patterns.

These surface layers can be repaired in other ways. Asphalt can be recycled, and often is, at very high rates. When resurfacing a road, a large percentage of the older pavement can be incorporated into the new mix, along with some new binder and aggregate. Rejuvenating oils, which rebalance the bitumen's chemical composition, are used to recover the reclaimed asphalt. While this technique is environmentally sound, and compatible with a circular economy, it is still a complex process that requires road closure.

Another method of restoring a pavement's original properties is spraying its surface with rejuvenating oils. This technique is simple, but only works for the first few centimeters of asphalt, with the oils being unable to penetrate further. It also requires road closure and causes a temporary reduction in surface friction. Any runoff oil may also be cause for environmental concern [10].

Studies using heating have shown great promise, as temperature is a very influential factor in asphalt's ability to self-heal [11]. Roads can be artificially heated using microwaves or induction if metallic fibers are added to their composition. These techniques reduce the bitumen's viscosity, facilitating healing through capillary mechanisms. While they appear effective so far, large amounts of energy are required.

A passive approach to boosting asphalt self-healing would be the best solution to this problem. This could theoretically be done by including rejuvenating oils in the asphalt mixture but only releasing them when necessary, which is what encapsulated rejuvenators try to achieve. These would then reduce the binder's viscosity in affected areas and rebalance its chemical composition, promoting healing. There have been many studies using encapsulated rejuvenators of various types yet results so far have been inconclusive. Some studies show great improvements under certain conditions, while others report little benefit to fatigue resistance, the main concern. Furthermore, the inclusion of these encapsulated rejuvenators often affects the other properties of asphalt, such as its stiffness modulus, and so their self-healing benefits might be counteracted by these other changes. One of the ways to learn more about rejuvenator and capsule behavior would be to produce an asphalt mixture where

rejuvenator release is visible, which is the premise of this work. Other techniques of assessing encapsulated rejuvenator equipment exist, such as computed tomographies, but often require specialized equipment or small specimens. Despite having limitations, the information provided by them is extremely useful, and this study is intended to complement it.

1.2 Aim and Objectives

The goal of this study is to produce self-healing asphalt concrete mixtures with added encapsulated rejuvenators, in which rejuvenator and capsule behavior is easily seen and studied. This can be accomplished by producing mixtures with a clear or light-colored binder and coloring the rejuvenating oil with an adequate pigment or dye, that needs to be selected. By subjecting samples of this mixture to realistic testing and then observing their internal structure, their behavior can be interpreted and correlated with the visual findings.

1.3 Thesis Overview

In Chapter 1 the context of this dissertation, its goals, and its structure are presented.

Chapter 2 contains a review of relevant literature, exploring different rejuvenator encapsulation techniques, their production methods, working principles, and techniques for the detection of rejuvenator release. It concludes with an overview of various studies that used encapsulated rejuvenators in asphalt mixtures.

Chapter 3 presents the materials and equipment used. The various methods and experimental procedures employed are discussed.

Chapter 4 examines the results of the aforementioned experimental procedures, analyzing the possible reasons that led to each result and the significance of the findings.

In Chapter 5 this dissertation's findings are summarized and used to suggest future research avenues.

2

State of the Art

2.1 Asphalt Self-healing with Encapsulated Rejuvenators

Over time, bitumen's chemical composition changes, along with its physical properties. Lighter, more volatile, compounds such as maltenes are lost, leaving behind a larger percentage of asphaltenes. Concurrently, exposure to air and sunlight promotes the binder's oxidation and photo-oxidation [12]. This process is called aging, and leads to a stiffer and more brittle material, prone to cracking. As the material ages, its ability to recover from damage worsens, and becomes slower (a process that is not fast to begin with [9]).

Asphalt's ability to self-heal is comprised of a variety of mechanisms, ranging in scale from the microscopic to the macroscopic level. Processes such as molecular interdiffusion and capillary flow are reported to contribute to self-healing [13]. In a broad sense, these processes are dependent on the binder's viscosity and its free surface energy, and can be divided into three key phases: flow, wetting, and interdiffusion [14], [15]. Flow describes the phase during which the sides of a crack come together. This enables the next step, wetting, which happens when the surfaces are close enough to start interacting, forming an interface. Molecular interdiffusion between the two sides finally leads to the recovery of the material's properties.

One possible way of accelerating this phenomenon is the introduction of rejuvenators into the mixture, intending to lower the binder's viscosity and rebalance the amounts of light and heavy elements. This procedure is typically used when recycling older pavement layers, along with the addition of new binder and aggregates [3].

Ideally, it would be possible to incorporate these rejuvenators within the asphalt mixture when it is produced, with the goal of activating them when the pavement layer incurs damage. This is what various authors have tried to achieve by encapsulating said substances [16]. By

adding these discrete pockets of rejuvenator into the asphalt's structure, it is expected that, whenever a crack develops, it will intersect some of them, resulting in the rejuvenator's release into the affected area.

Many substances can work as rejuvenators, yielding different results. Oils containing maltenes are often used, with the goal of compensating for the share of lighter compounds lost over time. Other oils, such as vegetable oil can also be used to modify the bitumen, which in some studies is referred to be inert, in the sense that there is mostly a physical interaction with the bitumen rather than a chemical one. Being soluble in bitumen, they work by loosening the binder, facilitating flow deformation in the cracked area. Rather than rejuvenators, these compounds can be called "Softening Agents"[17].

It is worth noting that there is limited research into the exact degree of chemical interaction between bitumen and sunflower seed oil. The chemical interaction between this oil and the binder can be expected to be lower than that of an oil formulated for that purpose, but likely not zero, as waste cooking oil has been found to reduce the ratio of asphaltenes to maltenes in bitumen, but not to an extent resembling virgin bitumen [18]. Waste vegetable oil has been shown to have good rejuvenation potential in reclaimed asphalt mixtures, comparable in many aspects to more traditional rejuvenators such as aromatic oils, with the exception of its impact on moisture resistance [19]. Many authors [3, 18] refer to sunflower seed oil as a rejuvenator, and so the same terminology will be used, despite its working principle likely differing from more traditional oils.

2.2 Rejuvenator Encapsulation Methods

There are various methods of encapsulating liquids, which can be divided into physico-mechanical, chemical, and physico-chemical ones [17].

Physico-mechanical methods rely on mechanical processes, which include:

- Spray drying - a process that involves spraying a mix of the target substance and polymers into a hot chamber, where rapid drying produces a shell on the outside of each droplet.
- Pan coating - where the target material is sprayed with the encapsulating compounds, forming a shell.
- Extrusion - methods by which the target substance is forced through a nozzle, forming droplets or streams depending on the flow's speed.

Chemical methods include:

- Interfacial polymerization - a technique that requires a multifunctional monomer to be dissolved in the core material which is in turn dispersed in an aqueous phase. By adding a reactant, polymerization will occur on both sides of the interface between core material droplets and the continuous phase [21].
- *In-situ* polymerization - while this technique is similar to the previous one, it does not require that reactants are included in the core material, with the reaction taking place in the continuous phase rather than at the interface between phases [21].

Physico-chemical methods, as their name implies, combine both physical and chemical processes. It is usual for droplet formation to be achieved using the former techniques, and shell creation using the latter ones. Some of these processes include:

- Ionic gelation - a technique where the target substance is mixed with a polymer bearing electrolyte groups and subsequently dropped into a catalyst solution, where a polymeric matrix forms by ionic exchange.
- Coacervation - a coacervate is a homogeneous mixture of charged macromolecules. Coacervation happens when it undergoes liquid-liquid phase separation caused by a change in pH, ionic exchange, or any other mechanism, giving rise to a dense polymer-rich phase and a dilute phase [22].

Concerning their use in asphalt mixtures, two main types of capsule structures exist: single cavity and multi-cavity. There are also fibers, which differ in morphology from capsules. Depending on how they are produced, they might have discrete pockets of rejuvenator or a continuous "tube". In the first case, the fiber's behavior will be closer to a multi-cavity system, while the second case will tend toward a single cavity like behavior.

In the following paragraphs some of the most common rejuvenator encapsulation techniques will be explored.

Saturated Porous Aggregates

Some of the first encapsulated rejuvenators to be tested were saturated porous aggregates, in 2010 [16]. In this case, porous sand was chosen. After sieving and drying, the particles were placed in a container with the rejuvenator, a dense aromatic oil, and a vacuum was pulled, forcing the oil into the aggregate. Afterwards, the oil-infused grains were coated with a mix of epoxy resin and cement, forming a shell. In this same paper, the capsules were shown to be thermally stable at asphalt mixing temperatures and strong enough to resist the mixing process.

The addition of these aggregates was found to lower the asphalt's mixture strength by up to 30%, with no effect on its fatigue resistance [10]. According to [23], it is difficult for the rejuvenator to flow out of the pores, due to capillary action and its high viscosity.

Core-shell Microcapsules

Using melamine-formaldehyde modified by methanol (MMF), to increase its thermal stability, the authors of [23] were able to produce microcapsules (diameters in the range of 10 to 25 μm) containing a very dense aromatic oil, commonly used as a rejuvenator in pavements. The production process employs both *in-situ* polymerization and coacervation, yielding single cavity capsules, covered by a polymeric shell. These MMF microcapsules were found to have minimal mass loss at asphalt mixing temperatures. The authors did not assess microcapsule performance in asphalt.

Besides MMF microcapsules, other types of core-shell single cavity capsules have been developed. In [24], double-walled microcapsules were obtained using *in-situ* polymerization, combining both urea-formaldehyde and polyurethane. The rejuvenator used is a proprietary green bio-oil product. These microcapsules were much larger in diameter than the previous ones, with a mean diameter of 152.91 μm.

Calcium-alginate Capsules

This type of capsule uses ionic gelation to produce a matrix of calcium alginate polymer and rejuvenator, resulting in a multi-cavity type of internal structure. The production process begins with the production of an emulsion containing the rejuvenator, water, and sodium alginate. This mixture is then dropped into a solution containing calcium ions, which will interact with the alginate strands, forming a hard polymeric structure. This process will be explained in further detail in chapter 3.2, as these are the type of capsules chosen for this work.

Behavior under mechanical loading is much different from the previous types, acting more like a somewhat rigid sponge than a brittle particle [17]. The first trials using this type of capsule employed external coatings of cement and epoxy resin, which were found to crack during the mixing process [3]. Additionally, the beads without shells were found to be strong enough to resist both this previous process and compaction.

The proportions between capsule constituents have profound effects on the end results. In [25], calcium alginate capsules using vegetable oil as a rejuvenator were produced using various ratios of oil and water (O/W ratio). Since the authors always used the same quantity of sodium alginate, oil to alginate ratio (O/Alg) also varied, but less dramatically. It was found that higher O/W ratios correlate with larger capsule diameters. Higher O/W ratios also resulted in weaker, more deformable capsules. With the formulation used by the authors, oil to water ratios higher than 0.5 led to capsules with less than 10 N of compressive strength at 130°C, rendering them inadequate for use in asphalt as the authors considered this the minimum amount of strength required to resist mixing and compaction. Capsules with higher O/W ratios had better healing ability (using the specific methodology in this paper) due to higher amounts of oil being released.

The influence of oil to alginate ratios is studied in [7]. The capsules and their production method were very similar to the ones described previously, although some poly(ethylene-alt-maleic anhydride) (PEMA) was added to the rejuvenator, to increase emulsion stability. In this study, increased O/Alg ratios resulted in more spherical capsules, while lower ratios led to elliptic ones. The author suggests that an increased water content (proportionally) and its subsequent evaporation might be the cause of this phenomenon. Higher O/Alg ratios also made for larger capsules, with large internal pores. Thermal stability was higher for capsules with higher proportions of rejuvenator. In terms of mechanical resistance, higher proportions of alginate (lower O/Alg) generally resulted in stronger capsules, although this relationship was not linear. The best performing capsules had an oil to alginate ratio of 1.5, and these were followed by capsules with O/Alg of 1 and 0.67. Capsules with higher proportions of alginate performed worse at higher temperatures, indicating that they could have degraded because of dehydration.

Thermal performance, a very important characteristic, has been studied by various authors. Usually, thermogravimetric analysis is used, in which changes in weight of a sample are recorded as a function of increasing temperature. This type of analysis can provide information on all phenomena that cause changes in mass, such as vaporization, sublimation, or oxidative degradation [26]. In [25] not only were various capsule compositions tested, but calcium

alginate polymer and sunflower seed oil were also tested individually. The polymer starts losing mass at around 100°C which is likely a product of the evaporation of any water that remained within it. The mass loss continues steadily to a level of 6% at 200°C. By 400°C, 39% of the original mass was lost. After this point there is a sharp increase in mass loss, with only 20% of the polymer remaining at 500°C, steadily decreasing to 9% at 1000°C. The oil's mass steadily decreases to 80% of the original amount at 400°C, after which there is a sharp drop-off in mass. The thermal behavior of capsules will naturally be a blend of the two previously described. Up to 200°C, the upper limit of asphalt mixing temperatures, mass loss was lower in capsules with higher proportions of oil, which is in accordance with the two previously described behaviors for their ingredients. The worst performer had 5% mass loss at this temperature, a negligible amount.

Compartmented Calcium Alginate Fibers

These types of fibers have been studied by the authors of [27] and [28]. Numerical simulations presented in these studies suggest that, due to their arrangement, fibers containing rejuvenators are more likely to be intercepted by random planar cracks than capsules, leading to much greater rejuvenator release. If the fibers were hollow, this release might have been so great in fact, that it could have led to over-saturation of the binder in areas where cracks form. Compartmented fibers were chosen instead, as a way of limiting possible over-saturation.

Sodium alginate was the polymer chosen for the shell of the fiber. Two different solutions were prepared, one containing sodium alginate and water, and the other containing poly(ethylene-alt-maleic anhydride) (PEMA) and the rejuvenator, which were later mixed. The mixing process must be carefully controlled as this is how the rejuvenator droplet size is set. The emulsion was then spun in a wet spinning process to form the rejuvenator-filled compartmented fibers.

Various proportions of alginate and rejuvenating oil were tested. Higher rejuvenator to alginate ratios generally resulted in fewer oil compartments per unit length, along with larger compartment size. The fibers using 70 grams of rejuvenator to 30 grams of alginate seemed to strike a balance which led to the highest rejuvenator volume per gram of fiber. Increased percentages of rejuvenator also resulted in a lower mass loss at 160 °C. At asphalt mixing temperatures mass loss was under 9% for all types of fibers. Uniaxial tensile strength varied greatly with temperature and fiber composition, but it can be stated that lower rejuvenator/alginate ratios resulted in stronger fibers.

2.3 Assessment of Asphalt Self-healing

2.3.1 Rejuvenator Release Detection Methods

Detecting rejuvenator release is one of the most important metrics through which an encapsulation system can be measured. If this release is inadequate, the technology loses its major purpose.

Many techniques can be used for this purpose. Given bitumen's dark color and the fact that rejuvenators are intended to dissolve in it, simple visual analysis often is not enough to draw any conclusions. As such, authors typically use techniques such as Fourier-transform infrared spectroscopy (FTIR spectroscopy), fluorescent microscopy, and computed tomography (CT scans) to directly measure changes in the binder's composition or asphalt microstructure, indicative of rejuvenator presence ([3], [20], [25], [29]). When these rejuvenator detection methods are coupled with techniques such as measuring changes in the sample's stiffness modulus or phase angle, a clear picture of the rejuvenator's release can be painted.

Fourier Transform Infrared (FTIR) Spectroscopy

Infrared spectroscopy is a technique that measures the interaction between infrared radiation and the sample being studied. Different parameters like emission or absorption can be measured, and the results are plotted as a function of the wavelength (or other related units like frequency or wavenumber). The resulting graph is called a spectrum. This technique makes use of the fact that different substances interact differently with infrared radiation because of their distinct molecular structures. Every molecule will have a number of vibration modes and "natural" frequencies, which when excited will produce characteristic spikes at certain radiation frequencies which can be used to identify them.

Fourier transform spectroscopy differs from monochromatic spectroscopy because it uses a beam of light containing various frequencies instead of a single one. While the second technique is of simpler comprehension, since slowly varying the frequency of light shone on the sample and measuring the absorption for each one will directly produce a spectrum, the technique employing various frequencies at once grants higher quality and faster results [30], [31]. The raw data from the multi-frequency analysis needs to be put through a Fourier transform to decompose the results into absorption for each light frequency.

An example of how this technique can be used is presented in [7]. The author uses FTIR spectroscopy to measure both the aging of bitumen and composition change after rejuvenator release. Knowing that certain compounds that form due to oxidation will have peaks at the wavenumbers of 1030 cm^{-1} and 1700 cm^{-1}, the spectra of samples subjected to long- and short-term aging were compared to the one of an unaged specimen (Figure 2-1). For this comparison the area under the aforementioned wavenumber peaks was normalized, added and called the combined aging index. The difference between the short-term aged (STA) and the long-term aged (LTA) samples is very clear.

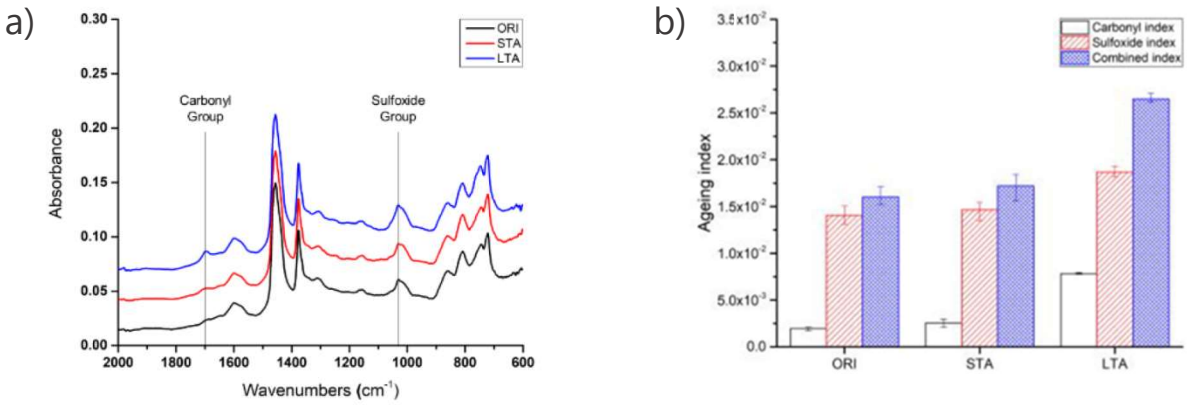

Figure 2-1: a) FTIR spectrogram of 70/100 bitumen at different aging levels [7]; b) Aging indices for the unaged (ORI), short-term aged (STA), and the long-term aged (LTA) bitumen samples [7]

A similar methodology was employed to measure rejuvenator presence in bitumen. Three distinct rejuvenators were tested, and their infrared spectral signature was studied. They were then mixed with bitumen at various concentrations to determine their rejuvenating capacity and efficiency after re-aging. By looking at the spectra of these rejuvenator-bitumen mixes and the absorption change at key wavenumbers (Figure 2-2), the performance of each

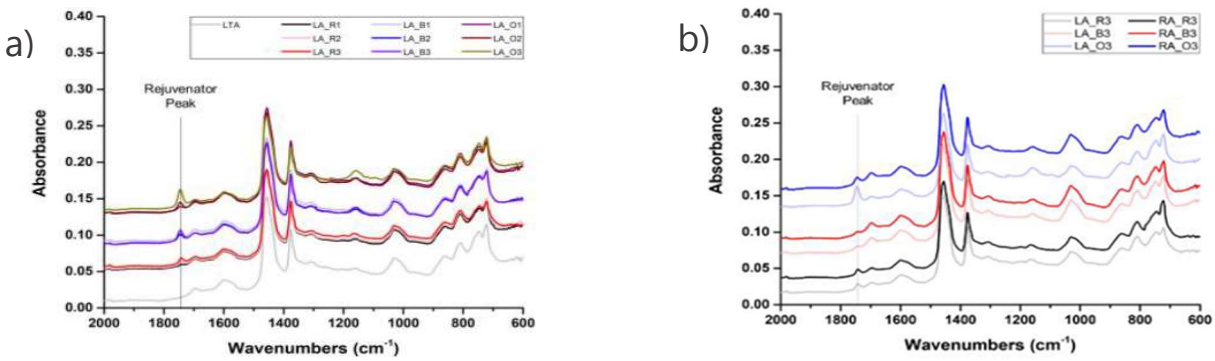

Figure 2-2: a) FTIR spectrogram of rejuvenated bitumen [7]; b) FTIR spectrogram of the re-aged bitumen ("RA" curves, with "LA" curves being prior to re-aging) [7]

rejuvenator can be measured. By relating this change to the concentration of rejuvenator necessary to produce it, its efficiency can be measured. In this case, while a rejuvenator called R20 was the best performer, having the lowest aging index after re-aging, rapeseed oil was the most efficient, producing the greatest change per volume added (Figure 2-3).

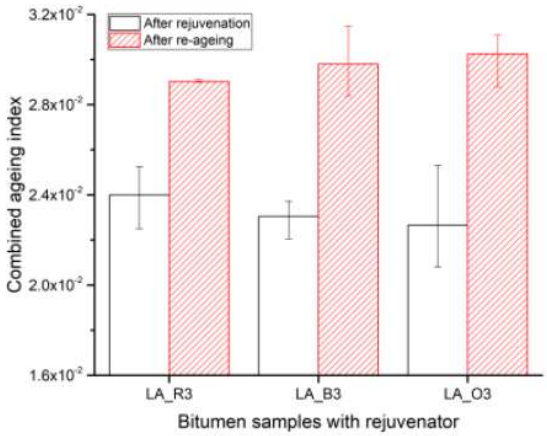

Figure 2-3: Aging index for the various rejuvenator types, with LA_R3 referring to R20 and LA_O3 referring to rapeseed oil [7]

This technique, while offering great insights into the compositional changes in a sample, presents some challenges when applied to the study of encapsulated rejuvenators. These challenges mainly stem from the fact that it can be difficult to extract the necessary samples from an asphalt mixture specimen. If, for instance, mastic samples are extracted from a specimen to be analyzed, the fact that rejuvenator release is concentrated around the capsules needs to be considered. If the overall compositional change of the mixture is to be studied, the binder must be extracted using solvents, which often also dissolve capsules, altering the results.

Fluorescence Microscopy

Fluorescence is the emission of light by a substance during exposure to electromagnetic radiation. If it persists after exposure, it is known as phosphorescence. A fluorescence microscope works by irradiating a sample with the required wavelength radiation (typically ultraviolet light) and separating the fainter, longer wavelength light emitted by it from the excitation light [32]. By coupling this phenomenon with the great visual detail enabled by a microscope,

very small details in a sample that would otherwise be invisible to the naked eye (due to size or not standing out in the visible light range) can be tracked.

This technique can be used to distinguish types of bitumen, or to detect substances dissolved in it that are not visible in its dark mass.

In [33] the authors used this technique to distinguish between aged and virgin bitumen (Figure 2-4) to study how the binders blend when using recycled asphalt. This is possible because the maltenes in bitumen are capable of fluorescence [34], and because bitumen's fluorescence decreases in brightness as it ages [35]. The authors quantified the fluorescence of each binder by processing the image and assigning each pixel a gray value, generalized as a mean gray value (MGV) for each binder.

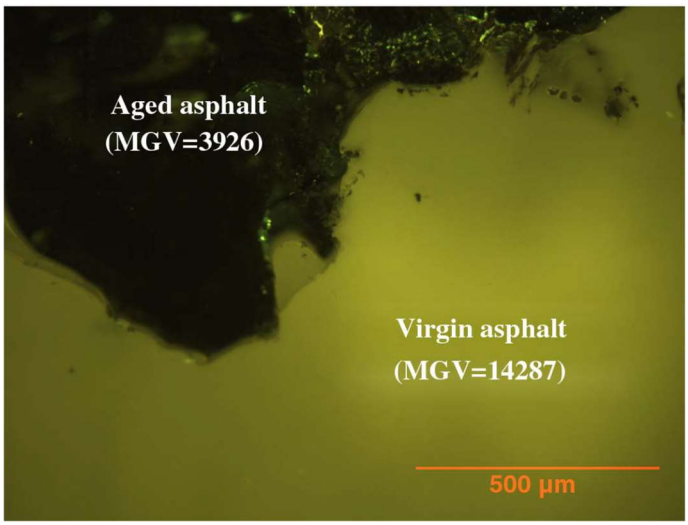

Figure 2-4: Fluorescence microscopy of virgin and aged bitumen samples [33]

This technique has also been employed in studies with microcapsules containing rejuvenators in [36]. The authors used microcapsules with shells made of melamine, urea, and formaldehyde, containing a rejuvenating oil. Diameters varied between 10 µm to 330 µm. When studying microcrack healing, oil release and crack closure can clearly be identified using fluorescence microscopy, as the oil and microcapsules have a much brighter yellow hue than the binder. In a specimen where a microcrack intersecting three capsules developed, oil can clearly be seen filling up the small void. After thirty minutes, the crack is no longer visible, and the oil appears to have dissolved in the bitumen (Figure 2-5).

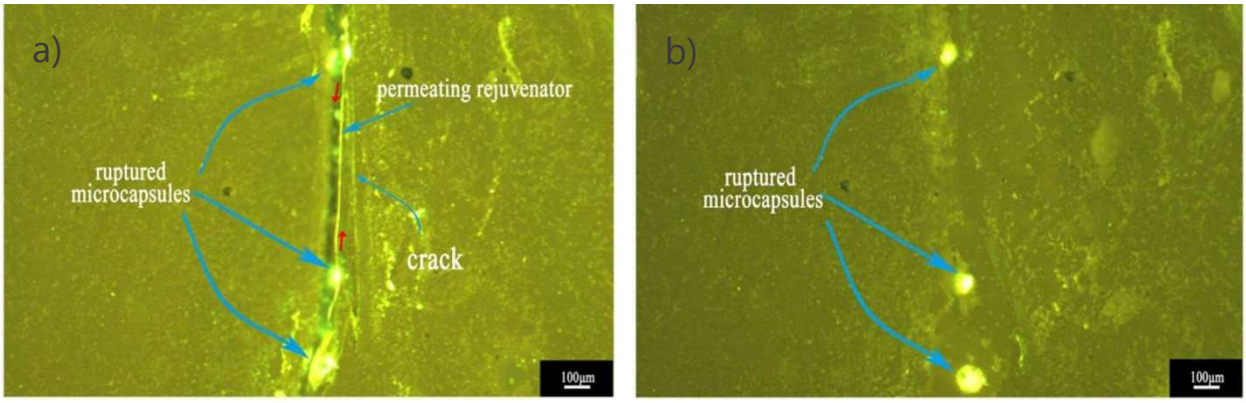

Figure 2-5: a) Fluorescent microscopy imaging of a crack in bitumen containing rejuvenating microcapsules [36]; b) Fluorescent microscopy imaging of a crack in bitumen containing rejuvenating microcapsules 30 minutes after damage was induced [36]

This technique's effectiveness is diminished when the contrast between the various materials in a sample decreases. When applied to asphalt mixtures containing encapsulated rejuvenators, fluorescent microscopy results in more complex images in which aggregates, capsules and rejuvenator may be hard to distinguish, such as the case in Figure 2-6 [29], where the authors tried to assess rejuvenator release in asphalt with this technique, yet the result is a confusing image, where the rejuvenator cannot easily be identified.

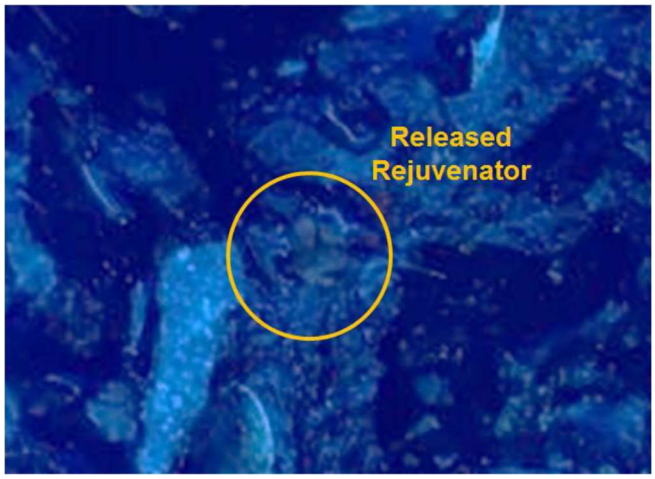

Figure 2-6: Fluorescent microscopy imaging of rejuvenator release in an asphalt mixture [29]

Computed Tomography with X-rays

Computed tomography (CT) scans have been an essential tool in the medical field for many decades. Their use in construction materials research became more widespread with the advent of the micro computed tomography, capable of much greater resolution than typical

medical devices [37]. This non-destructive technique uses an X-ray source which is rotated in relation to the sample, which can be achieved by moving either. Typically, in laboratory equipment, the radiation source is fixed, and the sample is rotated many times over the course of the scan. The resulting data is processed using tomographic reconstruction, which yields a slice with a set height of the sample's internal structure. These slices are then combined to form a complete scan of the specimen.

The reason this technique is able to produce models where the different components of a sample are distinguishable is that different materials typically will have differing atomic mass and density, which will influence X-ray absorption. While this distinction is not infallible, the very high resolution of modern scanners usually provides enough detail to visualize minute variations between components.

As its name suggests, this technique is highly dependent on computer processing. Nowadays, advanced quantitative analysis of the results goes hand in hand with sophisticated image processing software, with artificial intelligence starting to play a more prominent role. The resulting slices and three-dimensional models can be used to study several aspects. For concrete and asphalt samples, porosity can be measured, different phases and densities identified, and damage or failure modes can be studied, for example.

The type of analysis most authors have used to study rejuvenator microcapsules in asphalt is qualitative viewing, which is simple, and often enough to study capsule behavior. This is the type of analysis done in [3], where the authors compare microcrack healing in mixes with and without calcium alginate capsules containing oil. In Figure 2-7 part of a CT scan of a mixture without capsules is shown and no perceptible difference can be found after a rest period, in contrast to Figure 2-8, where the microcracks appear smaller.

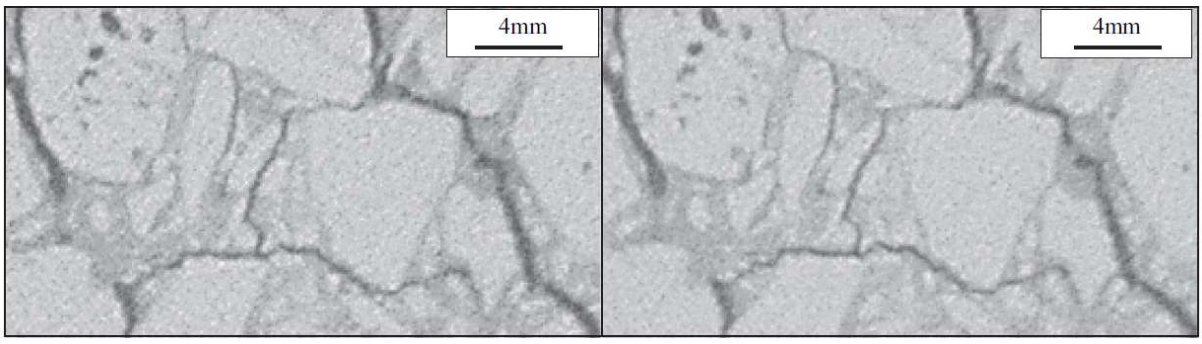

Figure 2-7: Computed tomography imaging of micro-cracks in traditional asphalt samples before (left) and after (right) resting [3]

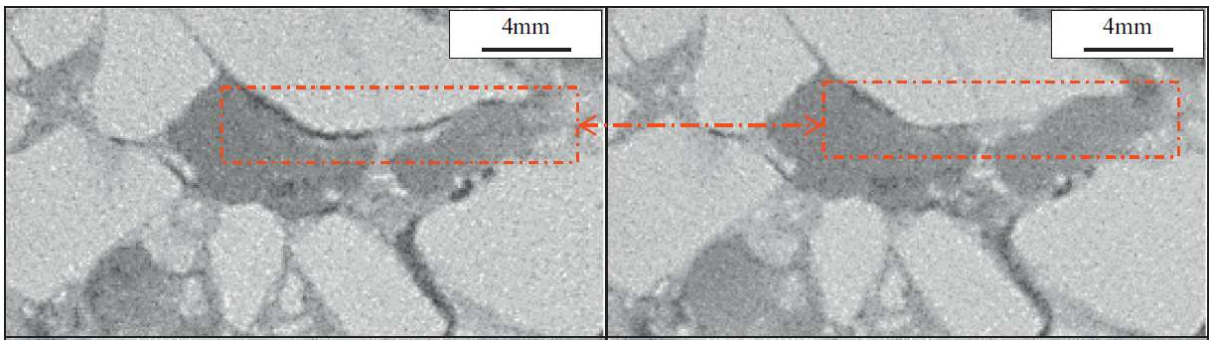

Figure 2-8: Computed tomography imaging of micro-cracks in asphalt samples containing calcium alginate micro-capsules before (left) and after (right) resting [3]

While very insightful, this technique also has its limitations. This method utilizes discrete slices of a specimen to form an image. While very small gaps between them can be reached, they are still present. This means that, when an asphalt sample is analyzed at two different points in time, miniscule differences in its size and position will influence what is visible in each slice, possibly hiding some micro-cracks. Studying a three-dimensional rendering of a crack instead of slices can attenuate this problem, yet it does not change the fact that the small samples can be exposed changes in ambient temperatures inside the scanner, capable of altering the mixture's internal structure to some degree. Additionally, the equipment required to perform these scans is often very expensive.

2.3.2 Crack Healing and Mechanical Performance

Given that asphalt degradation occurs in large part because of micro-cracks that eventually develop into macro-cracks, which increase its rate of degradation, a technology's effect on a pavement's crack healing ability should be its main performance indicator. A system should only be considered effective if produces meaningful, reproducible improvements in self-healing under real-world conditions, without greatly sacrificing other characteristics such as resistance to deformation or maximum strength.

As noted in the previous section, many factors affect self-healing ability, with the type of mixture (asphalt, mastic, or binder) being one of them. Tests using asphalt mixtures were considered the most relevant for this section. Most of the previously described encapsulation methods have been tested in asphalt mixtures, and some of the most relevant examples will be presented in the ensuing paragraphs.

2.3.2.1 Testing Methods and Criteria

The type of damage described in the previous paragraphs is known as fatigue cracking, one of the most common sources of damage to roadways [2]. In light of this fact, the effectiveness of an encapsulated rejuvenator is often measured through fatigue testing. Monotonic tests, simply applying load or strain until failure, are also common, and often used in the study of encapsulated rejuvenators.

Fatigue tests rely on the application of cyclical loads or strains, with slightly differing results. Strain-controlled tests always apply the same deformation on each cycle, varying the load needed to do so. When compared to load-controlled tests, the authors of [38] consider these to be better suited to thin asphalt layers, less sensitive to mixture variables, and more representative of *in-situ* conditions when it comes to crack propagation. These tests usually require more cycles to failure than load-controlled ones. Effects like increased stiffness from mixture aging will lead to lower fatigue life in strain-controlled conditions, while they increase fatigue life in load-controlled testing. A decrease in stiffness stemming from rejuvenator release would have the opposite effect, for example.

There are many ways of testing a specimen, each with their own advantages and disadvantages, which were readily summarized in [38]. Some of these techniques and their characteristics according to this source are:

- Simple flexure: where a specimen is subjected to loading, which can be applied at various points along the sample. These have the advantage of being widespread and well understood, but results can only be representative of *in-situ* conditions if a shift factor is used.
- Supported flexure: an iteration on the simple flexure test, where instead of simply being fixed to the testing apparatus, the specimen is supported by a resilient material like a thick rubber mat, that better simulates field support conditions.
- Direct axial tension or compression: where tension, compression, or both are applied along one of the specimen's axes, creating uniform stress field within the material. Realistic pulses (which apply compression-tension-compression) can be simulated, but other field conditions are not adequately represented.
- Diametral tests: cylindrical specimens have compressive loads applied along their vertical diametral plane that produces tensile stress in a direction perpendicular to this plane. While this test is simple and produces a biaxial state of stress, which

might better represent field conditions, it is known to underestimate fatigue life relative to other tests.

- Triaxial tests: typically, testing equipment capable of applying radial and axial stress is used. This is a common method of determining the properties of deformable solids, with the advantage of being able to faithfully replicate *in-situ* stress conditions, but shear stress must be controlled.
- Wheel-track testing: a loaded wheel with a pneumatic tire is repeatedly rolled over a specimen in the form of a slab supported by a rubber mat. This test offers a good simulation of field conditions and the ability to study crack initiation and growth but may be limited by the speed of the wheel, and rutting may affect fatigue measurements in low stiffness mixtures.

While load-controlled tests will eventually lead to specimen fracture, strain-controlled tests require the definition of criteria for failure. One of the traditional criteria is to stop the test when the loads applied, or the stiffness modulus becomes half of the initial value.

Healing can be measured in various ways. It is typical for authors to quantify healing by measuring the recovery of the mixture's stiffness modulus, maximum strength, number of loading cycles, or dissipated energy, among others. While this approach is very useful, it is important to note that asphalt is not an elastic material, but a viscoelastoplastic one with a complex behavior. When loaded, asphalt will display delayed deformation increase/recovery and dissipate energy through heat, that will slightly lower the bitumen's viscosity. These factors contribute to a perceived deterioration of its physical properties, which will increase the measured "level" of damage beyond what the specimen actually experiences. Some phenomena are reversible, and so when the sample is loaded a second time some of the measured recovery in its physical properties will simply be the reversal of these processes during the rest period. If the strain/load applied during the test is too great, asphalt's behavior might also go into its non-linear region, adding uncertainty to the results if not accounted for. During rest, asphalt will experience stress relaxation/strain recovery and steric hardening [2], which is the hardening of bitumen at room temperature over time after its heated due to the molecular restructuring of the asphaltenes [39]. These factors will increase the specimen's perceived healing.

Due to all these considerations, there has been a lot of research into how to correctly measure these factors and their contributions to the results, so as to approximate asphalt's viscoelastic behavior to an elastic one that can clearly be characterized through its stiffness modulus and the other previously described properties.

It can be argued that, while taking into account the previously described behaviors is important, when a comparative test is done, between mixtures with and without added encapsulated rejuvenators for example, the fundamental difference between them will be the addition of rejuvenator, while the other factors will mostly be equal between them, cancelling out their contributions.

2.3.2.2 Influence of Mixture Type on Asphalt Healing

As has been mentioned before, a multitude of factors affect a bituminous mixture's healing potential. Bitumen is itself one of them. Softer bitumen (high penetration grade) with lower softening temperature performs better in this regard than hard bitumen [9]. The authors of [40] also found that bitumen with low amphoteric and high aromatic contents had better healing ability.

Since bitumen is the component of asphalt that grants it its self-healing ability, it is not surprising to learn that bitumen content is a very important factor in healing speed and potential. In experiments done with bitumen and bituminous mortar healing speed was found to be very high, while in asphalt mixtures and pavements healing is much slower [9]. Asphalt mixtures with higher binder content show higher healing potential, as expected. This is also the case for mixtures with thicker bitumen films and lower air void content.

In [40] a stone mastic asphalt (SMA) specimen was tested against dense-graded mixtures in a direct tensile fatigue test to assess the difference a mastic-rich composition would present in fracture types and healing response. The authors expected the SMA to show cohesive fracture (through the mastic) and the dense-graded mixtures to show adhesive fracture (between the aggregates and binder), but in both types of mixture cohesive fracture was prevalent. Healing performance (measured through dissipated energy and corrected for asphalt's viscoelasticity) was also similar in both mixture types.

This result is somewhat unexpected, as SMA mixtures typically have higher bitumen content than traditional ones, which should increase their healing potential.

In [41] the authors tested different types of asphalt mixtures at low temperatures, the conditions they identified to be more conducive to fatigue damage. Using CT scans, fatigue cracking in an SMA 11 mixture was found to be more prevalent along aggregate-mortar

interfaces (adhesive fractures), while in AC-type mixtures (AC 8 and AC 11) cracking tended to happen in the mortar phase (cohesive fracture). In terms of healing, the SMA mixture had better damage recovery than the AC mixtures (with the AC 8 performing better than the AC 11) at both -5°C and 5°C, despite having the lowest binder percentage of the three. The results were not corrected for asphalt's viscoelasticity, yet they still offer a meaningful comparison. These findings are consistent with the conclusions made in [42] that in the 0°C to 20°C range the characteristics that most significantly affect healing have to do with the aggregate structure in the mix, with the effect of bitumen content becoming more relevant as the temperature increases.

In studies using calcium alginate capsules, authors have suggested that gap-graded mixtures, like SMA, might have a different response to encapsulated rejuvenators than continuously-graded mixtures [43]. This may happen because in a mixture like SMA the capsules will lodge themselves between "large" aggregates that are better able to compress them. This question will be investigated further in Section 4.3.4.

2.3.2.3 Assessment of Self-healing and Impact on Mechanical Performance for various Encapsulation Techniques

Saturated porous aggregates (SPAs) were first tested in asphalt mixtures in [44]. Two types of uniaxial compressive loading were applied: static and cyclic. Both were carried out at 20°C. The specimens used were small slabs containing 5% saturated porous aggregates, produced in the same way as described in Section 2.2, and averaged 3.64 mm in diameter.

The static load was used to quantify differences in the maximum compressive strength stemming from the use of SPAs. From the plots provided by the authors, it is visible that the mixture with encapsulated rejuvenator had lower stiffness, but similar yield strength. This may indicate that capsule breakage during loading is responsible for the added deformation, but once the majority of capsules are broken the mixture will act like a traditional one (for this kind of short time frame testing).

The cyclic loading test was intended to be representative of the loads created by traffic. A frequency of 0.5 Hz was used in load-controlled conditions (15 kN). Testing was interrupted at different points for different specimens to study the evolution of their behavior at various damage levels. During the initial loading phase, the slabs with capsules had up to twice the vertical deformation of the capsule-free slabs. This, along with visible oil leakage from specimens with SPAs confirms that the capsules were broken during this stage. Previously, it was stated that the oil might have difficulty leaving the aggregate's pores. The data presented in

this study does not necessarily counter that claim, as the mechanism behind the oil's release appears to be the crushing of the saturated aggregate, forcing it out. The claim would likely be valid if the aggregates were simply cracked.

After the initial loading, the slabs were rested at 55°C for 4 hours. They were then loaded again (at 20°C). Slabs containing capsules showed large amounts of deformation during the first cycles, while regular slabs displayed approximately the same amount as before rest, a sign that the binder had become less viscous in the first case. As loading went on, the amount of deformation became more constant in specimens with SPAs (matching the traditional mixture's behavior), likely due to their compaction.

Over the course of the tests, porosity of a capsule-containing specimen was studied using CT scans. Before testing, its value was 3.27%, which climbed to 12.07% after cyclical loading, and finally decreased to 8.54% after resting. While this does confirm that crack healing took place, it is unclear whether rejuvenator release or the increased temperature during rest was the biggest contributor. For the same circumstances, the porosity of the traditional mixture was 4.10%, 8.30%, and 6.39%. While there is less healing in this case (air void content decrease of 23% versus the SPAs' 29%), there is also less healing necessary, given that the overall values are lower. Coupled with the significant increase in deformation, the performance advantage of mixtures containing SPAs is uncertain in this study.

In a follow-up study, [20], various capsule diameters were studied, along with their influence on indirect tensile strength and indirect tensile fatigue tests. All testing was conducted at 5°C. An inverse relationship between the size of capsules and the asphalt mixture's tensile strength was found. Irrespective of capsule size, no influence on fatigue resistance was found. In light of this, the authors put forward that fatigue cracking was not the main mechanism for breaking the capsules. Given that indirect fatigue tests used 20% of the peak tensile strength, it is possible that internal stress in the samples was not sufficient to crack the SPAs.

While this study further shows that saturated porous aggregates might not work as a form of rejuvenator encapsulation, indirect tensile fatigue testing also might not be the best way of simulating real world loads as noted in Section 2.3.2.1.

In [24] asphalt mixtures containing core-shell double-walled microcapsules were produced, with the goal of assessing crack healing performance and stiffness recovery. In this experiment, crack healing ability was evaluated by measuring crack width after a rest period in comparison to the original width. Cracking was induced using a three-point bending test (3PBT) at room temperature and at high temperatures, and resting times were one, two, three,

and six days. As expected, longer resting periods corresponded to better crack healing. The mixture containing microcapsules also contained 5% post-consumer waste shingles (PWCS) by weight. When compared to a traditional mixture also containing 5% PWCS, the specimen containing microcapsules had slightly worse crack healing ability. Regarding stiffness recovery, the mixture with encapsulated rejuvenator had slightly worse or slightly better performance, depending on temperature (room temperature in the first case, and 50°C in the second case). It is important to note that stiffness recovery was measured in relation to the undamaged value and not in absolute terms.

From an observer's perspective, it is highly likely that the type of loading employed during these tests does not lead to loading of the microcapsules, producing a "clean" tension break in the lower part of the beam.

Asphalt mixtures containing calcium alginate capsules have been extensively researched. During some of the first trials with these capsules in [3], when subject to cyclical loading, specimens containing them showed decreasing stiffness over 500 cycles, whereas a traditional mixture displayed increasing stiffness, suggesting gradual capsule rupture due to loading (which would be desirable). Specimens containing capsules had better stiffness recovery after a rest period than traditional ones. Vertical deformation accumulation was greater in the formulations containing encapsulated rejuvenators. Micro-crack healing appeared to be much greater in specimens containing capsules, although this evaluation was made at a very small scale (cracks measuring about 0.3 mm), and so small variations of external factors (such as the time exposed to room temperature under a microscope) might influence results in a meaningful way.

Crack healing at a macroscopic scale was looked into by the authors of [45]. In an effort to test crack healing under simulated traffic loads, short asphalt beams were made and vertically cracked at their halfway point. Some contained capsules, and the remaining contained an amount of oil equivalent to what would be released from broken capsules during mixing and compaction. These beams were then subjected to uniform, uniaxial cyclical loading from the top, to promote rejuvenator release. After a rest period at 20°C, the beams were again broken using a three-point bending test, in order to quantify the strength regained during the rest period. The healing ratio was quantified as the amount of force needed to break the specimen for the second time over the amount necessary for the first time. In this regard, the beam containing 0.50% calcium alginate capsules was found to have up to 204% of the healing ability of a traditional mixture.

It is important to note that the bending tests were carried out at -20°C. The rejuvenator used in these experiments, sunflower seed oil, has the effect of lowering the bitumen's viscosity, allowing it to flow into cracks more easily. Yet, after crack healing is complete, its original viscosity is not regained, remaining more fluid than it would otherwise be, which would have a negative effect on the specimen's strength, despite the healing effect. By lowering the temperature at which tests are carried out this effect is minimized since the binder becomes stiffer in return.

In this same study, the effect of capsules on other mechanical properties of asphalt was studied. The researchers found that the presence of calcium alginate beads had a slight positive impact on air voids content (-8%), which could be explained by their high deformability and spherical shape allowing them to flow more easily during mixing and compaction than aggregates. Particle loss was 19% lower in mixes with capsules, while both kinds had the same indirect tensile strength, meaning that the adhesion between capsules and the rest of the components is very good. Water sensitivity tests showed no difference between the mixes with capsules and the ones without, and neither did rutting susceptibility tests. Stiffness modulus and fatigue resistance were lowered by 30% and 15%, respectively, in mixtures with capsules.

Loading of self-healed specimens at different temperatures was researched by [8]. In this study three types of asphalt mixture were produced: a standard AC 20 base 35/50, an AC 20 base 35/50 using 0.5% calcium alginate capsules containing sunflower seed oil (by mass), and the same AC 20 base 35/50 containing 0.1% sunflower oil (by mass). This last mixture intended to replicate the amount of oil that would be released by capsules during mixing and compaction. The various specimens were loaded in an indirect tensile strength test, to induce cracking, and allowed to rest at 20°C for various periods of time (24 hours to 96 hours, with 72 hours being the most common) before being loaded again. Temperatures during mechanical testing ranged from -14°C to 20°C. Before the rest period, the specimens were uniaxially statically loaded for 5 minutes (loads varied between 0, 5, 7.5, and 10 kN) to somewhat simulate traffic loads and encourage rejuvenator release. This was done at 20°C.

In general, strength recovery was very similar between the mixture containing capsules and the one containing oil under all conditions (varying temperatures or rest times, for example), and both edged out the traditional mixture in this regard. Critically, the varying uniaxial compressive loads applied to both the mixture containing oil and the one containing capsules showed no clear influence on strength and strength recovery, which suggests that rejuvenator release is not promoted by these loading conditions. This conclusion somewhat reduces the

meaningfulness of the remaining findings. As the author recommends, other types of loading should be studied, preferably, more realistic, cyclical ones.

As a follow-up study, the author of [46] aimed to test capsule influence on fatigue and rutting resistance under more realistic conditions. Two different tests were devised, one using small beams subjected to a four-point bending test (4 PBT) under a 10 Hz cyclic load, and another using slabs that would be put through a wheel tracking test. Both tests used an asphalt concrete mixture (AC 20 base 35/50), which was artificially aged at 85°C for 5 days for the first one.

This first test was picked as a way of studying fatigue resistance. It was done in strain-controlled conditions, using three different amplitudes, and the chosen frequency simulated traffic at 45 Km/h. After the first four-point bending test, the previously aged beams were confined and subjected to uniaxial static compression, resulting in 5 mm of deformation (10%) to their height. After this, they were allowed to rest for 5 days at 20°C before being tested again. When the fatigue curves before and after rest were compared, little difference between them was found for any of the specimens. Moreover, the ones containing 0.50% and 1% capsules performed slightly worse after resting.

The second test evaluated the rutting resistance of mixtures containing capsules, and was done at 60°C, the temperature recommended by the Standard NP EN 13108-1 for this test. No aging treatment was applied to the asphalt because it is precisely when new and more ductile that rutting poses a greater risk to it. During the first loading phase results showed greater vertical deformation accumulation in mixes containing 0.50% and 1% capsules than the ones with 0.75% or 0%, with the last two having very identical performance. After resting for 5 days at 20°C (no compression was applied), the testing resumed. Interestingly, specimens with capsules displayed slower rut evolution during this phase than the traditional mixture.

The authors of [47] devised a series of tests also aimed at loading the asphalt specimens in a realistic way. In this case, the specimens used were beams supported by concrete plates with a 30 mm gap between them, which in turn were supported by a neoprene base. The beam was loaded using a wheel track test capable of applying various loads (621 N up to 1032 N). This test setup is intended to mimic the conditions which lead to the development of a reflective crack in a pavement layer. This type of cracking often affects overlay asphalt layers, which are intended to quickly repair damaged pavements by paving over them. In these situations, discontinuities present in the old pavement layer, coupled with thermal expansion and traffic

loading, cause the new layer to quickly develop cracking patterns similar to the ones that previously existed [48].

The authors studied what effects calcium alginate capsules containing sunflower seed oil would have not only on fatigue life and crack healing, but also on skidding resistance and plastic deformation (rutting).

Four capsule diameters (0.7 mm, 1.3 mm, 2 mm, 3mm), each with two to three oil to sodium alginate ratios were tested. Capsule compressive strengths varied greatly, with the lowest value being 3.40 N and the highest 88.03 N. The asphalt mixture type used was a stone mastic asphalt (SMA) with a capsule content of 0.5% by mass (in the mixtures where these were added).

The various specimen's fatigue life was tested at five different load levels, with performance being recorded as the number of cycles the beams resisted until a crack with 50% of the specimen's height developed. A fatigue index was created, which related the number of cycles resisted by the specimen to the number of cycles resisted by the mixture without capsules (across all load levels). The results of the fatigue durability test showed that the mixtures with capsules tended to perform better with higher applied loads, which the authors theorized is the result of rejuvenator release aiding short-term healing. Smaller capsule diameters were found to have better performance than larger ones, with mixtures containing 1.3 mm (the second smallest after 1 mm) capsules showing the greatest fatigue resistance. This could be a sign of better integration within the asphalt mixture. When compared to the mixture without encapsulated rejuvenators, the majority of capsule-containing mixtures had worse fatigue resistance. One mixture (type I: 2 mm capsules with a compressive strength of 43.44 N) had comparable performance, and two mixtures (types A and B: 1.3 mm capsules, compressive strengths of 25.45 N and 11.62 N respectively) had better performance than the traditional one, seeing improvements of 10% and 12% to their fatigue life.

Crack self-healing was also measured. The authors first determined what level of damage would see the greatest recovery with a 24-hour rest period using a single capsule type, determining that 30% of the median number of cycles until failure was the optimum level of damage for this type of capsules, which was found to be in agreement with the findings of previous studies. Self-healing was measured through a healing index that relates the number of cycles resisted after a 24-hour rest period to the median number of cycles until failure for that mixture type. The worst performers in fatigue resistance generally showed the greatest strength recovery, with many mixture types showing healing indices between 39% and 43%, versus the traditional mixture's 9.2% healing index. The two best performers in the fatigue durability test had

the poorest healing ability. The mixture with comparable performance to the traditional one in the fatigue test showed a reasonable healing index of 33.5% These results reaffirm the notion that capsules which make the overall mixture weaker improve its self-healing ability by releasing greater volume of rejuvenator (often with a close to net-zero improvement in overall performance versus a traditional mixture). This finding was confirmed by measuring the volume of oil released by each capsule type after loading with a Fourier-transform infrared spectroscopy, which found a clear positive correlation between healing index and amount of oil released by the capsules. This was also done for rut depth, finding the same relationship.

The authors do not directly draw a comparison of rut depths across mixture types, but this data can be extracted from the figures showing rut depth versus oil release with an image processing software like *ImageJ*. The traditional mixture's rut depth at ten thousand cycles can be estimated to be 0.94 mm. The two best performing capsules, which were also the best performers in fatigue resistance, showed rut depths of about 1.04 mm, a 10.6% increase. There was a 22% increase for one capsule type (that underperformed in fatigue and self-healing tests), and the remaining capsule types had rut depth increases of over 43% versus a traditional specimen.

Overall, the best performing capsules appear to be the ones highlighted in the description of the fatigue resistance test, types A and B, that provide moderate increases in fatigue life and self-healing (about 11% and 5.3%) over a traditional mixture without excessively sacrificing resistance to plastic deformation. There are other capsule types which have a slightly higher sum of fatigue index and healing index but may not be useful if rutting performance is considered. Still, the total benefit of adding these encapsulated rejuvenators to a pavement layer is somewhat unclear, and heavily depends on its functional requirements.

A general conclusion that can be drawn from the previously presented studies is that the use of calcium alginate capsules seems to require tailoring to each specific mixture and use-case, as their concentration, integration within the mixture structure, size, and compressive strength all affect their performance. Their addition can easily result in a mixture with worse characteristics than the original.

3

MATERIALS AND METHODS

3.1 Materials

The materials necessary for the production of a light-colored asphalt mixture were kindly provided by two companies. The limestone aggregates were provided by Alves Ribeiro, from their facilities in Camarate. The binder, Recofal S100-P, was provided by Repsol. This product is a synthetic light-colored binder, with physical properties designed to resemble bitumen (Annex A). It is especially suited to applications where pigmentation is necessary. Bitumen (35/50 penetration value) was also used.

The calcium alginate capsules containing sunflower seed oil were produced in various batches by the author at NOVA University Lisbon's Department of Materials Science. Sodium alginate from Sigma-Aldrich and calcium chloride from Alfa Aesar were used.

The oil used in the calcium alginate capsules was regular, consumer-grade sunflower seed oil. The pigments used for this oil varied in nature. Blue and green Colorfalt pellets by Ventraco were used. These contain both pigment and binders (polymers). Ravasol COLOR+ R red pellets, from Ravago Chemicals, are the same kind of product, and these were also used. Carbon black (PBk7), pure chromium green (PG17 + PG8), and primary blue (PB15) powder pigments were tested. Finally, red fat-soluble food coloring (sunflower oil based) from Decora was also used.

During the mechanical testing of asphalt beams sheets of 10 mm thick natural vulcanized rubber (70 Shore A stiffness), 5 mm sheets of low-density polyethylene sponge, and 10 mm acrylic sheets were used to support the samples.

3.2 Pigment Selection

One of the most important aspects of this study is the adequate release of pigmented oil into the area surrounding capsules, so that its behavior can be studied. To this end, various pigments were studied with the goal of finding the one with the best coloring ability. Sunflower seed oil and pigment were mixed in various concentrations, depending on the pigment's solubility. The following colored oils were produced and tested (concentrations in pigment mass to oil mass):

- 1% green Colorfalt pellets
- 1% blue Colorfalt pellets
- 0.66% red Ravasol COLOR+ pellets
- 1% pure chromium green powder
- 1% primary blue powder
- 1% carbon black powder

Additionally, red fat-soluble food coloring (sunflower seed oil based) was also tested, with no dilution.

All the oils were produced with simple mixing and agitation, apart from the pellet-based ones, which also required heating to break down the pellet's binder.

The various oils were mixed with the binder at concentrations of 5%, 10% and sometimes 20% (all by mass) and spread in a thin layer on tracing paper. The resulting stripes were then visually compared against each other.

3.3 Production of Capsules

Calcium alginate capsules were chosen for this study because of their ease of production and safe ingredients. Given that it would be necessary to produce and experiment with the colored oil, a certain degree of flexibility was needed, which this encapsulation technique offers.

The steps followed for capsule production are based on the procedure described in [3].

The process begins with the mixing of sodium alginate, water, and the colored oil chosen for that batch. Notably, the red food coloring was diluted by 50% with sunflower oil. This was done because this coloring agent showed excellent pigmentation ability even at low

concentrations and was only commercially available in small quantities (17 g per package). This made it possible to produce a batch of capsules with a single bottle. The proportions between these three ingredients varied. The first batch produced used an oil to water ratio (O/W) of 0.1 by volume, and an oil to alginate ratio (O/Alg) of 3 milliliters per gram. In an attempt to increase capsule diameter, the following two batches used an O/W ratio of 0.2. Given the proportionally lower amount of water, the oil to alginate ratio was increased to 6 (ml/g) to keep the mixture's viscosity in a workable range. In this case, using an O/Alg ratio of 3 resulted in an emulsion which wouldn't flow through the dropping funnel. Once the constituents were measured, the oil and water were mixed with a high-shear laboratory mixer for three minutes. By this point, a dispersion of small oil droplets had been achieved. Sodium alginate was added, with the mixer still running to limit clump formation. The mixing process then went on for fifteen minutes.

Separately, a solution of water and calcium chloride was prepared, using a concentration of 2% CaCl by mass. This solution's volume, while not unimportant, does not need to be exact, requiring only that enough calcium ions be present to allow for the polymerization of the sodium alginate. For smaller batches as little as 400 ml were used, and for larger ones 800 ml were used. These volumes were adequately scaled for the volume of emulsion.

After the mixing process is complete, the now stable oil, water, and alginate emulsion was poured into a dropping funnel. The funnel was then placed over the calcium chloride solution at an adequate height, while the latter was slowly stirred by a magnetic stirrer. Dropping height should be limited to a few centimeters to ensure that drops do not assume a raindrop-like shape. Finally, the funnel's tap was regulated to allow for the steady dropping of the emulsion in small beads.

The newly formed calcium alginate capsules were allowed to remain in the calcium chloride bath for an additional fifteen minutes after the last drop, to ensure thorough polymerization of all capsules. As a final step, the capsules were removed from the calcium chloride solution and washed with ethanol, to limit the quantity of oil on their surface. They were now ready for drying and subsequent storage.

The sodium alginate capsules were stored in a freezer, using air-tight bags, to limit oxidation and any oil release.

The composition of the various capsule batches is presented in Table 3-1. The resulting capsules are pictured in Figure 3-1.

Table 3-1: Components and key ratios of the various calcium alginate capsule batches produced

Capsule Batch	A (Pellets; O/W 0.1; O/Alg 3)	B (Pellets; O/W 0.2; O/Alg 6)	C (Pellets; O/W 0.2; O/Alg 6)	D (Coloring; O/W 0.1; O/Alg 3)
Oil Type	Sunflower seed oil with 0.66% Ravasol COLOR+ R pellets by mass	Sunflower seed oil with 0.66% Ravasol COLOR+ R pellets by mass	Sunflower seed oil with 0.66% Ravasol COLOR+ R pellets by mass	Sunflower seed oil with 50% red food coloring by mass
Oil Volume (ml)	40.0	160.0	160.0	27.3
Water Volume (ml)	400.0	800.0	800.0	273.3
Sodium Alginate Mass (g)	13.4	26.7	26.7	9.1
O/W Ratio	0.1	0.2	0.2	0.1
O/Alg Ratio (ml/g)	3.0	6.0	6.0	3.0
Wet Yield (g)	394.4	836.3	824.7	294.3
Dry Yield (g)	36.0	122.7	119.0	33.2

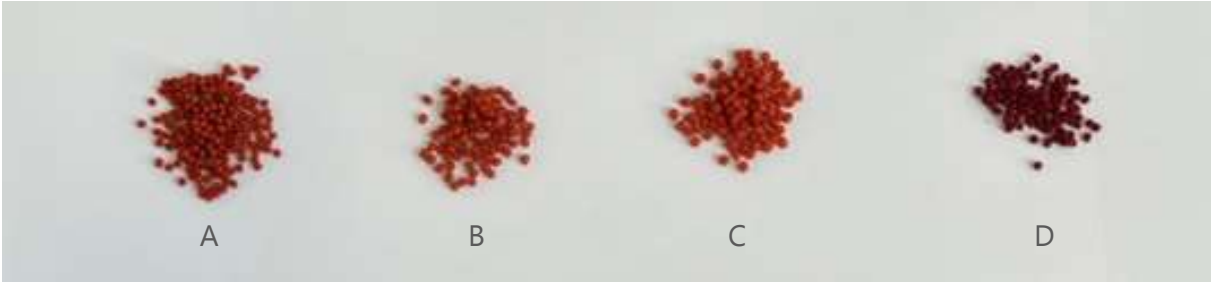

Figure 3-1: Samples from each capsule batch

3.4 Characterization of Capsules

There are various parameters that are relevant to capsule performance, such as size, thermal stability, compressive strength, and internal structure.

For each batch, capsule size was measured using photographs of capsules next to a ruler, which were later analyzed using *ImageJ*, an image processing program. Given their ellipsoidal shape, the capsule's two largest dimensions could be measured with a top-down photograph. The last dimension, their height, was measured in a similar way using a horizontally perpendicular photograph.

Mechanically the capsules were loaded to failure in a universal testing machine to determine their compressive strength. In the resulting force-displacement curves most capsules

showed a peak in force followed by a momentary decrease that corresponds to the beginning of crushing. This was determined to be their compressive strength. An example of a capsule form batch A is presented in Figure 3-2.

A second round of compressive testing was done on capsules that were heated to 150°C in a laboratory oven and then allowed to slowly cool to room temperature in the oven over two and a half hours. This simulated the temperatures experienced by the capsules during mixing, compaction, and mixture cooling. The beads were tested after this treatment to determine what effect heating had on their mechanical properties.

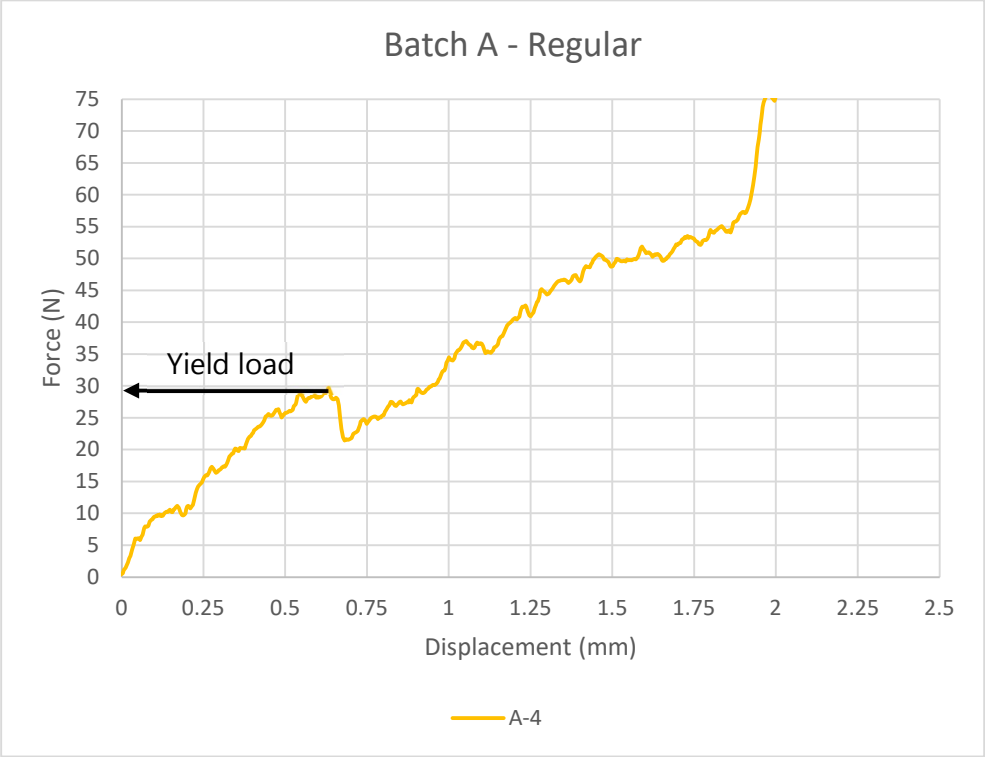

Figure 3-2: Force-displacement curve for a single capsule from batch A

The capsules were photographed after heating, to identify any differences in appearance, and after being compressed over a sheet of paper to show oil release.

Oil release after mechanical testing was also measured.

3.5 Production of Asphalt

Two types of asphalt mixtures were studied: a continuously graded asphaltic concrete (AC 14 surf/bin/reg 35/50) and a discontinuous stone mastic asphalt (SMA 11 PMB 45/80-65).

Both these mixtures used basalt aggregates in their formulations, which had to be switched out for limestone, to ensure the visibility of any oil released by capsules. Each mixture had its proportions adjusted to fit the original gradation curve as best as possible using the slightly different (in terms of particle size and density) limestone aggregates. Their gradation curves before and after limestone conversion are presented in Figure 3-3 and Figure 3-4.

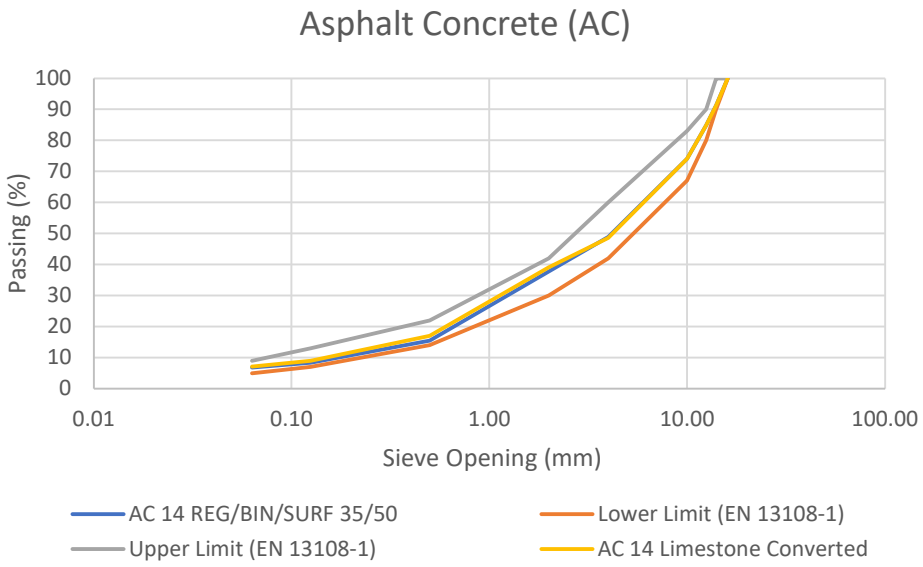

Figure 3-3: Gradation curve for the asphalt concrete mixture before and after being converted to limestone aggregate

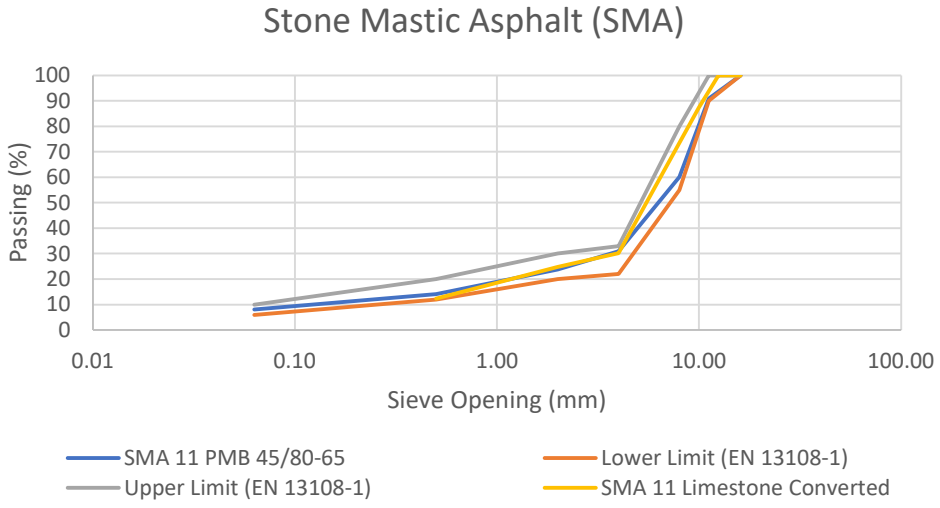

Figure 3-4: Gradation curve for the stone mastic asphalt mixture before and after being converted to limestone aggregate

The calcium alginate capsules were accounted for in the mixture formulation, with the mixture's theoretical maximum density being adjusted to reflect the addition of a certain percentage of capsules, but not in the gradation curves. The weight of each aggregate fraction was then calculated using this new density value, with the goal of obtaining a certain volume of asphalt.

The limestone aggregate fractions used were 12/20 mm, 4/12 mm, 0/4 mm, and filler (Figure 3-5).

The asphalt mixtures' densities before and after limestone conversion can be found in table Table 3-2.

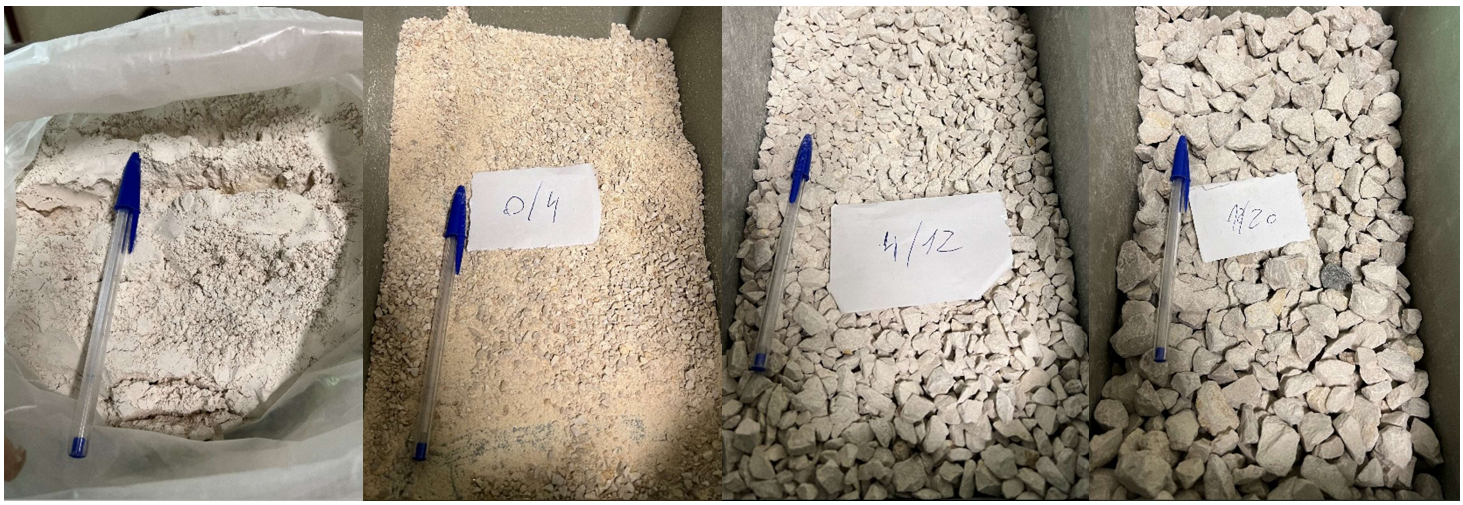

Figure 3-5: Limestone aggregate fractions used. From left to right: Filler, 0 to 4 mm, 4 to 12 mm, 12 to 20 mm

Table 3-2: Densities of the asphalt mixtures before and after limestone conversion

Mixture Type	Original		Limestone Only	
	Theoretical Bulk Density [kg/m^3]	Theoretical Maxiumum Density [kg/m^3]	Theoretical Bulk Density [kg/m^3]	Theoretical Maxiumum Density [kg/m^3]
AC	2440.0	2530.0	2365.9	2465.8
SMA	2540.0	2638.0	2357.4	2448.0

For the production of cylindrical test specimens (with a diameter of 101.6 mm and height of 63.5 mm), the aggregate mixes were weighed out and placed in a laboratory oven at 175°C for three hours, along with all the tools and molds which would be necessary. In a separate

oven, the binder was heated to 150°C for the same period. For each specimen, its constituent aggregates would be placed into a mixing bowl, after which the required amount of binder would be poured in. The bowl would then be attached to a Hobart asphalt stand mixer, and the mixing process would begin. This process would take a total of four minutes, during which the mixer's gas burner was carefully controlled to keep temperatures in the range of 140°C to 160°C. If capsules were to be added, this would be done at the third minute. If there were clumps or uneven capsule distribution these would be corrected by hand at the end of the mixing process. While the European Standard EN 12697-35:2016 does state that the asphalt concrete mixture should be mixed for 3 minutes, it was deemed to be far more homogenous at 4 minutes, possibly due to the binder used taking longer to adequately be incorporated. After mixing, the asphalt would be placed into Marshall molds and compacted using a Marshall compactor. For the asphalt concrete mix 75 blows were used on each side, while 50 were used for the stone mastic asphalt.

The composition of the specimens produced can be found in Table 3-3 and Table 3-4. Since not all cylindrical specimens were produced at the same time, their compositions were successively adjusted to ensure that specimen height would be 63.5 ± 1 mm, as stated by EN 12697-34:2020. This was done by increasing the theoretical volume of asphalt to be produced for each.

Table 3-3: Composition of the various asphalt concrete mixtures used in cylindrical specimens

		AC 14		AC 14 + 0.75% Capsules		AC 14 + 1.25% Capsules		AC 14 + 2.00% Capsules	
Density		2366		2339		2322		2297	
Theoretical Maximum Density		2457		2429		2411		2385	
Void Content		3.7%		3.7%		3.7%		3.7%	
Mixture Components		Mass (g)	% (of total mass)	Mass (g)	% (of total mass)	Mass (g)	% (of total mass)	Mass (g)	% (of total mass)
Encapsulated Rejuvenator		0.00	0.00%	9.03	0.75%	15.41	1.25%	24.39	2.00%
Binder		60.90	5.00%	59.77	4.96%	60.89	4.94%	59.76	4.90%
Aggregate	12/20 Limestone	266.13	21.85%	261.18	21.69%	266.07	21.58%	261.15	21.41%
	4/12 Limestone	323.99	26.60%	317.96	26.40%	323.91	26.27%	317.93	26.07%
	0/4 Limestone	532.26	43.70%	522.37	43.37%	532.14	43.15%	522.31	42.83%
	Limestone Filler	34.71	2.85%	34.07	2.83%	34.70	2.81%	34.06	2.79%
Total		1217.99	100.00%	1204.39	100.00%	1233.13	100.00%	1219.60	100.00%
Specimens Produced		1		1 (with pellet colored capsules)		3 (2 with pellet-colored capsules and 1 with food-coloring colored capsules)		2 (with pellet-colored capsules)	
Encapsulated Rejuvenator Batch		-		B		B and C; D		B and C	
Average Specimen Height (mm)		60.9		60.8		62.5		62.7	

Table 3-4: Composition of the various stone mastic asphalt mixtures used in cylindrical specimens

		SMA 11		SMA 11 + 0.75% Capsules		SMA 11 + 1.25% Capsules		SMA 11 + 2.00% Capsules	
Density		2357		2331		2314		2289	
Theoretical Maximum Density		2448		2421		2403		2377	
Void Content		3.7%		3.7%		3.7%		3.7%	
Mixture Components		Mass (g)	% (of total mass)	Mass (g)	% (of total mass)	Mass (g)	% (of total mass)	Mass (g)	% (of total mass)
Encapsulated Rejuvenator		0.00	0.00%	9.00	0.75%	15.13	1.25%	23.94	2.00%
Binder		64.32	5.30%	63.13	5.26%	63.33	5.23%	62.17	5.19%
Aggregate	12/20 Limestone	0.00	0.00%	0.00	0.00%	0.00	0.00%	0.00	0.00%
	4/12 Limestone	804.50	66.29%	789.60	65.79%	792.13	65.46%	777.54	64.96%
	0/4 Limestone	264.34	21.78%	259.44	21.62%	260.27	21.51%	255.48	21.35%
	Limestone Filler	80.45	6.63%	78.96	6.58%	79.21	6.55%	77.75	6.50%
Total		1213.61	100.00%	1200.13	100.00%	1210.07	100.00%	1196.87	100.00%
Specimens Produced		1		1 (with pellet colored capsules)		3 (2 with pellet-colored capsules and 1 with food-coloring colored capsules)		2 (with pellet-colored capsules)	
Encapsulated Rejuvenator Batch		-		B		B and C; D		B and C	
Average Specimen Height (mm)		62.1		62.9		62.6		63.0	

Specimens were allowed to cool down at room temperature for about 24 hours before being demolded. Some of the specimens were sawed using a circular saw with diamond blades.

For slab production, the same "limestone converted" AC 14 and SMA 11 mixtures, with the composition described in Table 3-5, were used. The mixture volume for each was 4651 cm^3, the volume of each mold (30.5 x 30.5 x 5 cm), with the mixture weight required being obtained with its theoretical maximum density. Mixing was done using at 125 rpm in a large floor-mounted mixer, fit for the large quantities of asphalt required. For compaction, a laboratory roller compactor equipped with a steel roller (EN 12697-33 compliant) made by Cooper Research Technology was used. Compaction was controlled by the specimen's height, as an indirect way of achieving the desired density. Mixing temperatures were kept between the same range as the previous specimens, with the aggregate and binder also being heated to 175°C and 150°C, respectively. The mixing times were 4 minutes for both types of asphalt. The slabs were allowed to cool down in their molds for 24 hours before being demolded. The molds, which were not pre-heated due to thermal expansion limitations, were previously coated with a thin layer of silicone compound. As a final step, the slabs were each cut into three beams, measuring 10 x 30.5 x 5 cm, which would then be used in the wheel tracking test.

Table 3-5: Composition of the asphalt slabs from which beams were cut

Mixture Components		AC 14		SMA 11	
		Mass (g)	% (of total mass)	Mass (g)	% (of total mass)
Binder		532.33	5.00%	562.23	5.30%
Aggregate	12/20 Limestone	2326.26	21.85%	-	
	4/12 Limestone	2831.97	26.60%	7032.18	66.29%
	0/4 Limestone	4652.53	43.70%	2310.57	21.78%
	Limestone Filler	303.43	2.85%	703.22	6.63%
Total		10646.52	100.00%	10608.20	100.00%
Specimens Produced		1		1	

3.6 Characterization of Asphalt Beams

It is very important to know certain parameters of an asphalt specimen, such as void fraction and density. These relate to the quality of production and the specimen's mechanical resistance.

The method used to measure bulk density, saturated surface dry (SSD), followed the procedures described in EN 12697-6:2012. This process requires the measurement of the specimen's mass in three distinct occasions. The first measurement (m_1) is the sample's dry mass. The samples were placed in a drying chamber for 36 hours, after which it was determined that their mass was constant (less than 0.1% variation between weightings), and the measurement could be taken. The second measurement (m_2) is the specimen's mass when submerged in water and saturated. The samples were immersed for 30 minutes prior, to make sure they were saturated with water. The final measurement (m_3) corresponds to the specimen's mass when saturated with a dry surface, which was obtained by removing the samples from the water bath, quickly patting their surface dry and measuring their mass.

This hydrostatic method requires the density of water to be known. The measurements were taken in a temperature-controlled room, set to 20°C. The equation (3.1) used to estimate water density as a function of temperature is provided in the European Standard:

$$\rho_w = 1.00052505 + \left(\frac{7.59 \times t - 5.32 \times t^2}{10^6}\right) \qquad \text{(Eq. 3.1)}$$

where ρ_w is the density of water in megagrams per cubic meter (Mg/m^3) and t is the temperature of the water in degrees Celsius (°C). In this case the density of water was approximately 0,99827585 Mg/m^3 or g/cm^3.

Bulk density then can be calculated using the following equation (3.2):

$$\rho_{bssd} = \frac{m_1}{m_3 - m_2} \times \rho_w \qquad \text{(Eq. 3.2)}$$

The determination of air void content can be made using the following equation (3.3), provided in EN 12697-8:2018:

$$V_a = \frac{\rho_m - \rho_b}{\rho_m} \times 100 \qquad \text{(Eq. 3.3)}$$

where V_a is the air void content of the bituminous specimen by volume (%), ρ_m is the maximum density of the bituminous mixture (Mg/m^3), and $\rho_b$is the bulk density of the specimen (ρ_{bssd} in this case, Mg/m^3).

The maximum density of each mixture was assumed to be the same as their theoretical maximum bulk density (published by Alves Ribeiro, Table 3-2) adjusted for limestone aggregate only, meaning that effects like differing particle shapes between limestone and basalt aggregate were not considered.

It was important to determine the asphalt beams' dimensions in order to calculate their density, verify any discrepancies between specimens, and to ensure they fit neatly into wheel tracking test molds. Their height was measured at four different points (one for each side) around the specimen using a digital caliper. Each side was measured twice with a metallic ruler, resulting in four measurements for each dimension.

3.7 Mechanical Testing

3.7.1 Compression of Cylindrical Specimens

To first establish whether oil release was indeed visible when the specimens were loaded, six Marshall specimens were subjected to uniaxial compression while confined. 200 kN were applied, which resulted in a vertical deformation of (approximately) 2 mm for the asphalt concrete mixtures with 1.25% capsules (both the one using pellet pigment and the one with food coloring), and a deformation of 4 mm for the stone mastic asphalt mixes with 1.25% capsules (also equal for both pigment types). The asphalt concrete mix containing 2% capsules experienced 6 mm of vertical deformation, and its stone mastic asphalt counterpart experienced 4 mm.

3.7.2 Flexural Loading applied with the Wheel Tracking Simulator

In a second phase, beams cut from the slabs produced as described in Section 3.4 were subjected to a wheel tracking test. Testing procedures were based on European Standard EN 12697-22:2020, but adapted for the required goal. The 5 cm high beams were placed in molds (measuring 30.5 x 30.5 x 8 cm). Below the beams, various combinations of support materials were tested, as well as wheel speeds. The tested beams were laterally confined by discarded asphalt slabs cut into similarly sized beams. These tests were not aimed at evaluating the rutting resistance of the asphalt produced. Rather, the test specimens were allowed to bend during the loading cycle, with the goal of causing fatigue damage with a realistic load type and support conditions. The arrangement used is pictured in Figure 3-6.

The equipment used was a small wheel tracking machine, built by Cooper Research Technologies, capable of applying 700 N to the specimen, as specified by the aforementioned European Standard.

Figure 3-6: Wheel tracking simulator configuration

When testing the various combinations of support layers, it was necessary to ensure that the specimen would crack within a reasonable number of cycles while not suffering excessive deformation. Specimen failure should not be too swift either, which would limit the fatigue effects of repeated loading. Before loading the specimens used in this study, the various support conditions were tested with waste beams. The various configurations are presented in Figure 3-7. A brief summary of each arrangement's performance will follow.

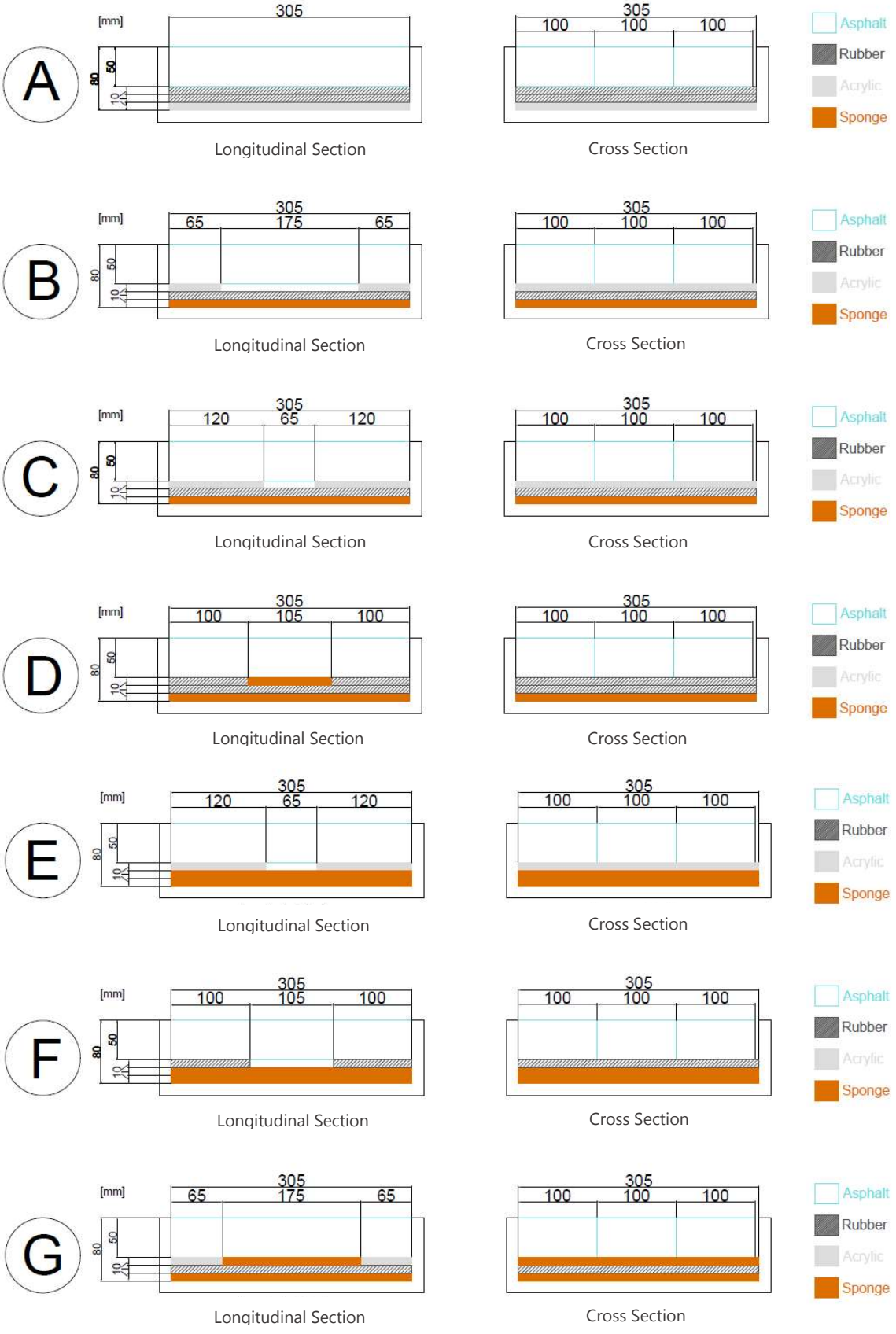

Figure 3-7: Schematic longitudinal sections and cross sections of the various support material combinations tested in the wheel tracking simulator

The simplest configuration (A) yielded no results, with the specimen not showing visible deformation or damage. This first trial clearly indicated that a less rigid substrate was needed. Configuration B was intended to induce a much higher moment at the specimen's half span than the previous. This arrangement resulted in prompt specimen cracking, but had the disadvantage of greatly deforming it. Less harsh configurations were studied with C and D. Both resulted in deformed specimens with only slightly widened cracks. Setup D was not taken to 20000 cycles (only doing about half that amount), yet damage progression appeared to noticeably diminish once the specimen started effectively compressing the sponge below it. Arrangements E and F were less rigid iterations of arrangement C, but both were ineffective since in the first case the specimen was deformed but not cracked, and in the second case it simply fractured too rapidly while accruing a lot of plastic deformation. The final and chosen setup was G. This was an attempt to improve setup B, by supporting the middle section of the specimen in an effort to reduce permanent deformation and increase the number of cycles required until failure. This configuration achieved the intended goals and was used with all three specimen sets.

During these initial trials the beams happened to rock back and forth as the wheel moved across them due to the gap between them and the mold. Samples with a closer fit did not have this issue, meaning the actual test specimens, which had dimensions very close to the mold, would also perform well. Other methods were tested to stop this swinging motion, such as packing the gap with cardboard or wooden wedges, but these proved ineffective. It is likely that gypsum plaster could have been more effective, as recommended by EN 12697-22:2020.

Colored oil was directly injected into the cracks that formed during this test, with the goal of visualizing oil propagation and distribution. In this way, the capsules were effectively circumvented, allowing the oil to retain the totality of its pigment.

Data from the set of cylindrical specimens was used to calculate the volume of oil to be injected, which would theoretically be released by calcium alginate capsules if they were present. It was established that the specimens would have a theoretical concentration of 1.25% capsules by weight. Based on previous works [25], the calcium alginate capsules were assumed to contain 50% vegetable oil (by mass). Capsule volume was known, and a value of 70 mm^3 was used. The number of capsules for a given fracture area for this concentration was also known. The cylindrical specimens had an average of 63 whole capsules and capsule fragments for a fracture area of about 60 cm^2, which means there were 1.05 of these occurrences per cm^2. In the case of the asphalt beams, the fracture surface would measure approximately 50 cm^2,

meaning 51.9 capsule occurrences would be intercepted. Using the previously presented information, a volume of 1.8 ml was assumed to correspond to the quantity of oil which would theoretically be released. This volume assumes that capsules would be capable of releasing the entirety of their contents when loaded, which is far from the truth. It is simply meant as an upper ceiling of a reasonable volume to add.

The quantity of oil used was the same for all specimen sets despite lower levels of damage. This was done because crack dimensions in the last two sets were unknown, and thus a correct estimate of the number of intercepted capsules could not be made. Additionally, the goal of adding this pigmented oil is simply visualization, so having excess oil would be preferable to an oil deficit.

Number of load cycles applied to each set of beams

The first pair of specimens (one AC and one SMA beam) were loaded until cracking could be noticed at their surface, along with some perceptible amount of differential movement between the two halves. To induce cracking at their mid span, an indentation with a depth of 7 mm was cut at half the specimens' length. A mixture of fat-soluble food coloring and vegetable oil (equal parts by weight) was added along their indentations with a syringe.

The second set of specimens was subjected to the same loading and support conditions as the first set, with the exception of the number of load cycles. It was determined that a lower level of damage should be studied, resulting in cracks that would not fully go through the specimen. Initially, the number of loading cycles for each mixture type was halved, which would result in about 5800 cycles for the asphalt concrete mixture and 4200 cycles for the stone mastic asphalt mixture. During actual testing, a very similar level of damage was experienced by both mixture types, with the AC specimen actually displaying a larger crack width than the SMA one at about 4200 cycles. As such, it was decided that loading should be stopped for both mixture types at this point.

There are two factors that may explain this behavior. Since the first set of tests employed a visual criterion, the number of cycles at which loading was stopped was not strictly objective. It is likely that the first AC specimen was overly loaded, since cracking at its surface was not as immediately obvious as the SMA one, that had some spalling along with an obvious crack. When testing was ended, the AC specimen displayed larger crack widths along its sides (which were not visible during the test) than its top would indicate.

The third set of specimens was loaded with the same support conditions, this time aiming to achieve an even lower level of damage by subjecting the samples to 25% of the number of cycles used in the first set. Given what was known from the second set of experiments, only small differences in performance between specimens were expected, and the number of load cycles required could be based on the cycles resisted by the first SMA beam. This would mean that both specimens should be subjected to 2079 cycles. Testing was stopped at 2186 cycles. At this point, the SMA beam had developed a thin crack, spanning about 1.5 cm along its side, which was illustrative of the low level of damage intended for this pair of specimens. The AC beam had no visible damage at this point, and so it was decided that loading should continue until a crack comparable to the one on the SMA beam developed, as simply adding oil to a specimen without damage would not yield meaningful information. Additionally, the target number of cycles was based on a limited number of tests that, when combined with the high variability associated with fatigue testing, may not actually be representative of this mixture's performance. This particular AC specimen proved itself much more durable than the previous AC one, withstanding about 5250 cycles without any visible evidence of damage, before a crack quickly developed and testing was stopped at 5343 cycles.

Handling of specimens after loading

After loading the first set of beams, the cracks on their sides and tops were covered with plastic adhesive tape to limit oil spillage. The specimens were placed upside down and oil was added along their indentations with a syringe. They were allowed to rest in these conditions for 4 days before being sawed lengthwise into 3 pieces (6 when the fractured halves are separated). The cut surface was inspected and photographed immediately after sawing and then once again 24 hours later.

Despite adhesive tape being used with the first set of beams, a significant volume of oil flowed out of the specimen's sides and bottom. To counter this, silicone compound was used to seal the cracks along the side of the second and third sets of beams, before wrapping their central section with plastic film. Colored oil was again added along the beams' indentations with a syringe. These specimens were rested for 5 days.

3.8 Assessment of Capsule Distribution and Rejuvenator Release

Internal structure and capsule distribution assessment was done visually, as this is one of the main goals of this dissertation. Photos of the specimens were taken at all stages of their production, to document both production and external appearance. Some of the cylindrical Marshall specimens were sawed, and their internal structure was photographed. Other Marshall specimens were opened using a chisel, after being uniaxially loaded. As will be discussed in Section 4.3 the sawing process also leads to some abrasion which can tamper with results. Resulting photographs were analyzed using *ImageJ's* color threshold and particle analysis tools. Some of those samples were also examined using a binocular microscope (Nikon SMZ800).

3.8.1 Capsule and Rejuvenator Identification Criteria

When quantifying the distribution of capsules in the specimens it was important to define clear criteria which would minimize the analysis' subjectivity. This is not to say that the results were not a product of the author's interpretation, but to ensure that the analysis is at least consistent.

Evaluation of the loaded specimens was done using *ImageJ* and simple visual examination. In both cases, the specimen's fractured surface was broken down into nine regular-sized sections, which was mostly necessary for the visual inspection, but still relevant for the sake of comparison for the results of the image processing software. Since the grid applied to the specimen's photographs was based on its general size, some particularly irregular samples had sections with less "specimen area" than others, but this was mostly nullified when the corresponding half was examined.

The asphalt beams were also analyzed with *ImageJ*, this time using it to measure the distance oil would cover and crack widths.

3.8.1.1 Visual Criteria

When inspecting the fractured surface of a specimen, it was decided to count the following quantities:

- Whole or mostly whole capsules: capsules that retained the majority of their mass and whose shape, even if somewhat deformed, is clearly recognizable. They can be distinguished from aggregate and mastic staining through their higher opacity ("deeper" red). Undamaged capsules also retained their smooth outer appearance.
- Deformed or crushed capsules and capsule remnants: all these particles are evidence of damage, although it might have occurred at different times. Deformed or crushed capsules are likely to have been damaged during loading, while capsule remnants are more likely to have been created when the specimen was fractured, although these are not mutually exclusive. Although capsules do not require damaging to release their rejuvenator, only deformation, these particles should provide a good indication of areas where loads were high and rejuvenator release was likely. They can be identified through their irregular shape and often irregular texture (where the capsule's inner polymeric structure is exposed).
- Altered aggregate: areas where the aggregate's original white hue has clearly morphed into reddish tones or a darker "oil-stained" white color indicates rejuvenator absorption by the rock.
- Altered mastic: similarly to the previous alterations, shifts in the mastic's color are a strong indication that colored oil was absorbed in that area. These can be identified through their lighter shades of red when compared to the capsules.

With the criteria established, an example of the identification of these occurrences can be found in Figure 3-8. It can clearly be noted that there is some difficulty in classifying certain particles. It can be especially difficult to distinguish between whole capsules and capsule fragments, which is why these results are combined when analyzing the final data. Since mastic and aggregate alteration are both indicative of the same rejuvenator release, these were also counted together in the combined results.

As an example, when identifying whole or mostly whole capsules, particles with a spherical shape are looked for. If the particle in question then appears to conserve most of its mass, it is counted as such. In the example these are marked by a blue circle. Similar particles that clearly display a higher level of damage are counted as deformed or crushed capsules, which can be seen in the lower part of the image. Other isolated capsule fragments are also included in this category and marked by a white circle, like the examples at the top of the image.

Aggregate and mastic staining are easier to distinguish since they tend to have a lighter color, and were then circled in green or black according to where they occurred.

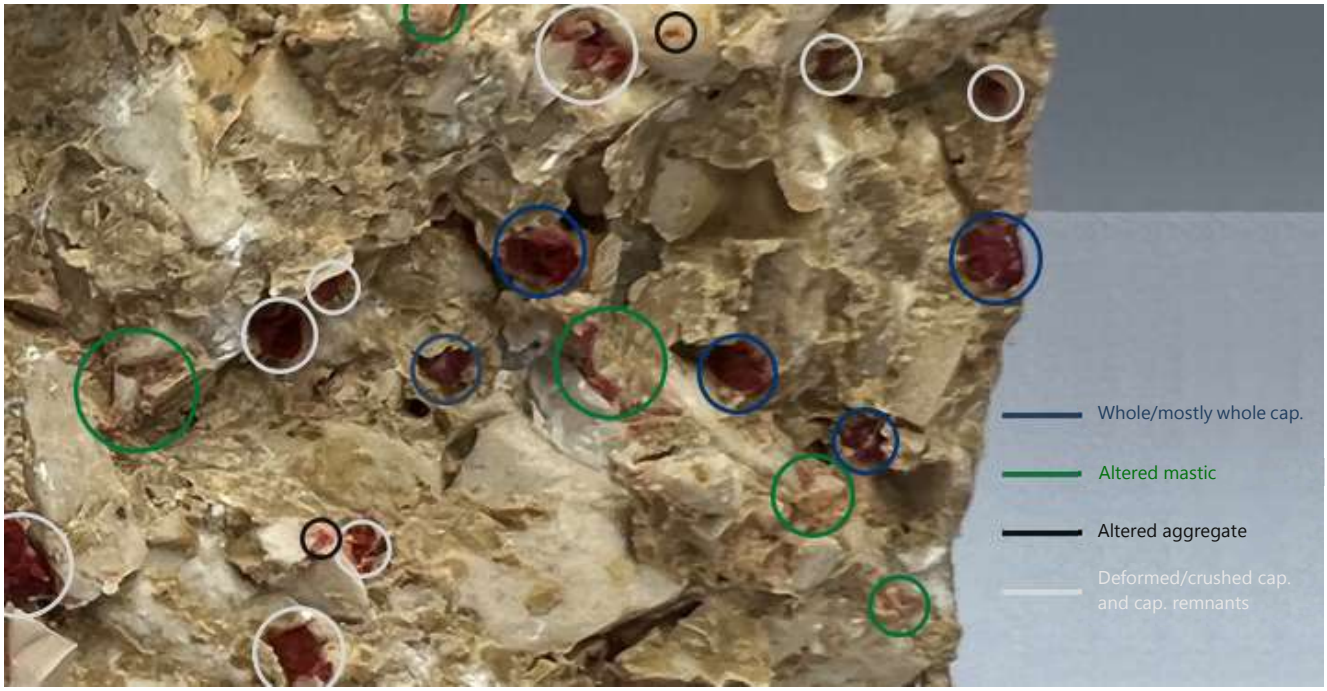

Figure 3-8: Example of the visual criteria used to identify the capsule-related occurrences

3.8.1.2 ImageJ's Color Threshold Criteria

ImageJ is a free to use open-source image processing software. One of its features allows the user to select certain parts of an image according to their hue. This feature is called "thresh-old" and is typically used with grayscale images. For this analysis, a variation of this technique using color was found to work better, and so it was the chosen method.

This analysis was done twice, once for the capsules themselves and another time for any staining present in the mastic or aggregate. This was done by changing the color selected by the software. In the first case, deeper shades of red would have been looked for, and in the second, tones closer to orange were chosen. Highlighting was done using the hue saturation and brightness (HSB) color space. It is not possible to fully define which hue is appropriate for every specimen photograph, since small differences in lighting will change each photograph's colors slightly. The general criteria used when highlighting capsules and capsule remnants was to fully highlight only the capsule material itself, with the hue interval that most faithfully

selected the largest number of capsules being used. For mastic, a hue range was picked so that the capsules themselves would not be highlighted nor would the broad mastic around them, with only a ring of altered mastic around each capsule being selected, along with any other reddish stains. This approach also generally worked for stained aggregate. In general, for specimens using capsules made with food coloring, hues between 0 and 7 worked best for capsule material selection, while a range of 8 to 17 picked up most of the red staining. For specimens using capsules with red pellet pigment, hues between 0 and 18 identified capsule material, and 19 to 21 found mastic and aggregate discoloration. The remaining parameters, saturation and brightness, were set to their full range.

This analysis was much more reliable for the more contrasting food coloring capsules, since they were clearly distinguishable from the remaining structure and the stains in these specimens also shared this deep red tone. For the paler, pellet-colored capsules, the results for capsule area are still somewhat relevant (although not as reliable as the previous case), but the program had difficulty in identifying the subdued red stains in these specimens.

By combining this thresholding with *ImageJ*'s particle analysis tool, it is possible to measure the highlighted areas. The setting "include holes" was turned on for capsule area measurement and turned off for mastic and aggregate staining measurement, as it would greatly overestimate the results in this last case. The resulting areas were measured in pixel squared, and relative measurements were obtained by relating these results with the pixel area of the specimen or specimen section in the photograph used.

3.9 Comparison of Synthetic Binder and Bitumen Solubility in Oil

As the various experiments were conducted, it became clear that many of the expected oil propagation and penetration results were not obtained despite variations in methodology. Some investigation was necessary to determine whether this was due to the rejuvenator/encapsulated rejuvenator themselves, or if there might be a problem with the experimental setups. One of the main assumptions made when devising the various experiments was that the synthetic binder would have similar properties to bitumen. Physically, this is the case, and verifiable through the technical data sheet provided by the manufacturer, yet chemically there are no such guarantees. As such, this material's interaction with sunflower seed oil may not resemble the behavior of bitumen.

To test this, an experiment inspired by the procedure for the determination of affinity between aggregate and bitumen (EN 12697-11:2020) was developed. The following steps were performed:

- Two mixtures were produced, one using 35/50 bitumen and the other Recofal S-100P synthetic binder
- After mixing, the mixtures were allowed to cool on trays which were lightly coated with silicone compound.
- The mixtures were placed over perforated plastic film that was then lightly wrapped around the aggregates
- The bundles were weighed and put into beakers, which were then filled with approximately 170 g of sunflower seed oil each.
- The aggregate bundles were weighed and photographed at one-hour intervals for six hours, and at 24, 25, and 48 hours. Each time, the oil was allowed to drain for two minutes before weighing the bundle.

For the mixtures, 150 g of aggregate between 8 mm and 11.2 mm were mixed with 16 g of binder in both cases. The binders were heated to their respective mixing temperatures, and the aggregate was heated to 175 °C. In a mixing bowl over a heating mantle, the aggregates were mixed by hand with the binder, ensuring they were thoroughly covered.

4

Results and Discussion

4.1 Binder Pigmentation

Photographs of the various tracing paper sheets with binder smears are presented in Figures 4-1 through 4-3. Various concentrations of each oil type in the binder were tested (measured by weight), which are indicated next to each smear.

Most pigmented oils produced little change to the color of the binder. Green pellet oil was by far the worst performer, closely followed by the blue and red pellet ones. While the former produced no visible changes, the latter ones slightly change the binder's hue, but only at high oil concentrations. The red pellet-based oil was deemed the best performer out of the three, as the resulting reddish tone had more contrast with the mastic in specimens (that has a yellow tone duller than the binder's original one).

Figure 4-1: Binder pigmentation tests for sunflower oil with (left to right) 1% Colorfalt green pellets, 1% Colorfalt blue pellets, 0.66% Ravasol Color+R red pellets

Coloring performance was lacking, and so the blue and black powders were experimented with. These produced better, but still lackluster results. The black oil naturally darkened the binder, but the resulting tones were thought to have poor contrast with the mastic and aggregates. Darkening the binder also hampers distinction between it and dim pores. The powder-based blue oil resulted in colors similar to the previous example (although with a greener hue), with the same problems.

Figure 4-2: Binder pigmentation tests for sunflower oil with 1% carbon black pigment (left) and 1% primary blue pigment (right)

Finally, red fat-soluble coloring (sunflower oil based) was tried. This was by far the best performing oil, with minimal concentrations producing very noticeable hue changes.

Figure 4-3: Binder pigmentation test for sunflower oil with 50% red fat-soluble food coloring

4.2 Calcium Alginate Capsules with Pigmented Oil

4.2.1 Capsule Size

The vast majority of capsules had ellipsoid shapes, causing them to have three distinct dimensions. The two largest, in the horizontal plane, will be called D and d, for the largest and smallest of the two respectively. The final measurement is the capsule's height and will be called h. Capsule dimensions for the various batches are presented in Table 4-1.

Table 4-1: Average capsule dimensions and volume for each batch produced (with P or C designating pellets/ food coloring, W meaning the O/W ratio, and A meaning the O/Alg ratio)

Capsule Batch	Average Largest Dimension (D) (mm)	Average Intermediate Dimension (d) (mm)	Average Smallest Dimension (h) (mm)	Average Dimension (mm)	Average Volume (mm^3)
A (P; W 0.1; A 3)	2.72	2.27	2.08	2.36	53.87
B (P; W 0.2; A 6)	3.24	2.55	2.36	2.71	81.51
C (P; W 0.2; A 6)	3.41	2.75	2.72	2.96	106.71
D (C; W 0.1; A 3)	2.73	2.38	2.05	2.39	55.71

Capsule composition was changed after for batches B and C. The oil to water ratio was increased from 0.1 to 0.2 which would have the effect of increasing the diameter. The composition used is very similar to the one used in [25], and this change would theoretically result in an equivalent diameter increase of 1.7 mm, but this was not the case. Differences in laboratory equipment between the batch in question and the one before it may be responsible, as a larger dropping funnel was used (due to an increased volume being produced at this time) and with the diameter of its needle being larger, droplet formation may have been affected.

4.2.2 Compressive Strength

The results from the compressive strength testing of capsules are presented in Table 4-2. The capsules from each batch exposed to the heating and slow cooling cycle were given the name "heated". The force-displacement curves for each capsule type can be found in Annex B1.

For the interpretation of these results, it is important to mention that batches A and D share the same ingredient ratios but differ in oil pigment type, and that batches B and C are equal in composition between them but differ in component ratios form the other two lots.

Table 4-2: Average yield load and yield deformation for each capsule batch before and after heating

Capsule Type		Average Yield Load (N)	Average Yield Displacement (mm)	Elastic Deformation Slope (N/mm)	Strength Change After Heating	Stiffness Change After Heating
Batch A	Regular	28.11	0.51	55.23	-1%	+24%
	Heated	27.83	0.41	68.58		
Batch B	Regular	17.30	0.49	35.31	+51%	-4%
	Heated	26.16	0.77	34.06		
Batch C	Regular	22.82	0.74	30.99	+19%	+21%
	Heated	27.07	0.72	37.62		
Batch D	Regular	29.17	0.58	50.16	-8%	+49%
	Heated	26.90	0.36	74.78		

The behavior of the regular capsules from batches A and D, which share the same ingredient proportions is mostly similar, both in terms of compressive strength (4% difference) and stiffness (10% difference). These differences are likely within the uncertainty associated with mechanical testing (capsules slightly shifting when loaded or differing in shape) and each capsule's production process (slightly different ratios between components or time spent in the calcium chloride solution). This suggests that the presence of polymers in the red pellet oil, used in batch A, does not influence mechanical behavior, or at least does so in the same way as the pigment in red food coloring.

It is important to note that the compressive strength shown by these capsules is similar to ones produced by other authors. In [43] calcium alginate capsules were produced using the same ratios and components, bar the pigments added to the oil, and showed a compressive strength of 33 N at an average deformation of 0.50 mm.

Batches B and C show a significant difference in compressive strength between them (32%). This is unexpected since the same ratios and composition and is indicative of discrepancies in the production process. Intriguingly, the difference in stiffness between them is not as pronounced (14%).

Despite the uncertainty associated with the mechanical performance of batches B and C, the difference between them and batches A and D is clear. The former were produced with twice the proportion of oil and half the proportion of sodium alginate of the latter. Both changes should result in weaker capsules, which is shown by the results.

Testing the capsules after they were heated produced varying results. Capsules from batch A retained the same strength but became stiffer. Capsules from batch B and C again differed greatly in their behavior, with the former becoming significantly stronger and maintaining their stiffness, while the latter became moderately stronger and stiffer. Capsules from batch D mostly maintained their compressive strength but had a large increase in stiffness.

After heating, most capsule types had sharper decreases in force after yielding in their force-displacement curves than previously.

The differences between batches A and D could suggest that the type of pigment used may influence mechanical behavior. The discrepancies between batches B and C indicate that capsule morphology and size (which is the main identifiable difference between the two) plays a very important role in mechanical behavior. Capsules from batches A and D are closer in terms of their dimensions, but differences in morphology may also interfere with the results.

4.2.3 Oil Release and Visual Appearance

Broken capsules from each batch are pictured in Figure 4-4. It is visible that some pigmented oil is released when the capsule is crushed. Large drops of clear oil also formed around the capsules. The oil seems to easily be absorbed by the paper, leaving the pigment behind, and creating larger clear stains around the original one. Capsules from batch D seem to release less pigmented oil, but overall capsule pigmentation ability is likely not affected due to this oil's great coloring capacity.

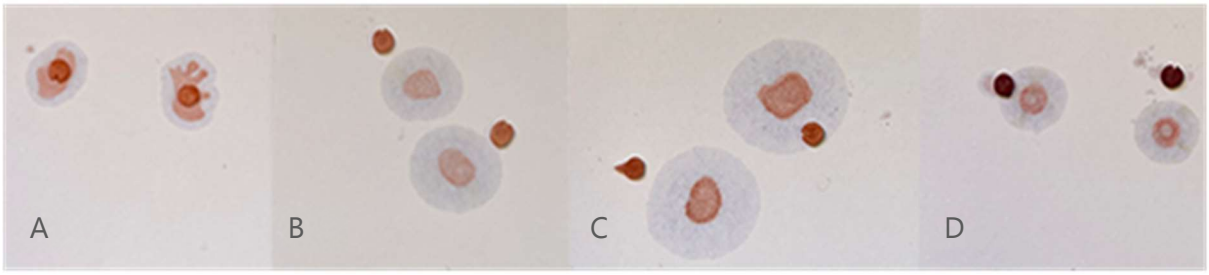

Figure 4-4: Calcium alginate capsules compressed on a paper sheet, showing oil release. Capsules from batches (left to right) A, B, C, and D

Two concurring mechanisms might explain a significant volume of the oil that flows out of the capsules is mostly colorless. Firstly, pigment is being used, and not a dye, which means that small particles in suspension are responsible for its color, and not a dissolved substance.

In the case of the pellet-colored oil, the pigment particles fell out of suspension a few days after mixing. This might also happen inside the capsule's pores, with the pigment and oil separating after some time. Additionally, a filtration effect might be present if the average pore size of the calcium alginate structure is smaller than the pigment particles, causing them to stay in the capsule while the oil is pushed out.

The release of oil onto the paper after capsule compression was measured. Total oil stain area and pigmented area were measured with *ImageJ*. The results are presented in Table 4-3. The ratio of pigmented area to total stained area was mostly similar for all capsule types. Capsules from batches A and D, which were on average smaller than the ones from B and C, tended to have a slightly higher ratio of pigmented area to total oil area. This is likely because, as pointed out before, most of the pigment is released in the vicinity of the capsule during its crushing, which means smaller capsules will have a smaller pigment "footprint". The clear oil stain results from capillary action, drawing oil from the capsule and into the paper, while filtering out the pigment. Larger capsules, with their larger total volume of oil, produced larger clear stains, that lowered the ratio of pigmented to total stain area. The results show that capsules from batch D do appear to release the least pigment and oil.

Although not ideal, since a fair amount of pigment was still released by the capsules, they were used in asphalt mixtures.

Table 4-3: Average oil stain and pigmented areas for each capsule type

Capsule Batch	Average Pigmented Area (mm^2)	Average Total Oil Area (mm^2)	Pigmented Area to Total Area	Average Capsule Diameter (mm)
A	30.97	226.37	13.7%	2.36
B	27.40	262.85	10.4%	2.71
C	32.06	340.93	9.4%	2.96
D	20.65	174.00	11.9%	2.39

Capsules before and after heating are pictured in Figure 4-5. Although the difference is faint, the heated capsules show a whiter color than the unheated ones. This can be indicative of a change within their structure or composition. This slight hue change is more visible in the capsules pigmented with red pellets, but it also seemed to affect the ones made with food coloring, where it is less visible due to their dark tone.

Figure 4-5: Calcium alginate capsules after being heated (top) compared to unheated ones (bottom)

4.3 Cylindrical Asphalt Specimens

4.3.1 Comparison Between Asphalt made with Synthetic Binder and Bitumen

Figures 4-6 and 4-7 show the internal structure of the limestone-converted mixtures made with 35/50 bitumen and synthetic Recofal S100-P binder side by side. The mixtures made with the synthetic binder may initially appear to have fewer small aggregates between the larger ones or more mastic, but this is a matter of contrast. Upon closer inspection, the mastic in the synthetic binder samples reveals many small aggregates whose shape and color appears to be masked by the surrounding binder.

Figure 4-6: Comparison between the internal structure of limestone converted asphalt concrete mixture made with 35/50 bitumen (left) and synthetic binder (right)

Figure 4-7: Comparison between the internal structure of limestone converted stone mastic asphalt mixture made with 35/50 bitumen (left) and synthetic binder (right)

4.3.2 Capsule Distribution and Behavior

During the production of the Marshall specimens it became clear that some capsules tended toward the outer parts of the specimen, which was confirmed when they were sawed. This might have occurred due to the wall effect, which drew the finer particles, like the capsules, toward the mold. On the top of the specimens additional capsules can be found because some tended to stick to the bottom of the mixer's bowl and whisk, and found themselves on top of the mixture when these were shaken into the mold to pour any remnants of bituminous mixture.

Internally, most cylindrical specimens appeared to have an even distribution of capsules. The capsules containing oil colored with red pellets were generally hard to distinguish, and while certainly visible, photographs of samples containing them had to be taken with a lot of light and fine tuning of camera settings. This was not ideal, and of the reasons another oil coloring technique was used. Samples of the internal structure for each type of mix can be found in Figures 4-8 and 4-9. It is important to note that the photographs of specimens

containing 1.25% and 2% capsules were taken right after sawing, while the others were taken days after. The cut surfaces were still wet, and oil released from the sawed capsules did not have time to spread. This results in capsules that are slightly more visible.

From inspection of these photographs, it is visible that the oil contained within the calcium alginate beads did not retain its pigmentation very well. The samples with 0.75% capsules show oil stains on some of the aggregates surrounding the capsules, with no red hue to them.

Figure 4-8: Internal structure of the cylindrical asphalt concrete specimens containing (left to right) no capsules, 0.75% capsules, 1.25% capsules, and 2% capsules

Figure 4-9: Internal structure of the cylindrical stone mastic asphalt specimens containing (left to right) no capsules, 0.75% capsules, 1.25% capsules, and 2% capsules

The fact that these stains are not visible just after sawing shows that the oil leaked from cut capsules and was not forced out during the compaction process (at least not in significant amounts). A clear example of these stains can be found in Figure 4-10, which shows photographs taken with a binocular microscope days after the specimen with 1.25% capsules was sawed, and now displays them.

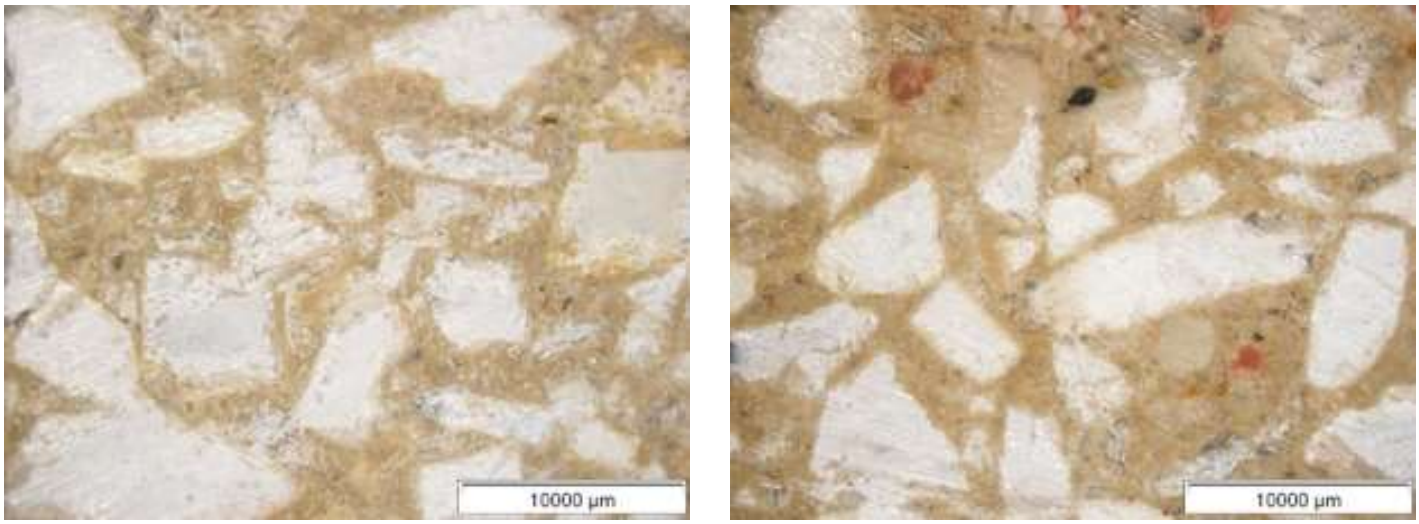

Figure 4-10: Clear oil staining in a stone mastic asphalt with 1.25% capsules (right) compared to a specimen with no capsules (left)

In other photographs taken with the binocular microscope some small air gaps can be seen around the calcium alginate capsules. This might be caused by the capsule's lower stiffness causing it to expand and contract during compaction, leaving a small gap when the load is removed. It might also be a sign of poor adhesion between the binder and capsule, which is unlikely since specimens opened with a chisel showed good adhesion, or evidence of damage caused by the sawing process.

After the initial compressive tests, oil could be seen leaking from capsules on the outside of the specimens. In all the specimens this oil appeared clear in color.

After opening the loaded specimens with a chisel, the appearance of their internal structure appeared very similar to the previously displayed sawed specimens. Upon closer inspection, some red staining of the mastic and aggregate is present, along with several instances of damaged or crushed capsules, which does suggest that some rejuvenator was released and retained its color, meaning the two mechanisms previously described did not completely block the pigment.

Despite some staining being present, colored oil release by the capsules was still deemed insufficient. The small amounts of staining present were not strictly correlated with damaged capsules. As an example, areas where many crushed or fragmented capsules could be found sometimes presented little staining. While some insights can be gained by studying the specimens made with these capsules, the pigmentation methods used here should not be regarded as particularly consistent. The problem of limited pigment release is also very likely to be compounded by the limited solubility of the synthetic binder in oil, which is explored in Section 4.5.

4.3.3 Quantification of Capsule Distribution and Rejuvenator Release in Loaded Specimens

As explained in Section 3.6.1., the various manifestations of capsules and rejuvenator release on the fractured loaded specimens were counted and measured. The results will be presented in Figures 4-11 through 4-16. Some of the findings from this data will be presented in the following paragraphs. The data for each specimen half was added, presenting a "combined" number of instances, representative of all the occurrences the fracture would intersect. For the highlighted area an average of the two sides was calculated. The data from which the figures were created is presented in Annex B2.

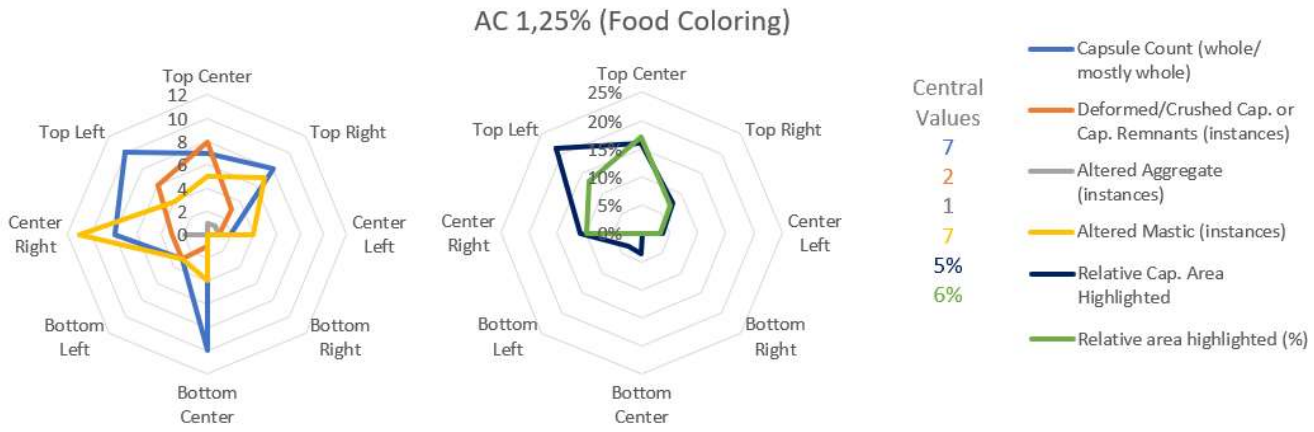

Figure 4-11: Capsule and staining distribution by zone in a loaded asphalt concrete specimen with 1.25% capsules pigmented with red food coloring

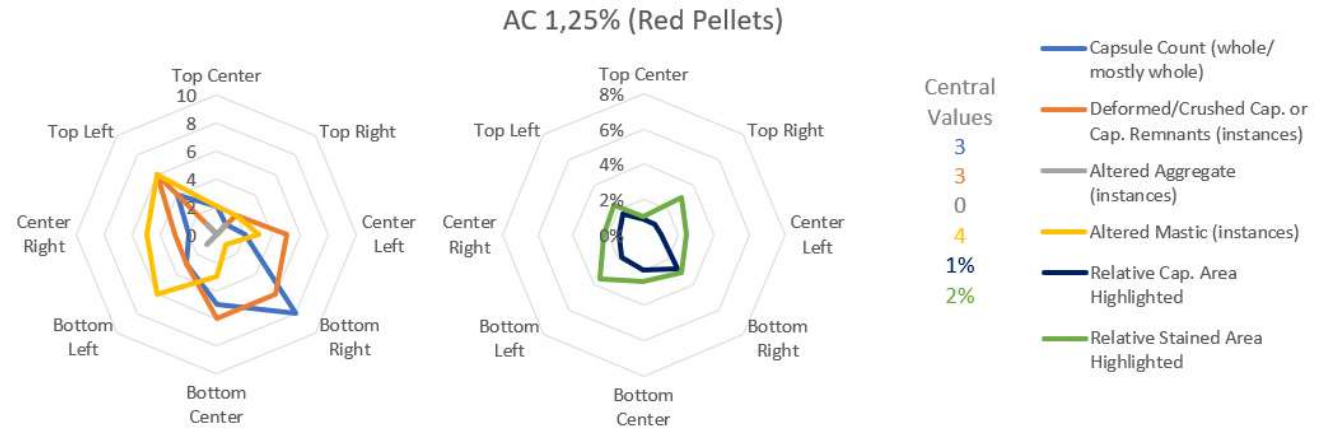

Figure 4-12: Capsule and staining distribution by zone in a loaded asphalt concrete specimen with 1.25% capsules pigmented with red pellets

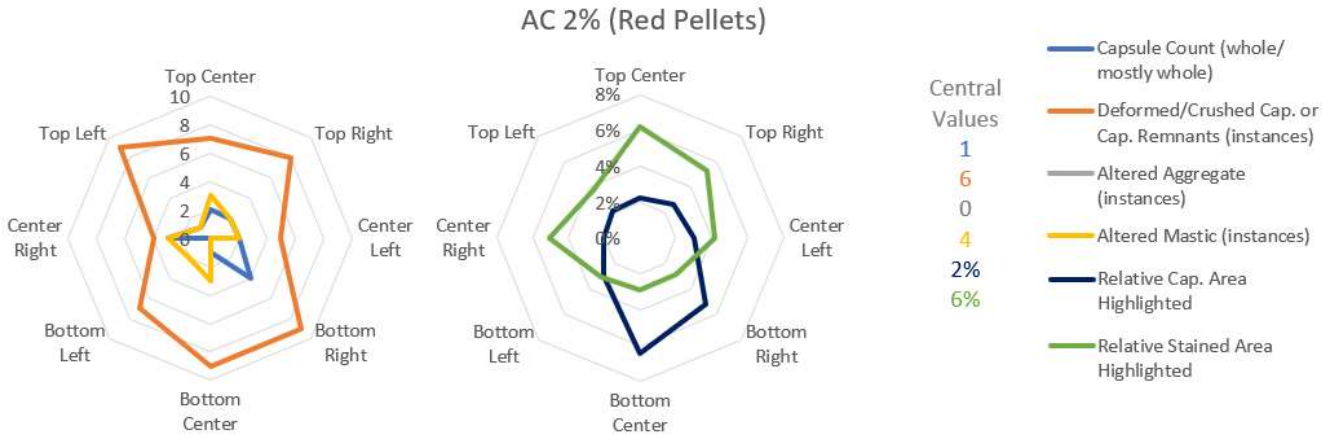

Figure 4-13: Capsule and staining distribution by zone in a loaded asphalt concrete specimen with 2% capsules pigmented with red pellets

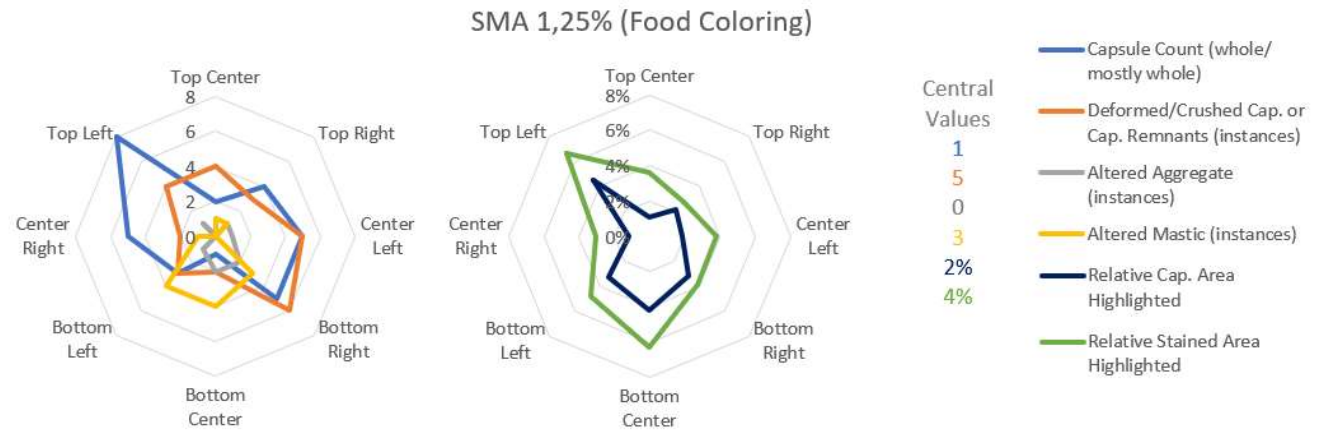

Figure 4-14: Capsule and staining distribution by zone in a loaded stone mastic asphalt specimen with 1.25% capsules pigmented with red food coloring

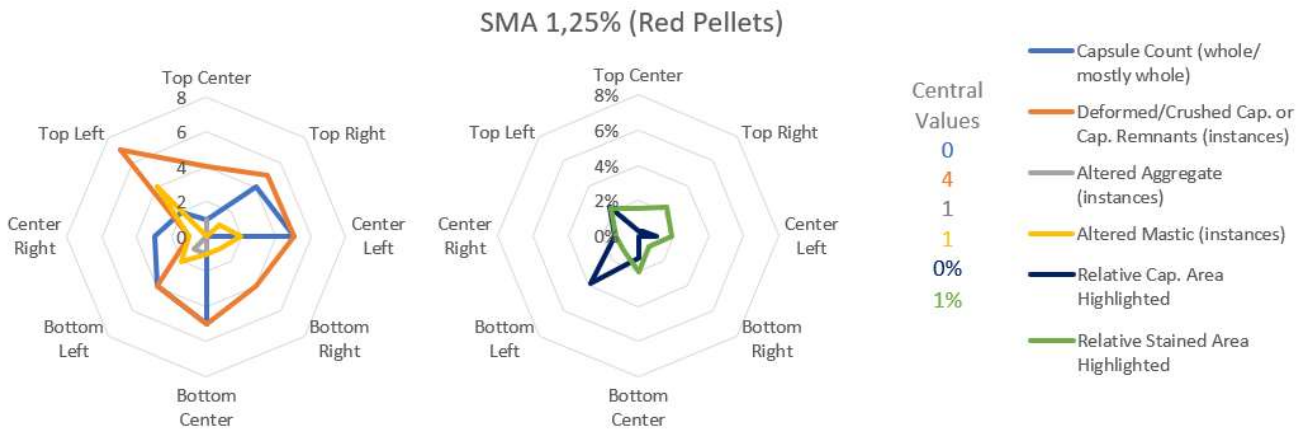

Figure 4-15: Capsule and staining distribution by zone in a loaded stone mastic asphalt specimen with 1.25% capsules pigmented with red pellets

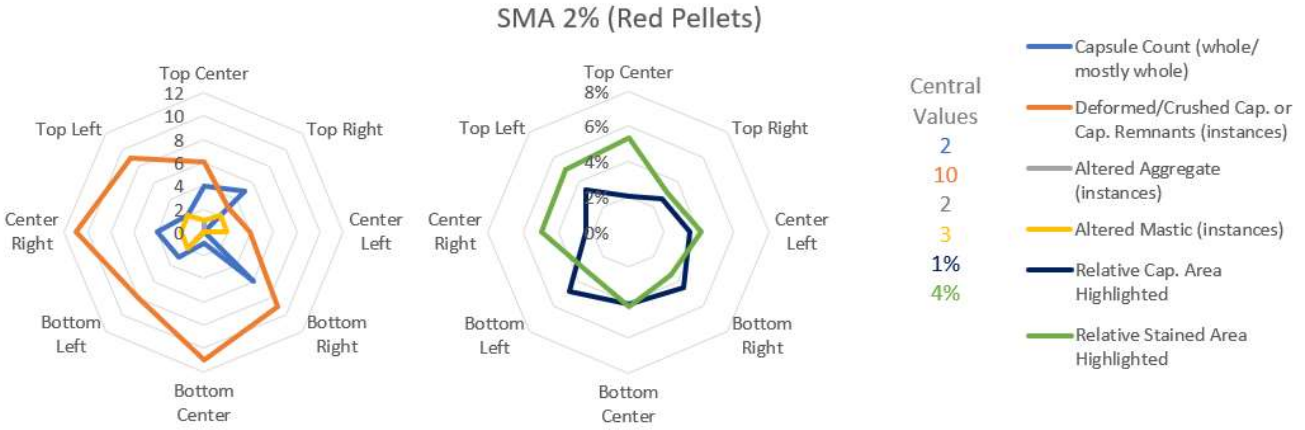

Figure 4-16: Capsule and staining distribution by zone in a loaded stone mastic asphalt specimen with 2% capsules pigmented with red pellets

Influence of capsule types

A clear correlation between the capsule concentration in the specimen and the number of capsules (whole or damaged) and capsule fragments present on its fractured surface was found, as would be expected. There was one outlier, the AC 14 mixture containing 1.25% capsules with food coloring, which displayed a higher number of capsule (whole or otherwise) occurrences than any other asphalt concrete specimen. There should not be any particular mechanism inherent to the encapsulated rejuvenators which would cause capsule distribution to be this uneven, especially when taking into consideration that the remaining specimens followed the expected distribution. It is possible that, given the small scale of the specimens

(with the fractured surface being a rectangle of approximately 10 x 6 cm) and the relatively large maximum aggregate size in the AC mixture (2 cm), some large aggregates elsewhere in the specimen displaced a significant number of capsules, with the fracture plane intersecting one of these higher concentration areas.

While the previously described AC mixture is an outlier, the 1.25% SMA mixture using capsules with food coloring does also show a higher number of capsules/capsule fragments and especially mastic and aggregate alterations than its equivalent made with pellet-colored capsules. A certain degree of bias may be present, since it is easier for both the human eye and an image processing software to identify the more contrasting red tones of the food coloring, with more capsules and staining going unidentified in the pellet-colored capsule specimen. It is also true that the food coloring demonstrated a substantially superior coloring power when compared to the red pellets, meaning that any release of it, even if in limited quantities, is more likely to produce visible staining than the pellet-colored oil, leading to the disparity in instances of dyed aggregate and mastic.

Another difference between the specimens using different capsule types is that fact that the ratio of crushed capsules and capsule fragments to whole/mostly whole capsules is significantly lower in the case of capsules made with food coloring. This should be expected, as the food coloring capsules have a lower oil to alginate ratio and should therefore be stronger. Another factor may also be at play, as the red pellets used to produce the first colored oil contain some polymer, and it is possible that they became more brittle after exposure to mixing temperatures due to it, whereas the food coloring capsules, containing only calcium alginate and vegetable oil, remained flexible and not as prone to crushing.

The data for the relative area highlighted has a reasonable correlation with the number of capsules, capsule remnants, and staining instances for the food coloring based capsules, while a much weaker correlation is found in the specimens using red pellet-colored capsules, along with much lower relative area values.

Influence of capsule concentration

For this analysis, the comparable specimens are the mixtures using 2% and 1.25% red pellet-colored capsules by mass. The quantity of capsules and capsule fragments is similar in the 1.25% AC and SMA mixtures. This number naturally increases for the specimens with a 2% concentration, with the SMA 2% displaying the expected 60% increase (1.25% to 2%) in number of capsules, while the 2% AC mixture displayed only a 25% increase in capsule concentration.

This may be explained by the previously noted capsule concentration non homogeneity in the AC specimens.

Both the SMA and AC 2% mixtures had a significantly higher proportion of broken capsules relative to the number of whole ones than the 1.25% mixtures. This may be caused by the additional capsule content creating a more deformable internal structure, whose larger aggregate shifts tend to crush more capsules. Interestingly, the number of aggregate or mastic staining instances either remained the same or decreased in these mixtures. It is important to note that, due to the very limited pigment release with these capsules, these results must be interpreted critically. It may be the case that, as would be expected, the mixtures with higher capsule concentrations had proportionally higher rejuvenator release, with it simply not being visible due to the oil coloring technique used. On the contrary, if oil pigmentation was thought to be reliable, this would suggest that less rejuvenator was released in these specimens. Since all the samples were subjected to the same 200 kN uniaxial compressive force (yielding the same or higher strains in the 2% mixtures when compared to the 1.25% ones), and a larger number of capsules were broken in the higher concentration specimens, there is no reason to suppose that the capsules were not adequately loaded in these mixtures, making the first scenario more likely.

Influence of mixture type

The number of whole capsules and damaged/fragmented capsules more closely matches the expected distribution in the SMA mixtures, with the 1.25% specimens having an identical number of capsules, and the 2% mixture displaying the expected increase. As previously explained, the AC mixtures are more irregular in this regard. Only the AC 1.25% red pellet capsule mixture matches its SMA equivalent in this regard, with the remaining 1.25% AC specimen displaying a much higher number of occurrences than expected, and the 2% AC specimen a lower-than-expected number. A possible explanation for this phenomenon has been put forward previously.

Regarding the number of staining instances, a clear trend can be seen. There is no SMA specimen that has a higher number of these occurrences than its AC counterpart. This difference becomes especially evident when the ratio of staining instances to capsule/capsule fragment instances is studied, with the 1.25% food coloring capsule mixtures having a ratio of staining to capsule instances of 59% in the AC specimen, and 36% in the SMA specimen. Since the capsules employing food coloring appeared to color the aggregate and mastic more

reliably, the results for these specimens should be given greater consideration, but the trend here identified holds true for all.

These findings seem to counteract the hypothesis presented in Section 2.3.2.2 that a discontinuously graded mixture like SMA would better be able to load the calcium alginate capsules and induce rejuvenator release. It is possible that, instead of lodging themselves between large, similarly sized aggregates and then being pinched when load is applied, the capsules found themselves in the mastic-filled voids between large aggregates with the smaller 0-to-4-millimeter aggregate also present bearing the load after the capsule's initial deformation. This mechanism can explain why the number of deformed/crushed capsules is similar between mixture types but staining clearly differs.

4.3.4 Binocular Microscope Observation of Capsules in Loaded Specimens

By closely looking at the structure of the specimens studied in the previous Section some insights can be gained about their behavior and the hypotheses previously put forward. Photographs representative of each specimen were used.

Figure 4-17 shows photographs of the internal structures of AC and SMA specimens, using differing capsule types but the same concentration. Capsule distribution appears the same for both capsule types, with some clumping and capsule fragments present in both. Some capsule disaggregation can be identified in the capsules colored with red pellets, such as the ones in the center of the red pellet capsule AC and SMA specimen photographs, with capsules that clearly underwent loading. Their equivalents in the mixtures using food coloring capsules do appear to better conserve their structure despite deformation, suggesting either higher compressive strength or elasticity.

Differences in staining are also immediately obvious between capsule types. While more limited in the stone mastic asphalt mixture, red staining is clearly noticeable in the mixtures using capsules with food coloring. Oil release is likely to also have occurred in the mixtures using red pellet-colored capsules, given that a similar level of damage is present in all the photographs. Additionally, some of these capsules show a certain softness in the color of the

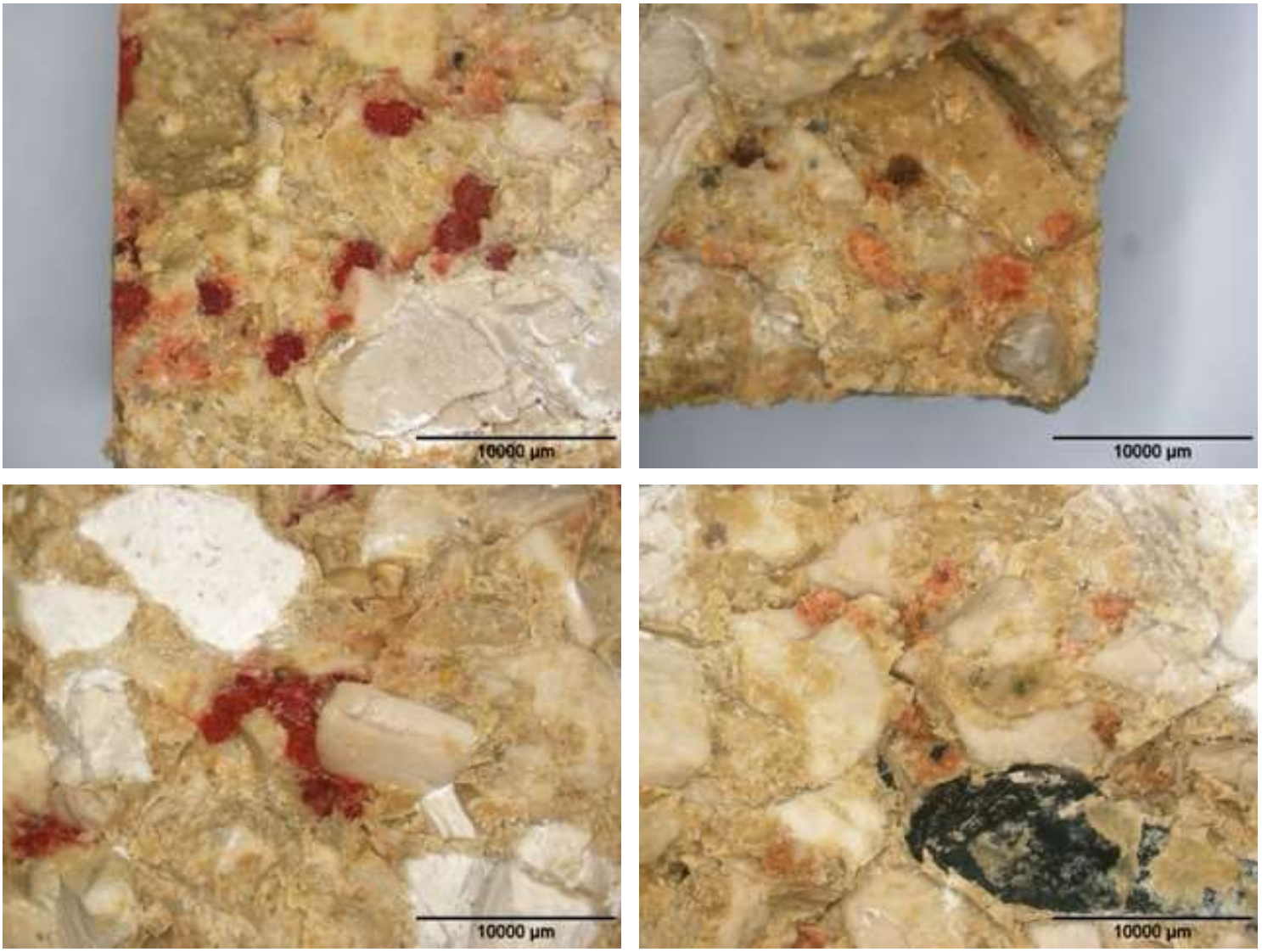

Figure 4-17: Magnified photographs of the internal structure of the following loaded specimens: AC 1.25% food coloring capsules (top left), AC 1.25% red pellet capsules (top right), SMA 1.25% food coloring capsules (bottom left), and SMA 1.25% red pellet capsules (bottom right)

mastic around them, which is likely caused by oil release. A clear example of this is found in Figure 4-18, which shows the type of staining often found around capsules with food coloring. It is important to note that these are individual examples representative of the most common occurrences in the specimens, but in all samples there were instances where no oil release can be found with food coloring and oil capsules or large amounts of discoloration are present with red pellet-colored capsules.

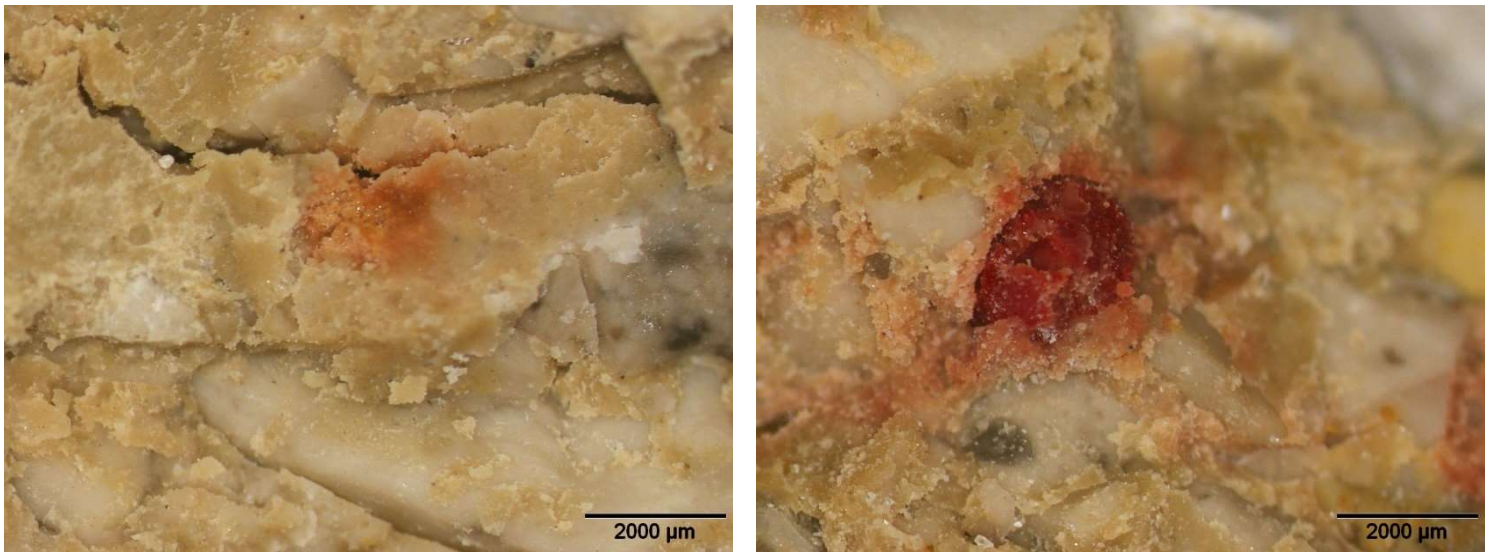

Figure 4-18: Staining around a red pellet-colored capsule (left) and around a food coloring colored capsule (right)

Differences in oil release between mixture types are presented in Figure 4-19. As mentioned in the previous Section, more staining is present in the AC mixture than the SMA. In these photographs, the arrangement of the capsules within the aggregate structure does appear to differ between mixture types. In the AC mixture, capsules appear to have a random distribution, often be surrounded by aggregate of a various sizes. In the SMA mixture, it is noticeable that the capsules often fit into pockets of smaller aggregate and mastic between larger aggregates.

In Figure 4-19, the capsules identified by a blue circle show cases where the capsule was likely "protected" by nearby aggregates of similar size. This shielding effect is not easily identifiable in the AC mixture.

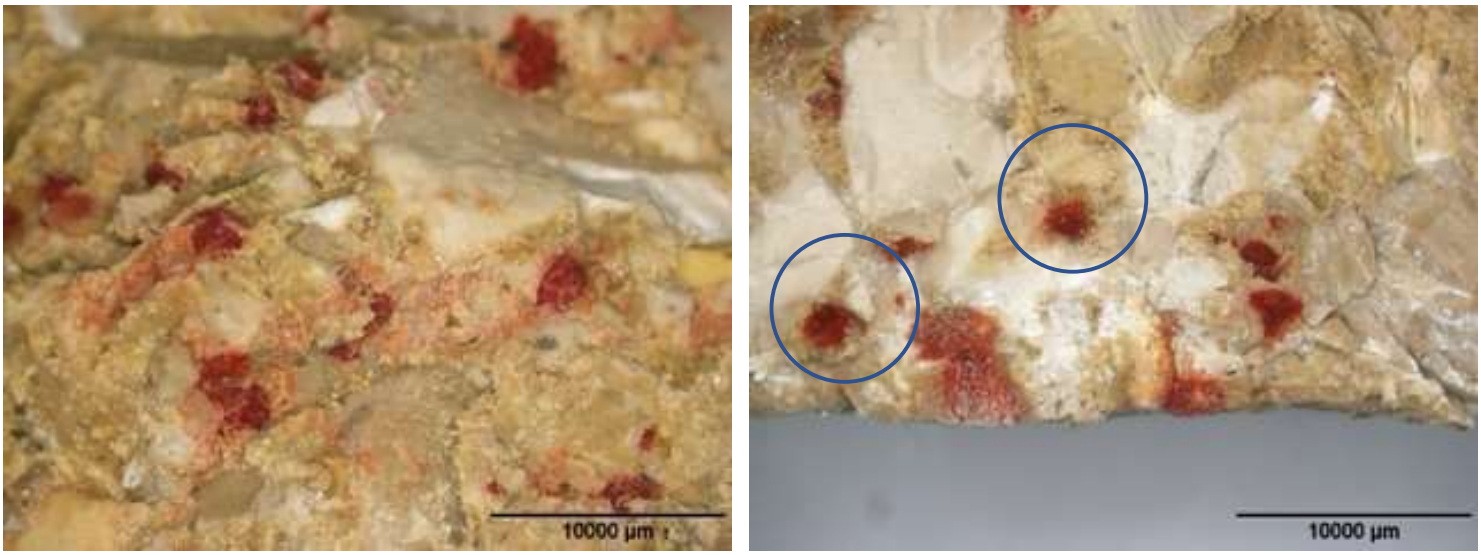

Figure 4-19: Comparison of capsule integration within the mixture between an asphalt concrete specimen (left) and a stone mastic asphalt specimen (right)

The mixtures using 2% capsules are pictured in Figures 4-20 and 4-21. Both display large quantities of damaged capsules, matching the findings in the previous quantitative analysis. Staining is limited in both cases, apart from a few aggregates in the SMA 2% mixture, which were completely dyed red. One of these aggregates is visible in the center of Figure 4-21. The aggregate in question does have some capsules in its vicinity, likely responsible for the oil release, yet the mastic around it retains its original color. From the available data, no clear explanation can be formulated for the reason only a few aggregates in this specific mixture displayed such behavior.

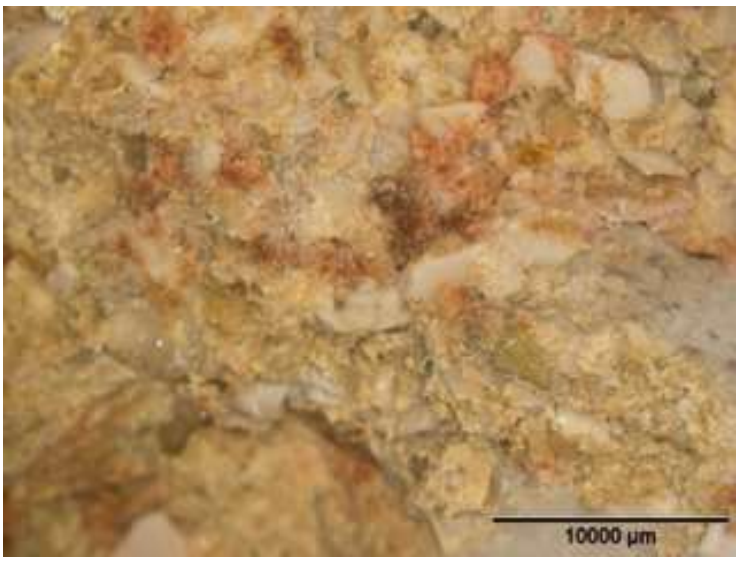

Figure 4-20: Internal structure of an AC specimen containing 2% red pellet-colored capsules

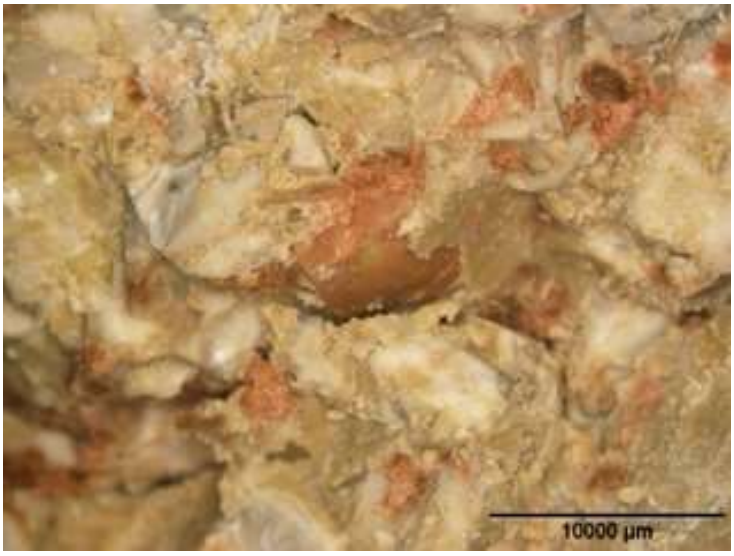

Figure 4-21: Internal structure of a SMA specimen containing 2% red pellet-colored capsules

As general observations, most of the oil released affected only the mastic, with very limited absorption by the aggregate present, with the exception of Figure 4-21. Oil propagation appeared mostly random, along mastic veins between the aggregates. No clear directionality or obvious signs of damage were associated with these streaks. This is likely motivated by the type of loading used, uniaxial compression with confinement, that mostly aimed to push the oil out of the capsules to test its coloring ability, not to generate the fatigue cracking where this technology would be most useful, and where oil release should follow the cracks. From the photographs presented, capsule adhesion to the mastic appears very good, with many being split by the fracture plane instead of being forced to one of the halves, indicating that the weakest link is the capsule itself and not the bond with the binder.

4.4 Asphalt Beams

4.4.1 Asphalt Beam Dimensions and Volumetric Properties

The asphalt beams were measured as described in Section 3.6, with the results being presented in Table 4-4. In terms of height, the specimens were very close to the specified 5 cm, which is expected since this dimension was controlled during compaction. On their longest side, the specimens also had a length very similar to the mold size (30.5 cm), which is expected. On their shortest side the specimens generally had a shorter than desired length, but were reasonably close to 10 cm. This is due to abrasion during the sawing process, which erodes away some of the material.

Table 4-4: Asphalt beam dimensions

Mixture Type	Specimen Number	Average Dimensions [cm]			Specimen Volume [cm3]
		Height	Longest Side	Shortest Side	
AC	1	4.89	30.35	9.89	1468.5
	2	4.95	30.36	9.94	1493.0
	3	4.94	30.43	9.75	1463.9
SMA	1	4.98	30.42	9.74	1475.4
	2	5.03	30.46	10.00	1531.6
	3	5.02	30.44	9.90	1511.3

The specimens' bulk density and void fraction is presented in Table 4-5. The asphalt concrete mixture appears to have been over-compacted, displaying a void fraction that is half the mixture's theoretical one. There are certain factors that may influence a sample's bulk density measurement when using the hydrostatic method. If, for example, the specimen has a very rough surface its density may be miscalculated due to the draining of water from these surface pores. It is also likely that the conversion of some of the aggregate from basalt to limestone affected the mixture's volumetric properties in ways that were unaccounted for, such as slightly differing particle shapes and sizes affecting their spatial arrangement. The stone mastic asphalt mixture's void fraction was slightly above expectations, but within a reasonable range. Interestingly, the specimen's all had dimensions close to those projected.

Table 4-5: Bulk densities and void fractions of the asphalt beams

Mixture Type	Specimen Number	Specimen Masses [g]			Real Bulk Density [kg/m^3]	Theoretical Bulk Density [kg/m^3]	Theoretical Maximum Density [kg/m^3]	Real Void Fraction	Theoretical Void Fraction
		Dry (M1)	Submerged (M2)	Saturated (M3)					
AC	1	3460.8	2032.9	3466.8	2413.6	2365.9	2465.8	1.93%	3.70%
	2	3529.6	2077.8	3534.6	2422.8			1.55%	
	3	3414.9	2002.7	3419.2	2410.8			2.04%	
SMA	1	3355.8	1934.6	3364.9	2346.2	2357.4	2448.0	4.32%	3.70%
	2	3468.1	1998.6	3474.8	2349.3			4.19%	
	3	3436.9	1979.6	3443.0	2348.6			4.23%	

4.4.2 Analysis of Oil Propagation

After resting the specimens were cut into three lengthwise slices, inspected, and photographed. These photographs were also analyzed with *ImageJ* to measure the cracks in them presented. The beams were also inspected and photographed again a day after sawing.

The first set of specimens were split along their cracks before sawing. During this operation, it was apparent that the oil had covered most of the fracture's surface in both cases. There were a few areas that oil did not reach, possibly due to the specimen not being fully fractured there or due to the method used to add the rejuvenator, since a significant part flowed out of the crack once a path of least resistance was found.

ImageJ enabled the measurement of oil penetration in the asphalt and the distance oil traveled in cracks, along with their width. For this analysis, the software's "set scale" feature was used, calibrated with the ruler visible in every photograph. These measurements are presented in Annex C, with the general results being discussed in the following paragraphs.

High Damage Level Beams

For the first set of wheel tracking beams, Figures 4-22 and 4-23, it is immediately noticeable that oil, or at least pigment penetration is limited to a few millimeters of asphalt in the vicinity of the crack. A distinction between the presence of pigment and the presence of oil can be made, since there are areas where a darker hue of the mastic and aggregate, similar to the effect an oil stain has on cloth, can be spotted that are not red in color. This suggests that the pigment might have greater difficulty in dispersing through the asphalt than the oil. There are also areas where red staining can be spotted, especially near zones where oil was free to flow, meaning the pigment was not completely ineffective.

Oil staining appeared to have been much more prevalent in the mastic and small aggregates contained within it than in the larger aggregate.

In many of the smaller cracks, which were generally perpendicular to the primary one and developed during loading, colored oil was present, usually filling them in their entirety regardless of their length. This generally occurred in cracks that were in contact with the main crack, and likely the result of capillary action. There are also occurrences where cracks further away from the primary one appear filled by colored oil. This means that the oil not only was capable of travelling significant lengths away from the initial crack but was also able to navigate the network of smaller secondary cracks. In the immediate vicinity of these cracks red staining and a hazier appearance of the mastic were again present.

A day after their initial inspection, the beams now displayed bands of oil-stained aggregate and mastic either side of the main crack. This staining did not show any red hue. It is likely that, after sawing, the porous aggregate and mastic were able to come into contact with the thin film of oil present in the primary crack, drawing some of it. It is possible that due to pore size, the pigment particles happened to be filtered out of this oil.

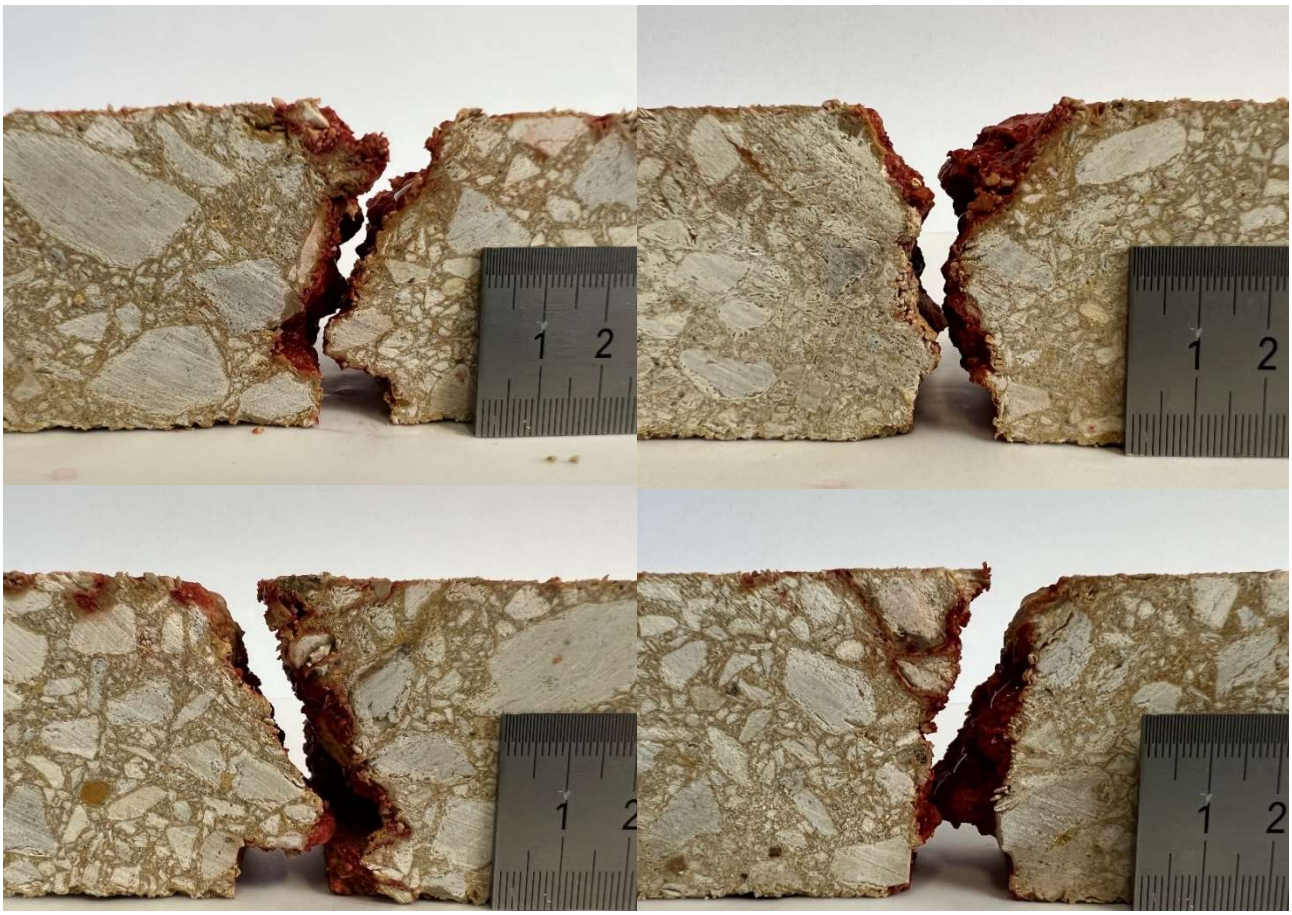

Figure 4-22: Photographs of the cracking in the AC High Damage Level beam

Oil penetration varied greatly and was inconsistent. In most photographs there are areas where some staining is visible, most commonly not red in color, immediately followed by zones where it is not noticeable. The typical oil penetration depths were between 1 and 2 mm for both mixture types. If an area was comprised of looser asphalt or had many air voids oil would tend to penetrate further, up to 4 mm (approximately).

Oil presence was identified in cracks spanning a few millimeters to cracks that spanned up to 2.5 centimeters. Crack width was not uniform, usually ranging from 0.2 to 0.5 millimeters.

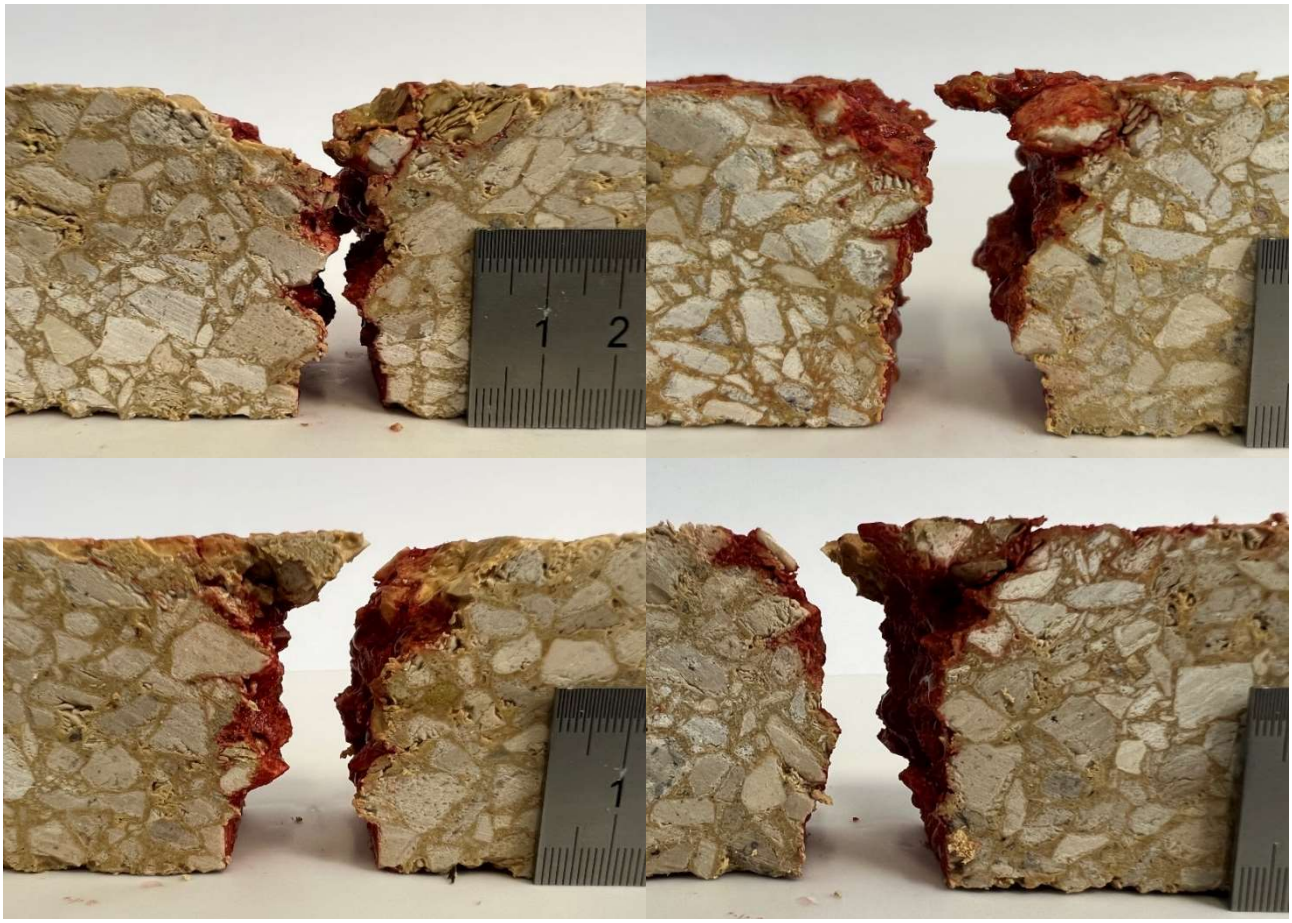

Figure 4-23: Photographs of the cracking in the SMA High Damage Level beam

Medium Damage Level Beams

The second set of wheel tracking beams is very similar to the first one in most aspects. Since these specimens were not completely fractured there was still a considerable volume of oil within the crack. This was not accounted for, and during sawing some of this oil was spread across the specimen's side by the blade, which interfered with the results. The smearing seen in Figure 4-24 is a product of an oversight during the drying process. This type of smearing, especially visible in Figure 4-25, is likely to have been caused by the sawing process since it has a clear directionality. Preparing the samples to be photographed involved drying them slightly, so that water and excess oil would not obscure the crack's details. Some oil pooled at the crack's surface and, when patted with a paper tower, some was spread onto the specimen's surface instead of being absorbed.

The beams clearly display a lower level of damage than the previous ones. The SMA beams had a smaller crack than the AC beams that decreased in height over the specimen's

width. This was not immediately apparent before sawing the specimens. Two of the SMA beams also broke during the sawing process.

The AC beam showed cracking between 33 and 38 mm, with one slice showing a 35 mm pigmented crack followed by a 14 mm section without colored oil. It is likely that oil simply could not access this extension since crack width in this segment is similar to the pigmented section. Crack width averaged 0.231 mm in this beam, usually being slightly wider at the base and narrowing towards the top of the specimen. Oil penetration was reminiscent of the previous set, with most measurements between 0.9 to 1.5 mm. Areas where there were more air voids or damage was present tended to have higher penetration, up to 5 mm in this case.

The SMA beam had crack pigmentation lengths between 25 and 38 mm. The slice that fractured during sawing showed a 15 mm unpigmented crack following the pigmented one. Crack width averaged 0.356 mm for this specimen, with a much clearer narrowing along its height than the previous. Oil penetration was slightly lower than the previous cases, averaging 0.9 mm. This is probably caused by the smaller crack containing less oil.

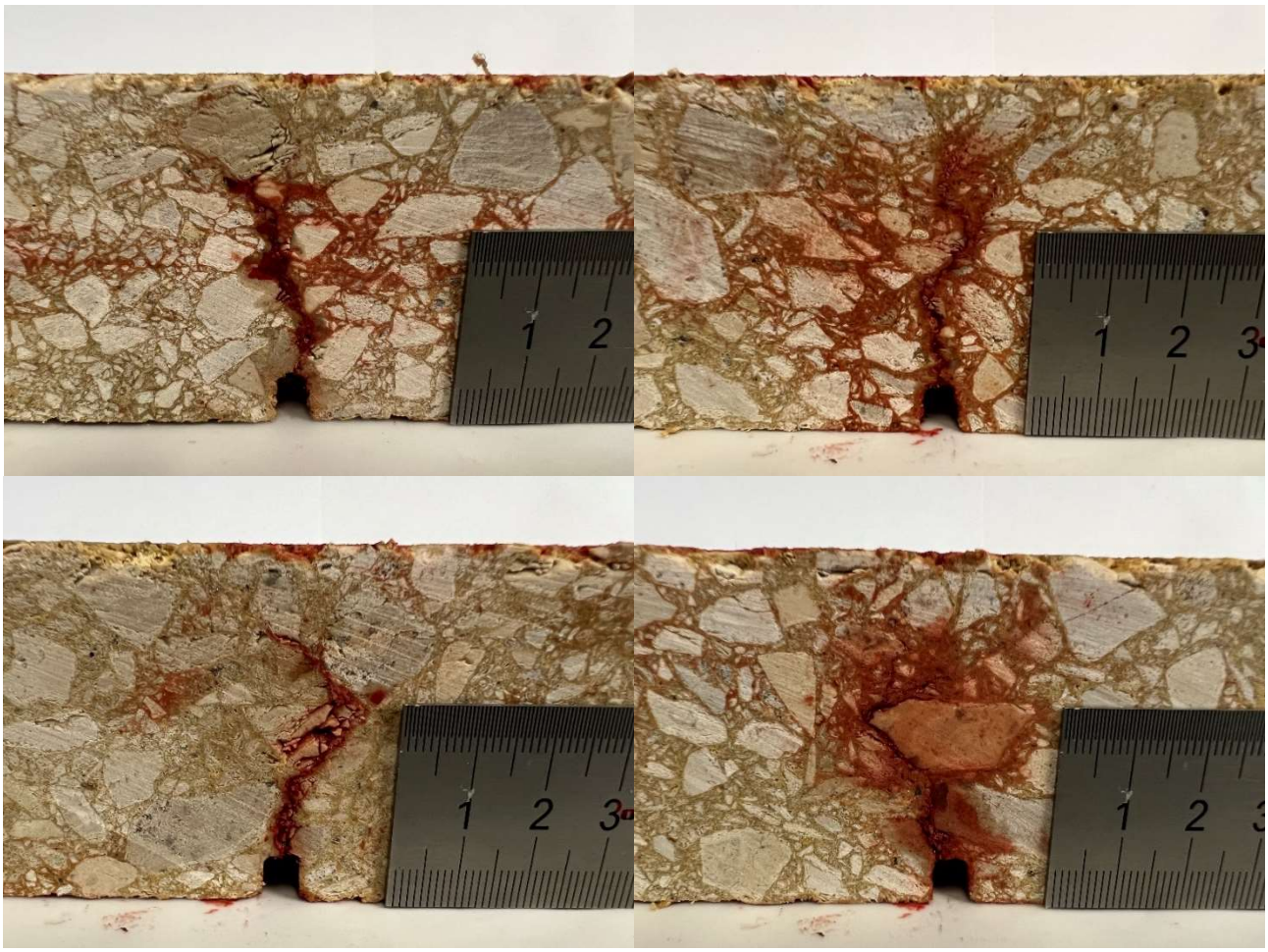

Figure 4-24: Photographs of the cracking in the AC Medium Damage Level beam

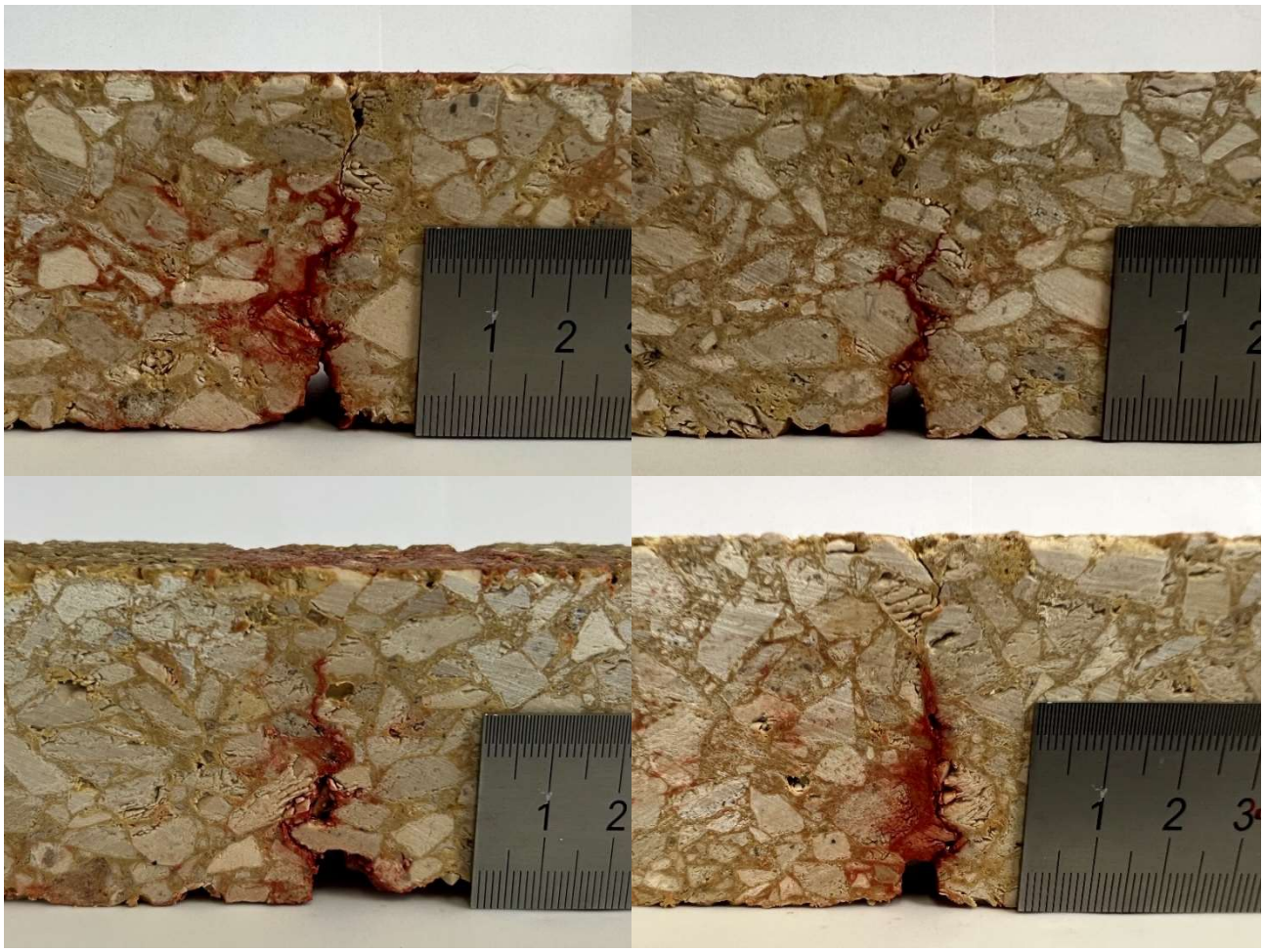

Figure 4-25: Photographs of the cracking in the SMA Medium Damage Level beam

Low Damage Level Beams

The third and final set of wheel tracking specimens was subjected to a lower level of damage than the second one. The cracks in these beams have very little visible oil, apart from the areas where it pooled into larger drops after sawing. No attempt to dry the specimens was made with this set, yet these oil droplets were still absorbed by the asphalt in their vicinity in a matter of minutes, creating the appearance of high oil penetration in these areas. When measuring oil penetration and crack width these areas were avoided.

As discussed in Section 3.8.2, the AC beam did not have the expected behavior. It becomes apparent when inspecting the specimen that the height of its crack is similar to the previous AC beam. Measurements confirm this notion, with crack height varying between 35 and 38 mm. This specimen is pictured in Figure 4-26. Its crack is noticeably thinner than the previous case, due to testing being interrupted almost as soon as it developed, which limited

its growth. Crack width averaged 0.158 mm if the two largest measurements (an air void and a gap between aggregates at the initiation of the crack) were excluded. Its width narrowed down to the 0.05 mm range at points. Oil penetration was lower than in the previous set, in the 0.2 to 0.4 mm range.

The SMA beam, Figure 4-27, had the intended level of damage of 25% the number of cycles of the first one. Crack length varied between 13 and 31 mm, with the intermediate values being 21 and 26 mm. Crack width measurements averaged 0.132 mm. Oil penetration was similar to the AC specimen, usually in the 0.2 to 0.4 mm range.

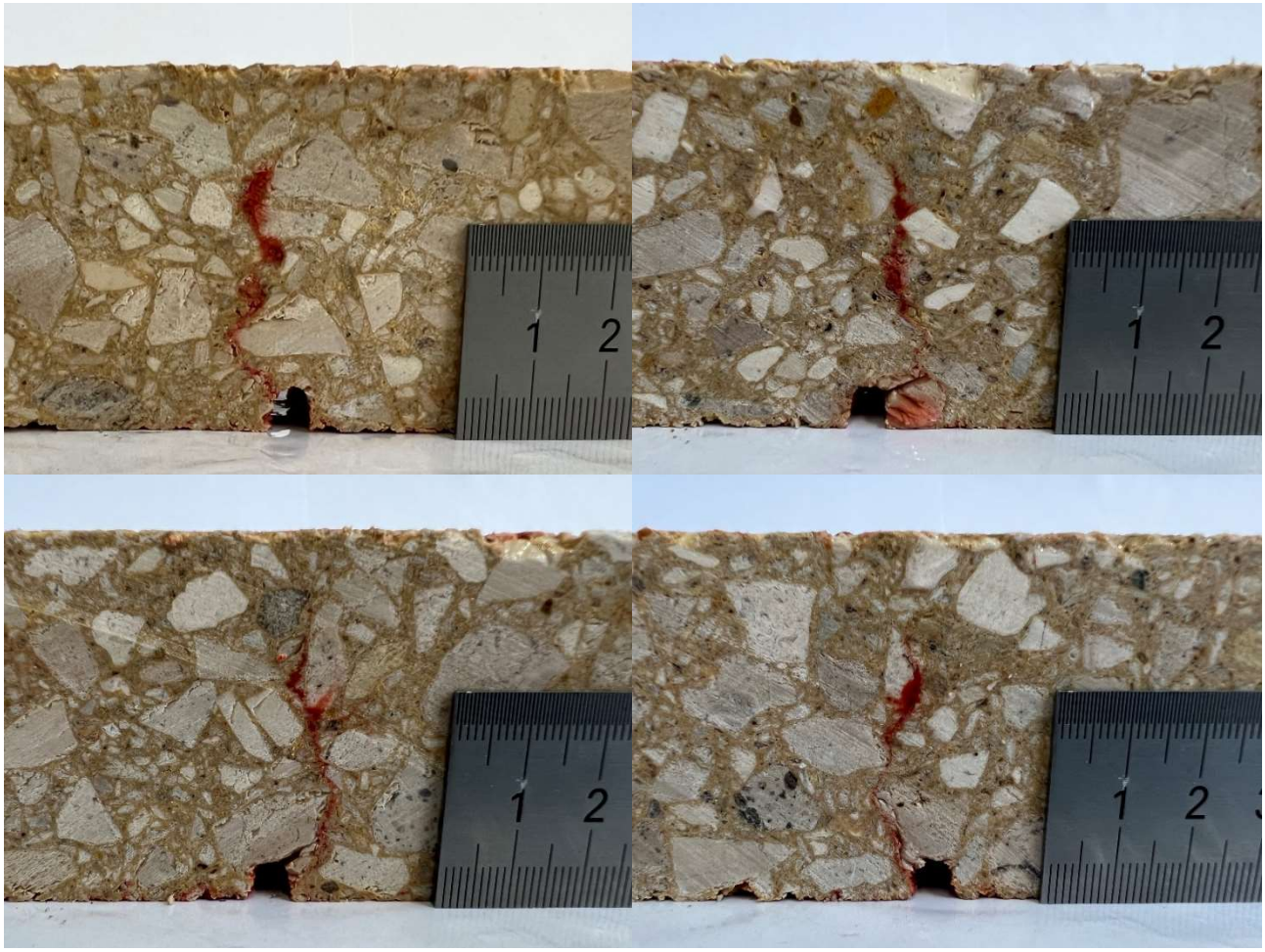

Figure 4-26: Photographs of the cracking in the AC Low Damage Level beam

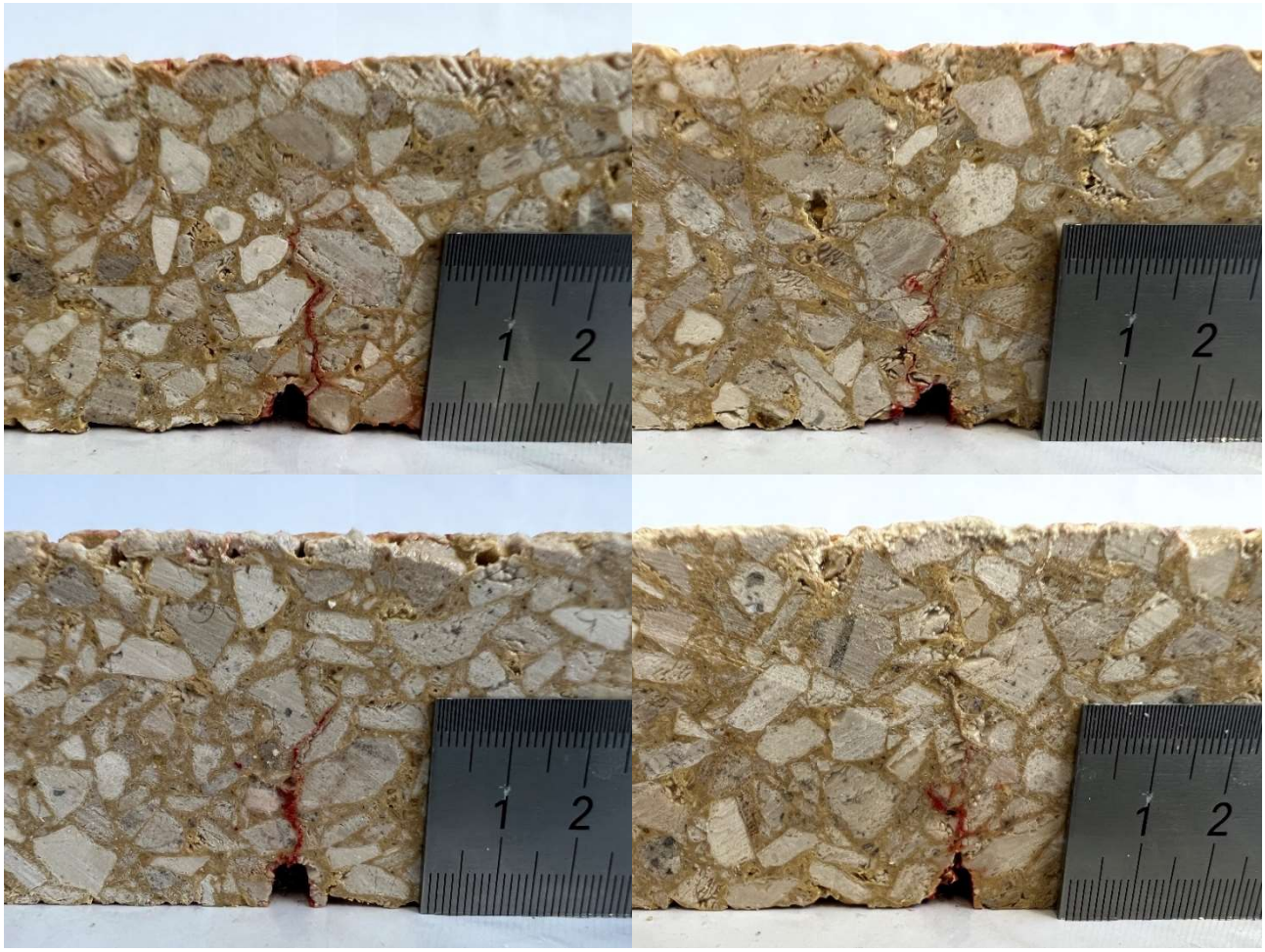

Figure 4-27: Photographs of the cracking in the SMA Low Damage Level beam

4.5 Comparison of Synthetic Binder and Bitumen Solubility in Oil

Figures 4-28 and 4-29 show the visual appearance of the two mixtures over the course of the test. Visually, it is clear that the mixture made with traditional bitumen lost a lot of its binder coating to the oil, as the aggregate gradually becomes more exposed over time.

In the mixture using the clear binder differences in binder coverage are naturally harder to identify. Some aggregates show darker areas where the binder happened to pool, and differences in their tone could be used to identify binder loss. Although not immediately noticeable, there is a difference in coverage between 0 and 48 hours. The areas where binder pooled appear smaller, and zones where a thinner layer was present appear whiter, revealing the aggregate's color.

Figure 4-28: Photographs of the bitumen-covered aggregate after (left to right) 0, 6, 24, and 48 hours in oil

Figure 4-29: Photographs of the synthetic binder-covered aggregate after (left to right) 0, 6, 24, and 48 hours in oil

It is worth noting that the oil in which the mixtures were submerged also changed. In the case of the sample with bitumen, the oil immediately became opaque and dark as soon as the aggregate pouch was lifted for the first weighing. The oil in contact with the synthetic binder mixture did not display sudden changes, but gradually became more orange as the test went on, resembling the synthetic binder's color, as is visible in Figure 4-30.

Figure 4-30: Sunflower seed oil before the experiment (left), after 48 hours in contact with the synthetic binder mixture (center), and after 48 hours in contact with the bitumen mixture (right)

The evolution of each mixture's mass was also monitored. These results are presented in Table 4-6. The recorded masses are only intended for comparison between the two samples as the methodology did not completely drain the oil out of the aggregate bulk. In all measurements except the first the aggregates are coated in oil. At 48 hours, after a standard weighing procedure, the aggregates were spread out on strainers until oil drops stopped forming. This left only a coating of oil on the surface of the aggregates, which could not be removed without disturbing the remaining binder film.

Table 4-6: Mixture mass over the course of the experiment

Time (hours)	Aggregate + Binder Mass (g)		Binder + Remaining Oil Mass (g)		Binder + Remaining Oil Mass Change Relative to Initial Binder Mass	
	Recofal S-100P	35/50	Recofal S-100P	35/50	Recofal S-100P	35/50
Initial (dry)	160.63	157.27	(no oil) 10.03	(no oil) 7.17	0%	0%
1	167.53	165.14	16.93	15.04	+69%	+110%
2	168.09	163.36	17.49	13.26	+74%	+85%
3	167.64	162.18	17.04	12.08	+70%	+68%
4	167.30	160.98	16.70	10.88	+67%	+52%
5	168.10	160.21	17.50	10.11	+74%	+41%
6	167.80	159.29	17.20	9.19	+71%	+28%
25	168.56	160.43	17.96	10.33	+79%	+44%
26	166.88	159.38	16.28	9.28	+62%	+29%
48	169.31	159.99	18.71	9.89	+87%	+38%
Drained (48 h)	161.97	153.81	11.37	3.71	+13%	-48%

These results reiterate that a large part of the traditional binder was lost to the oil. While some loss was visually identified for the synthetic binder, the sample's mass still shows an increase relative to the start, which means that binder loss was not enough to offset the mass gain from the oil coating/absorption. Intermediate measurements show a clear downward trend in mass of the sample with bitumen, while the mass of the synthetic binder mix mostly remained stable.

5

Conclusions and Further Research

This work intended to visually study the behavior of sunflower seed oil when applied in asphalt as a rejuvenator, be it directly or in encapsulated form. To this end, the feasibility of various techniques had to be evaluated.

A commercially available synthetic colorless binder combined with limestone aggregate made it possible to produce light-colored asphalt, an essential first step.

To be able to perceive the sunflower seed oil inside this mixture, it was necessary to find a pigment or dye which could be added to it. A number of colored oils were produced using various pigments. Since this oil was expected to mix with the binder, several tests were carried out to find which colored oil would best change a binder sample's color. It was found that oil mixed with fat-soluble food coloring had the best performance, although oil mixed with asphalt coloring pellets was also used for comparison.

It was now necessary to produce calcium alginate capsules containing these oils, which was successfully done. These capsules had an appearance and dimensions in line with ones produced through the same methods in the literature. The compressive strength of these capsules, when unheated, was in line with previous findings. After heating, capsule strength and stiffness varied greatly and requires further research. Pigmented oil release was present, although somewhat limited in volume.

The light-colored asphalt mixture was then combined with the pigmented capsules, to learn if it was possible to produce this type of mixture and to study its internal structure. Cylindrical Marshall-type specimens were produced and sawed. Some were uniaxially compressed before sawing to promote rejuvenator release. The production of these samples had no issues, with the only noteworthy difference between them and a traditional mixture being

the release of oil on their tops and bottoms during compaction due to capsule damage in these areas. Capsule distribution in the mixture was found to be mostly homogenous.

Oil release in the unloaded cylindrical specimens was not completely accompanied by pigment release. The capsules in these specimens all used oil pigmented with pellets. Colorless oil release was identified many hours after sawing (and associated damaging of the cut capsules), but not immediately after. This indicated that minimal amounts of oil were released due to mixing and compaction.

Both capsules pigmented with food coloring and ones pigmented with pellets were used in loaded specimens. These specimens were then fractured with a chisel, showing some evidence of oil release, with discoloration of the mastic and aggregate. This staining was not uniform or easily predictable, and often had no pigmentation. Capsules containing food coloring performed better, due to their greater coloring ability.

The distribution of capsules, capsule fragments, and staining instances was studied in these specimens. A positive correlation between capsule concentration and the number of capsules and capsule fragments was found. A higher proportion of broken capsules was found in the mixtures with higher capsule concentrations. The ratio of crushed capsules and capsule fragments to whole/mostly whole capsules is significantly lower in the case of capsules made with food coloring, that had a higher proportion of sodium alginate in their composition and should therefore have higher compressive strength. The amount of staining was found to be higher in asphalt concrete specimens than in stone mastic asphalt ones.

Microscopic observation of the capsules in these previous specimens showed that oil release mostly affected the mastic, and that capsule adhesion to the mixture was good.

Asphalt beams were produced and loaded in a modified wheel tracking test. Pigmented oil was directly added to the specimens' cracks. Oil penetration was found to be limited, decreasing with the width of the crack likely due to a smaller volume of oil being present. Oil was able to propagate through most visible cracks, even their width was very small. Oil was also able to fully traverse long cracks.

Binder solubility in oil was studied in a comparative test between traditional bitumen and the synthetic clear binder. Aggregates coated with bitumen had lost most of their coverage after 48 hours, while aggregates coated with synthetic binder showed noticeably lower binder loss.

Going forward, there are many matters addressed in this work that can be investigated further. It would be important to find a different type of oil or similar substance that is more

capable of modifying this synthetic binder for example. It would also be interesting to find a type of pigment or dye that is better able to flow out of the calcium alginate capsules. More research into wheel tracking tests with flexion is needed, as it offers the possibility of realistically simulating a pavement layer yet there were difficulties in predicting and monitoring the level of damage that samples would have. Higher temperatures during the rest time of the specimens could also be explored, possibly allowing the oil to penetrate the synthetic binder in a way that is closer to bitumen. The effect that calcium alginate capsules have on rejuvenators with particulates or additives could also be an interesting subject of future projects.

BIBLIOGRAPHY

[1] A. Schroten, L. van Wijngaarden, M. Brambilla, M. Gatto, S. Maffii, F. Trosky, H. Kramer, R. Monden, D. Bertschmann, M. Killer, V. Lambla, K. El Beyrouty, S. Amaral, "Road taxation and spending in the EU," CE Delft, 2019.

[2] R. Varma, R. Balieu, and N. Kringos, "A state-of-the-art review on self-healing in asphalt materials: Mechanical testing and analysis approaches," *Constr. Build. Mater.*, vol. 310, p. 125197, Dec. 2021, doi: 10.1016/j.conbuildmat.2021.125197.

[3] R. Micaelo, T. Al-Mansoori, and A. Garcia, "Study of the mechanical properties and self-healing ability of asphalt mixture containing calcium-alginate capsules," *Constr. Build. Mater.*, vol. 123, pp. 734–744, Oct. 2016, doi: 10.1016/j.conbuildmat.2016.07.095.

[4] S. Burningham and N. Stankevich, "Why road maintenance is important and how to get it done," p. 10, 2005.

[5] John Read and David Whiteoak, *The Sell Bitumen Handbook*, Fifth Edition. Thomas Telford Publishing, 2003.

[6] S. Xu, A. García, J. Su, Q. Liu, A. Tabaković, and E. Schlangen, "Self-Healing Asphalt Review: From Idea to Practice," *Adv. Mater. Interfaces*, vol. 5, no. 17, p. 1800536, Sep. 2018, doi: 10.1002/admi.201800536.

[7] Shi Xu, "Self-healing Porous Asphalt: A Combination of Encapsulated Rejuvenator and Induction Heating", PhD Thesis, Faculty of Civil Engineering and Geosciences, Delft University of Technology, Delft, Netherlands, 2020.

[8] E. D. Paciência, "Auto-regeneração de misturas betuminosas com agentes encapsulados," MSc Dissertation, Dept. of Civil Engineering, NOVA University Lisbon, Lisbon, Portugal, 2018.

[9] J. Qiu, "Self Healing of Asphalt Mixtures", PhD Thesis, Faculty of Civil Engineering and Geosciences, Delft University of Technology, Delft, Netherlands, 2012.

[10] Á. García, E. Schlangen, and M. van de Ven, "Properties of capsules containing rejuvenators for their use in asphalt concrete," *Fuel*, vol. 90, no. 2, pp. 583–591, Feb. 2011, doi: 10.1016/j.fuel.2010.09.033.

[11] A. Garcia, M. Bueno, J. Norambuena-Contreras, Q. Liu, and M. Partl, "The model for induction-healing asphalt concrete," in *Asphalt Pavements*, CRC Press, 2014, pp. 1431–1440. doi: 10.1201/b17219-173.

[12] José Neves and António Correia Diogo, "Ligantes e Materiais Betuminosos," in *Ciência e Engenharia de Materiais de Construção*, IST Press, 2012, pp. 273–319.
[13] D. Sun *et al.*, "A comprehensive review on self-healing of asphalt materials: Mechanism, model, characterization and enhancement," *Adv. Colloid Interface Sci.*, vol. 256, pp. 65–93, Jun. 2018, doi: 10.1016/j.cis.2018.05.003.
[14] J. Qiu, M. F. C. van de Ven, S. P. Wu, J. Y. Yu, and A. A. A. Molenaar, "Investigating self healing behaviour of pure bitumen using Dynamic Shear Rheometer," *Fuel*, vol. 90, no. 8, pp. 2710–2720, Aug. 2011, doi: 10.1016/j.fuel.2011.03.016.
[15] R. Micaelo, "CARACTERIZAÇÃO E AVALIAÇÃO DO DESEMPENHO DE MISTURAS BETUMINOSAS COM AGENTES ENCAPSULADOS," presented at the 10º Congresso Rodoferroviário Português, Laboratório Nacional de Engenharia Civil, Lisbon, July 2022, p. 10.
[16] Á. García, E. Schlangen, M. van de Ven, and G. Sierra-Beltrán, "Preparation of capsules containing rejuvenators for their use in asphalt concrete," *J. Hazard. Mater.*, vol. 184, no. 1–3, pp. 603–611, Dec. 2010, doi: 10.1016/j.jhazmat.2010.08.078.
[17] I. Gonzalez-Torre and J. Norambuena-Contreras, "Recent advances on self-healing of bituminous materials by the action of encapsulated rejuvenators," *Constr. Build. Mater.*, vol. 258, p. 119568, Oct. 2020, doi: 10.1016/j.conbuildmat.2020.119568.
[18] H. Asli, E. Ahmadinia, M. Zargar, and M. R. Karim, "Investigation on physical properties of waste cooking oil – Rejuvenated bitumen binder," *Constr. Build. Mater.*, vol. 37, pp. 398–405, Dec. 2012, doi: 10.1016/j.conbuildmat.2012.07.042.
[19] M. Zaumanis, R. B. Mallick, L. Poulikakos, and R. Frank, "Influence of six rejuvenators on the performance properties of Reclaimed Asphalt Pavement (RAP) binder and 100% recycled asphalt mixtures," *Constr. Build. Mater.*, vol. 71, pp. 538–550, Nov. 2014, doi: 10.1016/j.conbuildmat.2014.08.073.
[20] A. Garcia, C. J. Austin, and J. Jelfs, "Mechanical properties of asphalt mixture containing sunflower oil capsules," *J. Clean. Prod.*, vol. 118, pp. 124–132, Apr. 2016, doi: 10.1016/j.jclepro.2016.01.072.
[21] G. Nelson, "Microencapsulated colourants for technical textile application," in *Advances in the Dyeing and Finishing of Technical Textiles*, Elsevier, 2013, pp. 78–104. doi: 10.1533/9780857097613.1.78.
[22] S. Sawant and R. Shegokar, "Bone scaffolds," in *Nanobiomaterials in Hard Tissue Engineering*, Elsevier, 2016, pp. 155–187. doi: 10.1016/B978-0-323-42862-0.00005-5.
[23] J.-F. Su and E. Schlangen, "Synthesis and physicochemical properties of high compact microcapsules containing rejuvenator applied in asphalt," *Chem. Eng. J.*, vol. 198–199, pp. 289–300, Aug. 2012, doi: 10.1016/j.cej.2012.05.094.
[24] M. A. Aguirre, M. M. Hassan, S. Shirzad, L. N. Mohammad, S. Cooper, and I. I. Negulescu, "Laboratory Testing of Self-Healing Microcapsules in Asphalt Mixtures Prepared with Recycled Asphalt Shingles," *J. Mater. Civ. Eng.*, vol. 29, no. 9, p. 04017099, Sep. 2017, doi: 10.1061/(ASCE)MT.1943-5533.0001942.
[25] T. Al-Mansoori, J. Norambuena-Contreras, R. Micaelo, and A. Garcia, "Self-healing of asphalt mastic by the action of polymeric capsules containing rejuvenators," *Constr. Build. Mater.*, vol. 161, pp. 330–339, Feb. 2018, doi: 10.1016/j.conbuildmat.2017.11.125.
[26] A. W. Coats and J. P. Redfern, "Thermogravimetric analysis. A review," *The Analyst*, vol. 88, no. 1053, p. 906, 1963, doi: 10.1039/an9638800906.

[27] A. Tabaković, W. Post, D. Cantero, O. Copuroglu, S. J. Garcia, and E. Schlangen, "The reinforcement and healing of asphalt mastic mixtures by rejuvenator encapsulation in alginate compartmented fibres," *Smart Mater. Struct.*, vol. 25, no. 8, p. 084003, Aug. 2016, doi: 10.1088/0964-1726/25/8/084003.
[28] A. Tabaković *et al.*, "The compartmented alginate fibres optimisation for bitumen rejuvenator encapsulation," *J. Traffic Transp. Eng. Engl. Ed.*, vol. 4, no. 4, pp. 347–359, Aug. 2017, doi: 10.1016/j.jtte.2017.01.004.
[29] S. Xu, X. Liu, A. Tabaković, and E. Schlangen, "Investigation of the Potential Use of Calcium Alginate Capsules for Self-Healing in Porous Asphalt Concrete," *Materials*, vol. 12, no. 1, p. 168, Jan. 2019, doi: 10.3390/ma12010168.
[30] B. H. Stuart, "Infrared Spectroscopy: Fundamentals and Applications," John Wiley & Sons, 2004, p. 208.
[31] P. R. Griffiths, "Fourier Transform Infrared Spectrometry," vol. 222, p. 6, 1983.
[32] Kenneth R. Spring, *Encyclopedia of Optical Engineering*. Taylor & Francis, 2011. doi: 10.1081/E-EOE.
[33] Y. Ding, B. Huang, and X. Shu, "Utilizing Fluorescence Microscopy for Quantifying Mobilization Rate of Aged Asphalt Binder," *J. Mater. Civ. Eng.*, vol. 29, no. 12, p. 04017243, Dec. 2017, doi: 10.1061/(ASCE)MT.1943-5533.0002088.
[34] F. Handle *et al.*, "The bitumen microstructure: a fluorescent approach," *Mater. Struct.*, vol. 49, no. 1–2, pp. 167–180, Jan. 2016, doi: 10.1617/s11527-014-0484-3.
[35] D. Grossegger, H. Grothe, B. Hofko, and M. Hospodka, "Fluorescence spectroscopic investigation of bitumen aged by field exposure respectively modified rolling thin film oven test," *Road Mater. Pavement Des.*, vol. 19, no. 4, pp. 992–1000, May 2018, doi: 10.1080/14680629.2017.1281833.
[36] D. Sun, Q. Pang, X. Zhu, Y. Tian, T. Lu, and Y. Yang, "Enhanced Self-Healing Process of Sustainable Asphalt Materials Containing Microcapsules," *ACS Sustain. Chem. Eng.*, vol. 5, no. 11, pp. 9881–9893, Nov. 2017, doi: 10.1021/acssuschemeng.7b01850.
[37] A. du Plessis and W. P. Boshoff, "A review of X-ray computed tomography of concrete and asphalt construction materials," *Constr. Build. Mater.*, vol. 199, pp. 637–651, Feb. 2019, doi: 10.1016/j.conbuildmat.2018.12.049.
[38] S. C. S. Rao Tangella, J. Craus, J. A. Deacon, and C. L. Monismith, "SUMMARY REPORT ON FATIGUE RESPONSE OF ASPHALT MIXTURES," Institute of Transportation Studies, University of California, Berkeley, California, Feb. 1990.
[39] J.-F. Masson, P. Collins, and G. Polomark, "Steric Hardening and the Ordering of Asphaltenes in Bitumen," *Energy Fuels*, vol. 19, no. 1, pp. 120–122, Jan. 2005, doi: 10.1021/ef0498667.
[40] D. Williams, D. N. Little, R. L. Lytton, Y. R. Kim, and Y. Kim, "Microdamage healing in asphalt and asphalt concrete," Federal Highway Administration, Volume II: Laboratory and field testing to assess and evaluate microdamage and microdamage healing., 2001.
[41] G. Sun, D. Sun, A. Guarin, J. Ma, F. Chen, and E. Ghafooriroozbahany, "Low temperature self-healing character of asphalt mixtures under different fatigue damage degrees," *Constr. Build. Mater.*, vol. 223, pp. 870–882, Oct. 2019, doi: 10.1016/j.conbuildmat.2019.07.040.
[42] B. Kim and R. Roque, "Evaluation of Healing Property of Asphalt Mixtures," *Transp. Res. Rec.*, p. 8, 2006.

[43] R. Micaelo, G. Pereira, and A. C. Freire, "Asphalt self-healing with encapsulated rejuvenators: effect of calcium-alginate capsules on stiffness, fatigue and rutting properties," *Mater. Struct.*, vol. 53, no. 1, p. 20, Feb. 2020, doi: 10.1617/s11527-020-1453-7.

[44] A. Garcia, J. Jelfs, and C. J. Austin, "Internal asphalt mixture rejuvenation using capsules," *Constr. Build. Mater.*, vol. 101, pp. 309–316, Dec. 2015, doi: 10.1016/j.conbuildmat.2015.10.062.

[45] T. Al-Mansoori, R. Micaelo, I. Artamendi, J. Norambuena-Contreras, and A. Garcia, "Micro-capsules for self-healing of asphalt mixture without compromising mechanical performance," *Constr. Build. Mater.*, vol. 155, pp. 1091–1100, Nov. 2017, doi: 10.1016/j.conbuildmat.2017.08.137.

[46] Gonçalo Moura Pereira, "Avaliação das propriedades mecânicas e de autorregeneração de misturas betuminosas com rejuvenescedores encapsulados", MSc Dissertation, Dept. of Civil Engineering, NOVA University Lisbon, Lisbon, Portugal, 2019.

[47] N. Ruiz-Riancho, S. Tahseen, A. Gracia, D. Grossegger, and R. Hudson-Griffiths, "Optimisation of self-healing properties for asphalts containing encapsulated oil to mitigate reflective cracking and maximize skid and rutting resistance," *Constr. Build. Mater.*, p. 12, 2021, doi: https://doi.org/10.1016/j.conbuildmat.2021.123879.

[48] N. Dhakal, M. A. Elseifi, and Z. Zhang, "Mitigation strategies for reflection cracking in rehabilitated pavements – A synthesis," *Int. J. Pavement Res. Technol.*, vol. 9, no. 3, pp. 228–239, May 2016, doi: 10.1016/j.ijprt.2016.05.001.

A

DATA SHEETS

A.1 Repsol Recofal S100-P Data Sheet

CHARACTERISTICS	UNIT	TESTING METHOD	SPECIFICATION
Density	g/cm^3	EN 15326	0.95-1.15
Penetration at 25˚C	0.1 mm	EN 1426	20-50
Softening Point	˚C	EN 1427	≥ 85
Resistance to hardening			
• *Retained penetration*	%	EN12607-1	≥ 80
•*Softening Point Increase*	˚C		≤10
•*Change in mass (absolute value)*	%		≤1.5
Brookfield viscosity at 160 ˚C	cP	EN 13303	≥ 400
Fraass Breaking Point	˚C	EN 12593	≤-20

B

Experimental Data

B.1 Force-Displacement Curves for the Various Capsule Batches

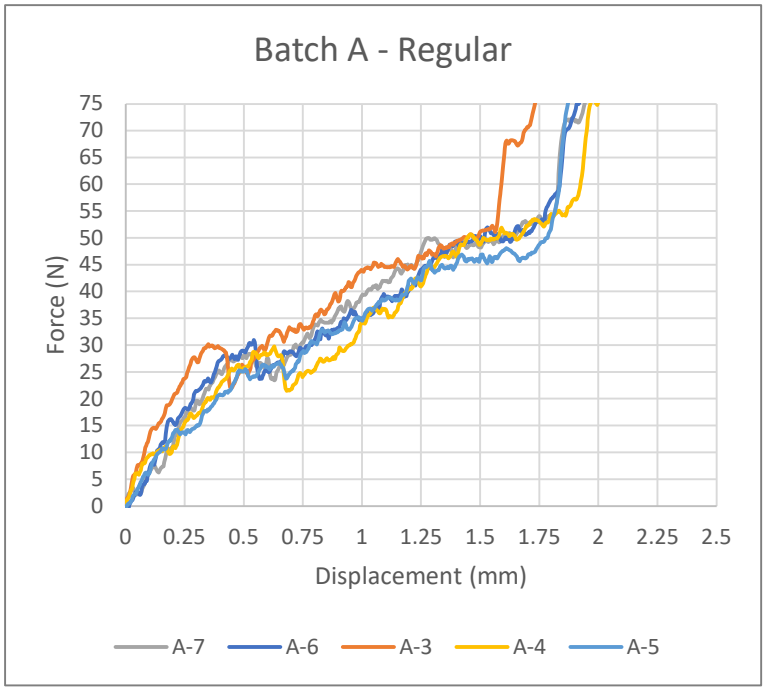

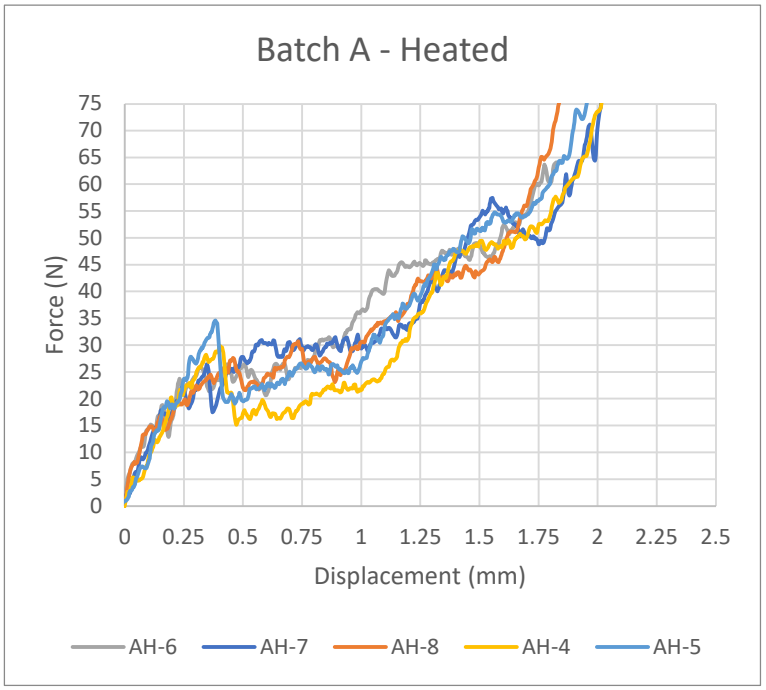

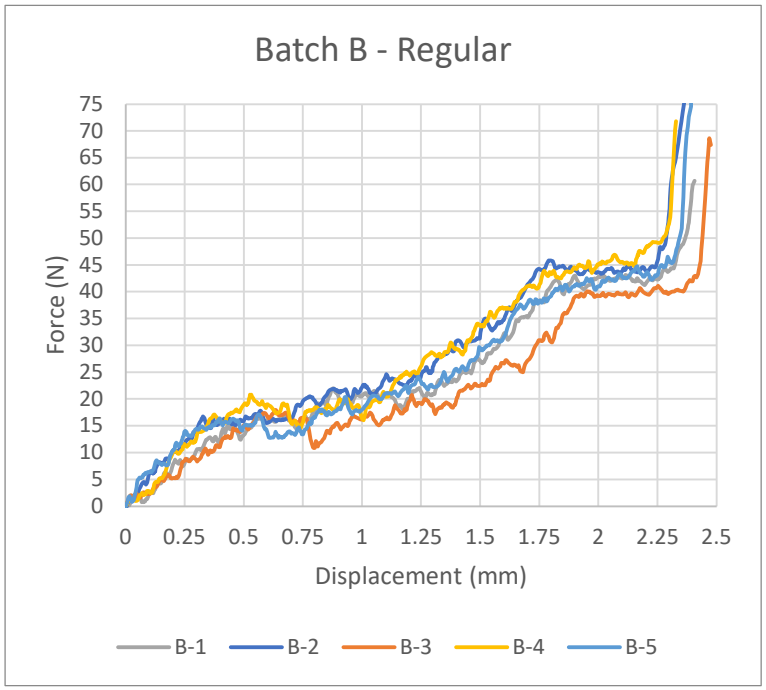

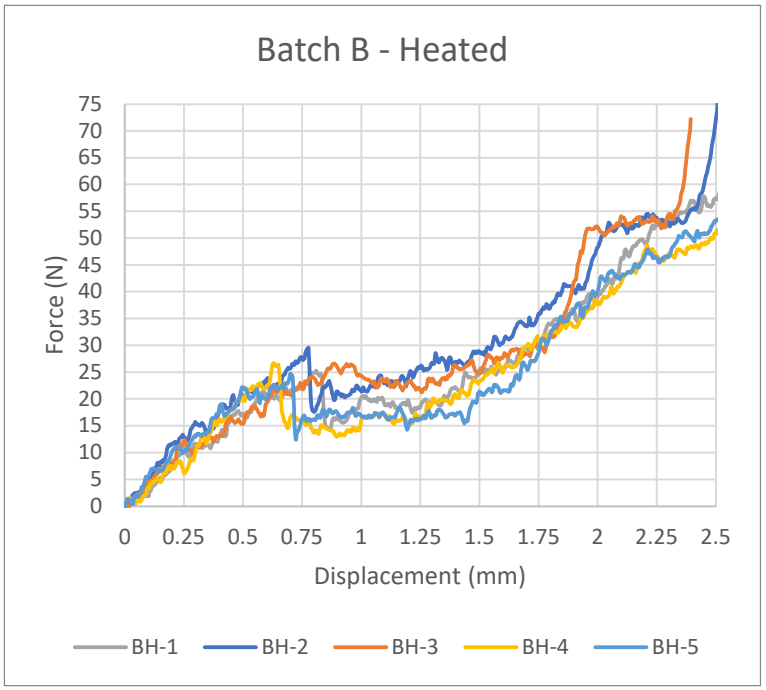

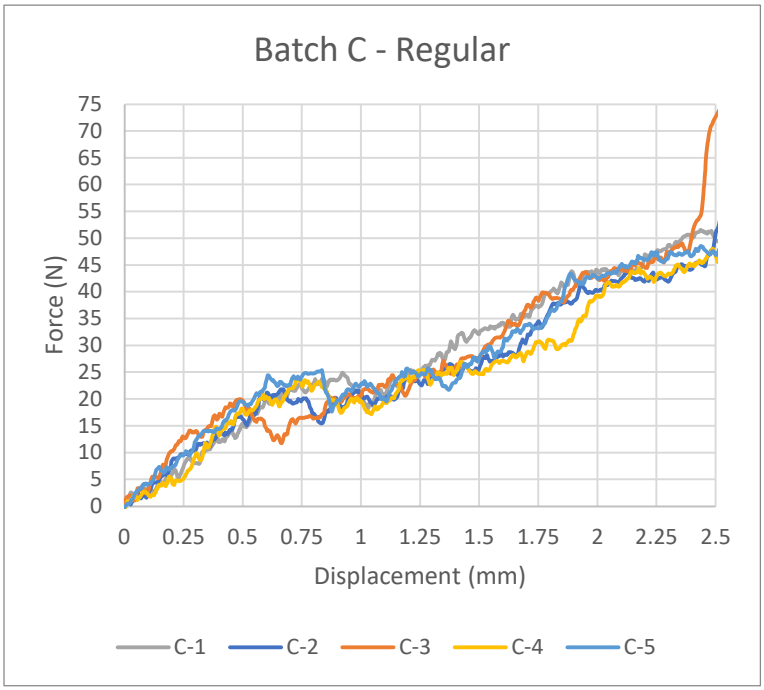
Batch C - Regular
Force (N)
Displacement (mm)
C-1
C-2
C-3
C-4
C-5

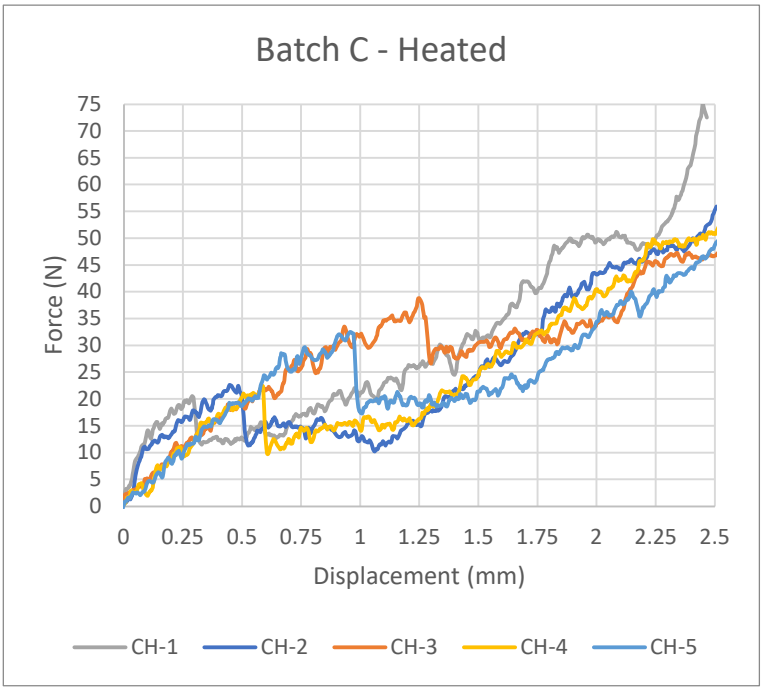
Batch C - Heated
Force (N)
Displacement (mm)
CH-1
CH-2
CH-3
CH-4
CH-5

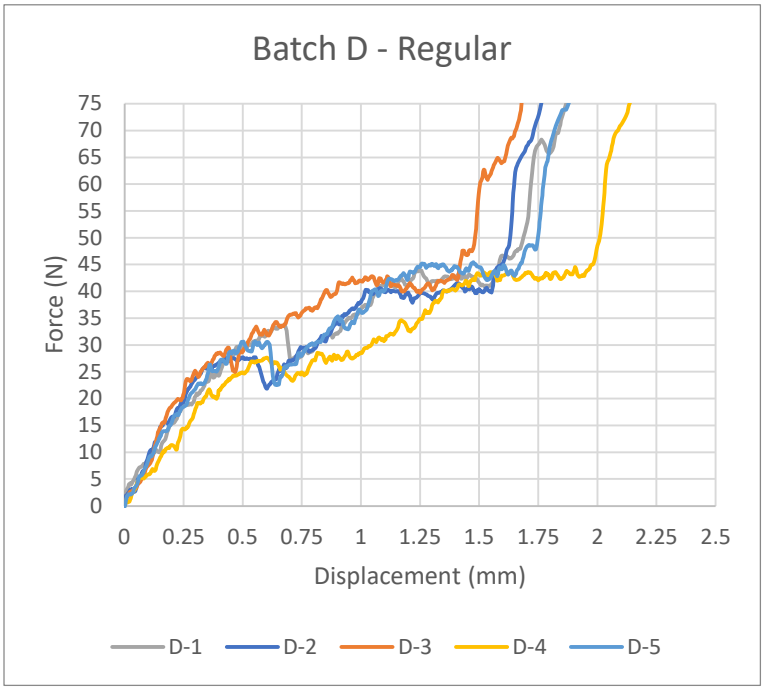
Batch D - Regular
Force (N)
Displacement (mm)
D-1
D-2
D-3
D-4
D-5

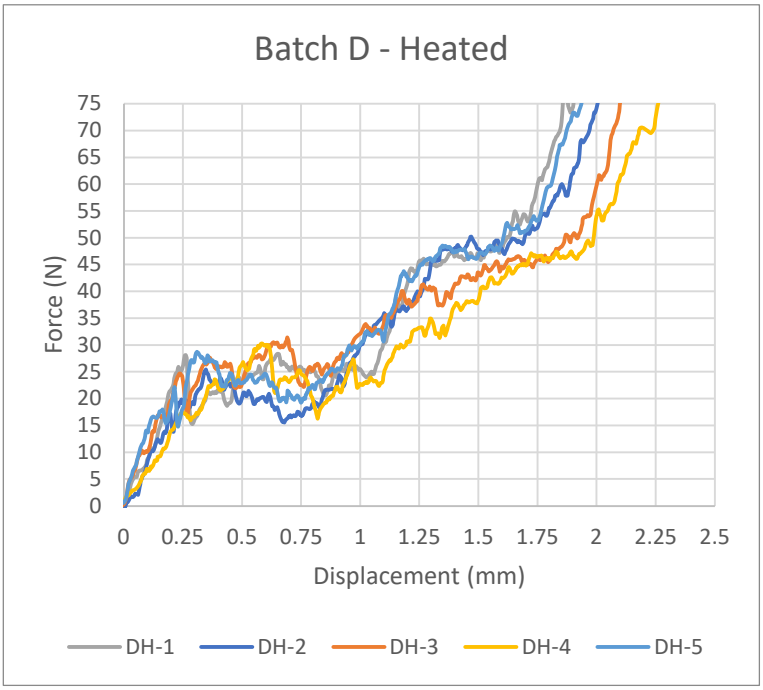
Batch D - Heated
Force (N)
Displacement (mm)
DH-1
DH-2
DH-3
DH-4
DH-5

B.2 Capsule and Staining Distribution in Loaded Cylindrical Specimens

AC 1.25% Red Food Coloring

Relative Cap. Area Highlighted			
	Col. 1	Col. 2	Col. 3
Row 1	21%	16%	8%
Row 2	11%	5%	4%
Row 3	3%	4%	0%

Cap. and Remnants (instances) (Cap. Count + Deformed/Crushed)			
	Col. 1	Col. 2	Col. 3
Row 1	26	19	12
Row 2	15	10	4
Row 3	9	13	0

Relative Stained Area Highlighted			
	Col. 1	Col. 2	Col. 3
Row 1	13%	17%	7%
Row 2	10%	6%	3%
Row 3	0%	0%	0%

Staining (instances) (Altered Aggrgate + Altered Mastic)			
	Col. 1	Col. 2	Col. 3
Row 1	4	6	8
Row 2	13	8	5
Row 3	3	4	0

Capsule Count (whole/ mostly whole)			
	Col. 1	Col. 2	Col. 3
Row 1	10	7	8
Row 2	8	7	2
Row 3	3	10	0

Deformed/Crushed Cap. or Cap. Remnants (instances)			
	Col. 1	Col. 2	Col. 3
Row 1	6	8	3
Row 2	3	2	1
Row 3	3	1	0

Altered Aggregate (instances)			
	Col. 1	Col. 2	Col. 3
Row 1	0	1	1
Row 2	2	1	1
Row 3	0	0	0

Altered Mastic (instances)			
	Col. 1	Col. 2	Col. 3
Row 1	4	5	7
Row 2	8	7	4
Row 3	3	4	0

AC 1.25% Red Pellets

Relative Cap. Area Highlighted			
	Col. 1	Col. 2	Col. 3
Row 1	2%	1%	1%
Row 2	1%	1%	1%
Row 3	2%	2%	3%

Cap. and Remnants (instances) (Cap. Count + Deformed/Crushed)			
	Col. 1	Col. 2	Col. 3
Row 1	10	2	3
Row 2	5	6	7
Row 3	6	11	14

Relative Stained Area Highlighted			
	Col. 1	Col. 2	Col. 3
Row 1	2%	1%	3%
Row 2	2%	2%	2%
Row 3	3%	3%	3%

Staining (instances) (Altered Aggrgate + Altered Mastic)			
	Col. 1	Col. 2	Col. 3
Row 1	7	2	3
Row 2	5	4	3
Row 3	7	3	1

Capsule Count (whole/ mostly whole)			
	Col. 1	Col. 2	Col. 3
Row 1	4	2	1
Row 2	2	3	2
Row 3	3	5	8

Deformed/Crushed Cap. or Cap. Remnants (instances)			
	Col. 1	Col. 2	Col. 3
Row 1	6	0	2
Row 2	3	3	5
Row 3	3	6	6

Altered Aggregate (instances)			
	Col. 1	Col. 2	Col. 3
Row 1	1	0	1
Row 2	0	0	0
Row 3	1	0	0

Altered Mastic (instances)			
	Col. 1	Col. 2	Col. 3
Row 1	6	2	2
Row 2	5	4	3
Row 3	6	3	1

AC 2% Red Pellets

Cap. Relative area highlighted (%)			
	Col. 1	Col. 2	Col. 3
Row 1	2%	2%	3%
Row 2	2%	2%	3%
Row 3	3%	6%	5%

Cap. and Remnants (instances) (Cap. Count + Deformed/Crushed)			
	Col. 1	Col. 2	Col. 3
Row 1	10	9	10
Row 2	7	7	7
Row 3	7	10	13

tained Relative area highlighted (%			
	Col. 1	Col. 2	Col. 3
Row 1	4%	6%	5%
Row 2	5%	6%	4%
Row 3	3%	3%	3%

Staining (instances) (Altered Aggrgate + Altered Mastic)			
	Col. 1	Col. 2	Col. 3
Row 1	1	3	2
Row 2	3	4	3
Row 3	2	3	0

Capsule Count (whole/ mostly whole)			
	Col. 1	Col. 2	Col. 3
Row 1	1	2	2
Row 2	3	1	2
Row 3	0	1	4

Deformed/Crushed Cap. or Cap. Remnants (instances)			
	Col. 1	Col. 2	Col. 3
Row 1	9	7	8
Row 2	4	6	5
Row 3	7	9	9

Altered Aggregate (instances)			
	Col. 1	Col. 2	Col. 3
Row 1	0	0	0
Row 2	0	0	1
Row 3	0	0	0

Altered Mastic (instances)			
	Col. 1	Col. 2	Col. 3
Row 1	1	3	2
Row 2	3	4	2
Row 3	2	3	0

SMA 1.25% Red Food Coloring

Cap. Relative area highlighted (%)			
	Col. 1	Col. 2	Col. 3
Row 1	4%	1%	2%
Row 2	1%	2%	2%
Row 3	3%	4%	3%

Cap. and Remnants (instances) (Cap. Count + Deformed/Crushed)			
	Col. 1	Col. 2	Col. 3
Row 1	13	7	7
Row 2	9	8	14
Row 3	6	4	15

tained Relative area highlighted (%			
	Col. 1	Col. 2	Col. 3
Row 1	7%	4%	3%
Row 2	3%	4%	4%
Row 3	5%	6%	4%

Staining (instances) (Altered Aggrgate + Altered Mastic)			
	Col. 1	Col. 2	Col. 3
Row 1	1	1	2
Row 2	1	3	1
Row 3	5	6	5

Capsule Count (whole/ mostly whole)			
	Col. 1	Col. 2	Col. 3
Row 1	8	2	4
Row 2	5	1	5
Row 3	3	1	5

Deformed/Crushed Cap. or Cap. Remnants (instances)			
	Col. 1	Col. 2	Col. 3
Row 1	4	4	3
Row 2	2	5	5
Row 3	3	2	6

Altered Aggregate (instances)			
	Col. 1	Col. 2	Col. 3
Row 1	1	0	1
Row 2	0	0	1
Row 3	1	2	2

Altered Mastic (instances)			
	Col. 1	Col. 2	Col. 3
Row 1	0	1	1
Row 2	1	3	0
Row 3	4	4	3

SMA 1.25% Red Pellets

Cap. Relative area highlighted (%)			
	Col. 1	Col. 2	Col. 3
Row 1	2%	0%	0%
Row 2	1%	0%	1%
Row 3	4%	1%	0%

Cap. and Remnants (instances) (Cap. Count + Deformed/Crushed)			
	Col. 1	Col. 2	Col. 3
Row 1	9	5	9
Row 2	4	4	10
Row 3	8	10	4

Stained Relative area highlighted (%)			
	Col. 1	Col. 2	Col. 3
row 1	2%	2%	2%
row 2	1%	1%	2%
row 3	1%	2%	1%

Staining (instances) (Altered Aggrgate + Altered Mastic)			
	Col. 1	Col. 2	Col. 3
Row 1	4	1	1
Row 2	1	2	2
Row 3	3	2	1

Capsule Count (whole/ mostly whole)			
	Col. 1	Col. 2	Col. 3
Row 1	2	1	4
Row 2	3	0	5
Row 3	4	5	0

Deformed/Crushed Cap. or Cap. Remnants (instances)			
	Col. 1	Col. 2	Col. 3
Row 1	7	4	5
Row 2	1	4	5
Row 3	4	5	4

Altered Aggregate (instances)			
	Col. 1	Col. 2	Col. 3
Row 1	0	1	0
Row 2	0	1	0
Row 3	1	1	0

Altered Mastic (instances)			
	Col. 1	Col. 2	Col. 3
Row 1	4	0	1
Row 2	1	1	2
Row 3	2	1	1

SMA 2% Red Pellets

Cap. Relative area highlighted (%)			
	Col. 1	Col. 2	Col. 3
Row 1	3%	2%	3%
Row 2	2%	1%	3%
Row 3	5%	4%	4%

Cap. and Remnants (instances) (Cap. Count + Deformed/Crushed)			
	Col. 1	Col. 2	Col. 3
Row 1	11	10	8
Row 2	15	12	4
Row 3	11	12	15

Stained Relative area highlighted (%)			
	Col. 1	Col. 2	Col. 3
Row 1	5%	5%	3%
Row 2	5%	4%	4%
Row 3	3%	4%	3%

Staining (instances) (Altered Aggrgate + Altered Mastic)			
	Col. 1	Col. 2	Col. 3
Row 1	2	2	2
Row 2	2	5	3
Row 3	3	0	0

Capsule Count (whole/ mostly whole)			
	Col. 1	Col. 2	Col. 3
Row 1	2	4	5
Row 2	4	2	0
Row 3	3	1	6

Deformed/Crushed Cap. or Cap. Remnants (instances)			
	Col. 1	Col. 2	Col. 3
Row 1	9	6	3
Row 2	11	10	4
Row 3	8	11	9

Altered Aggregate (instances)			
	Col. 1	Col. 2	Col. 3
Row 1	0	1	0
Row 2	0	2	1
Row 3	1	0	0

Altered Mastic (instances)			
	Col. 1	Col. 2	Col. 3
Row 1	2	1	2
Row 2	2	3	2
Row 3	2	0	0

C

Specimen Photographs

C.1 Wheel Tracking Beams

AC High Damage

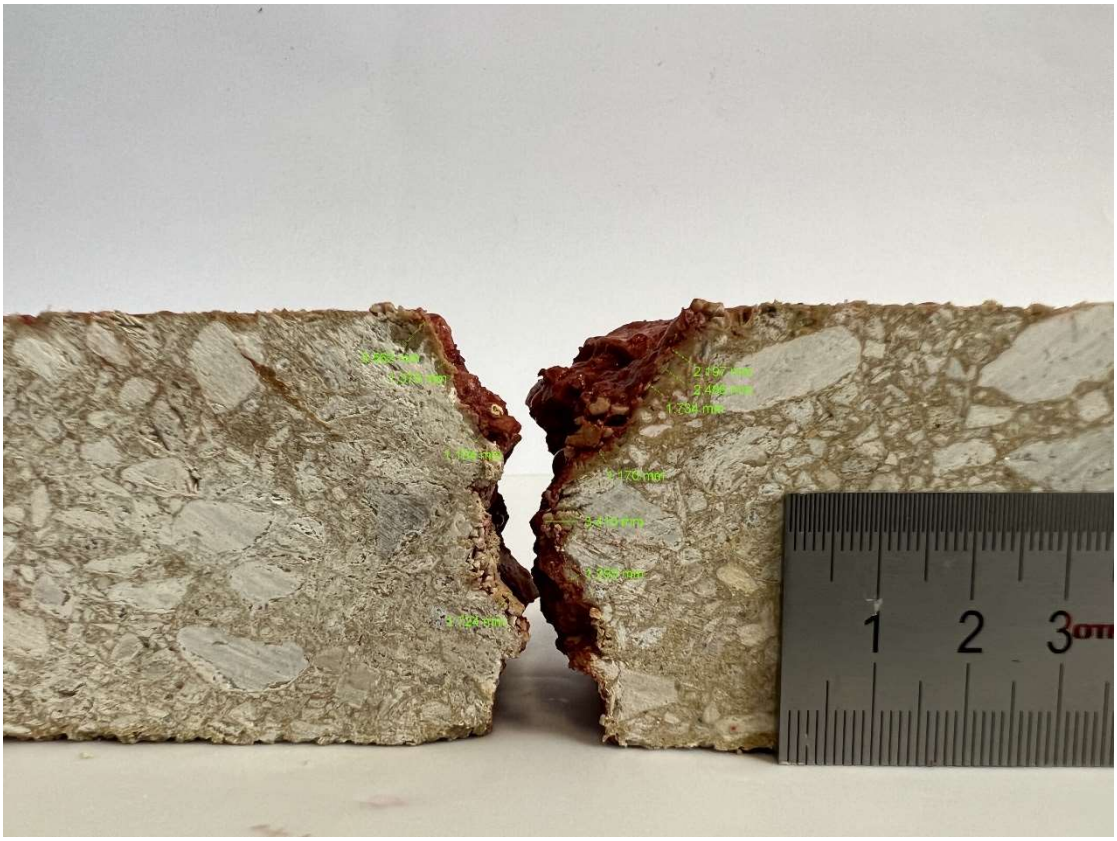

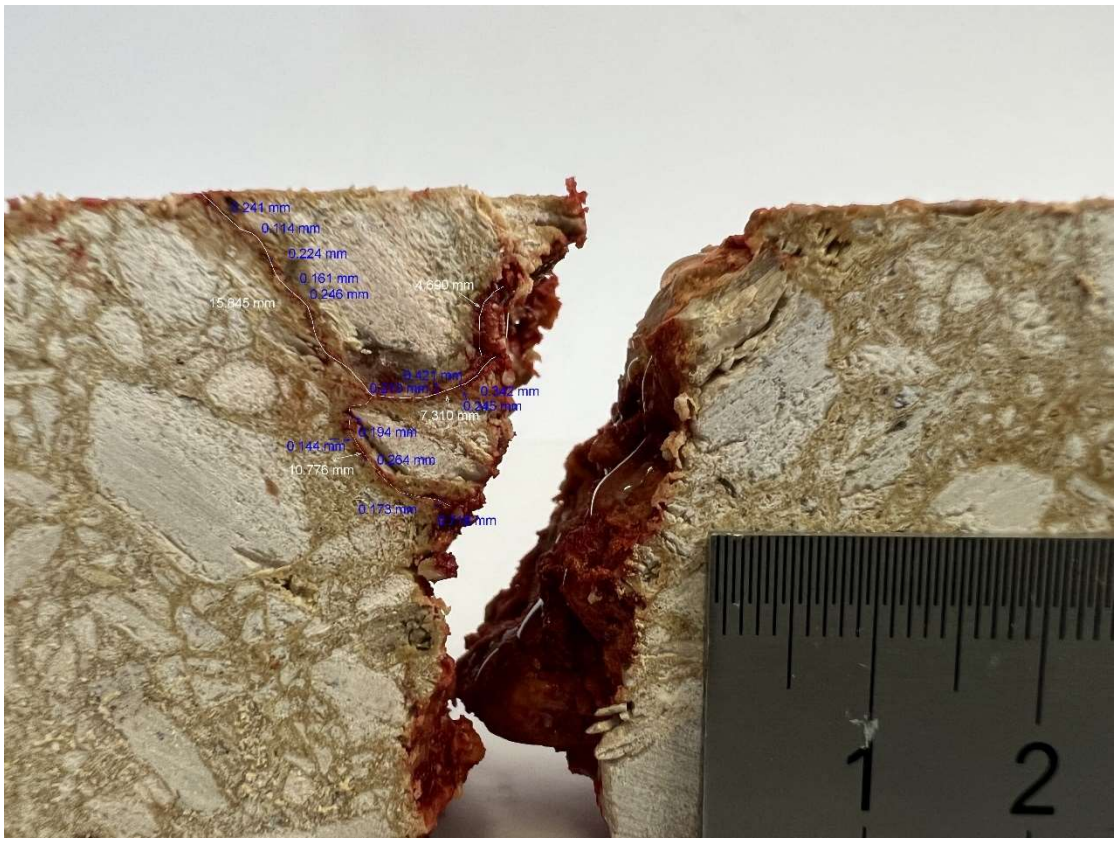
0.241 mm
0.114 mm
0.224 mm
0.161 mm
0.246 mm
15.845 mm
4.690 mm
0.421 mm
0.342 mm
0.245 mm
7.310 mm
0.194 mm
0.144 mm
10.776 mm
0.264 mm
0.173 mm
1
2

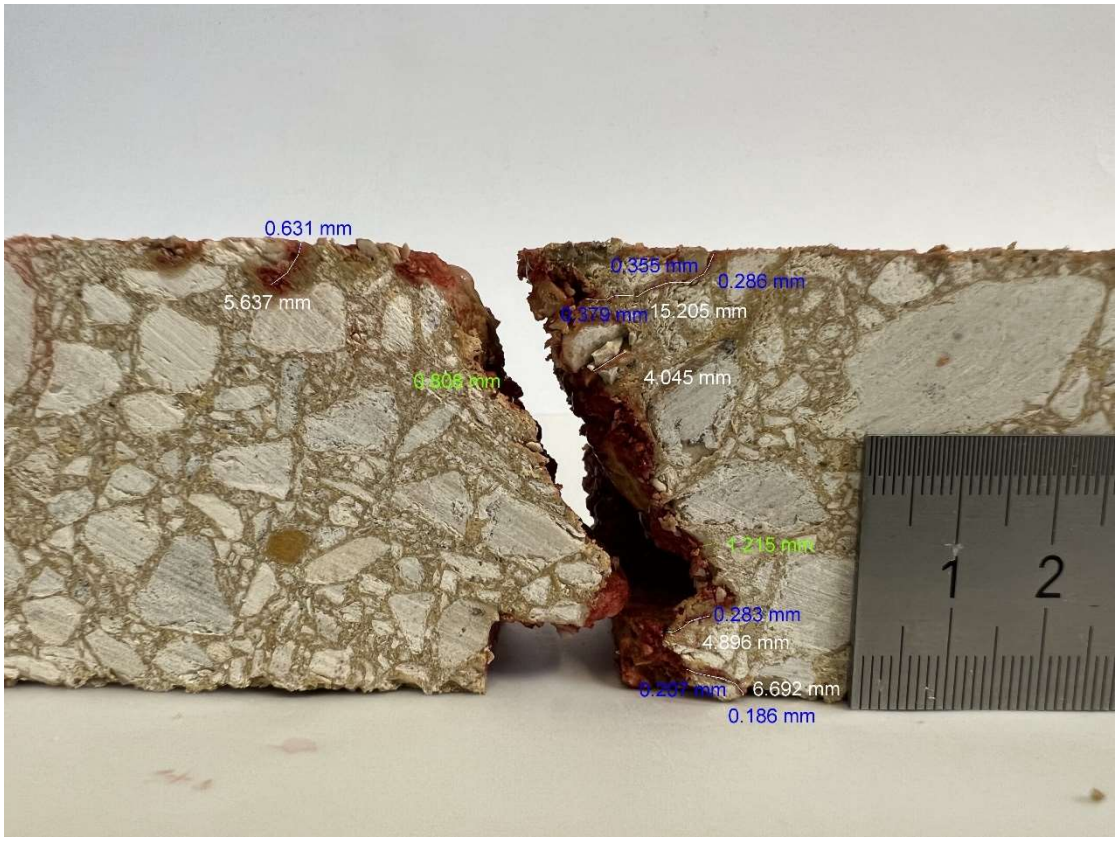
0.631 mm
5.637 mm
0.355 mm
0.286 mm
0.379 mm
15.205 mm
6.805 mm
4.045 mm
1.215 mm
0.283 mm
4.896 mm
0.231 mm
6.692 mm
0.186 mm
1
2

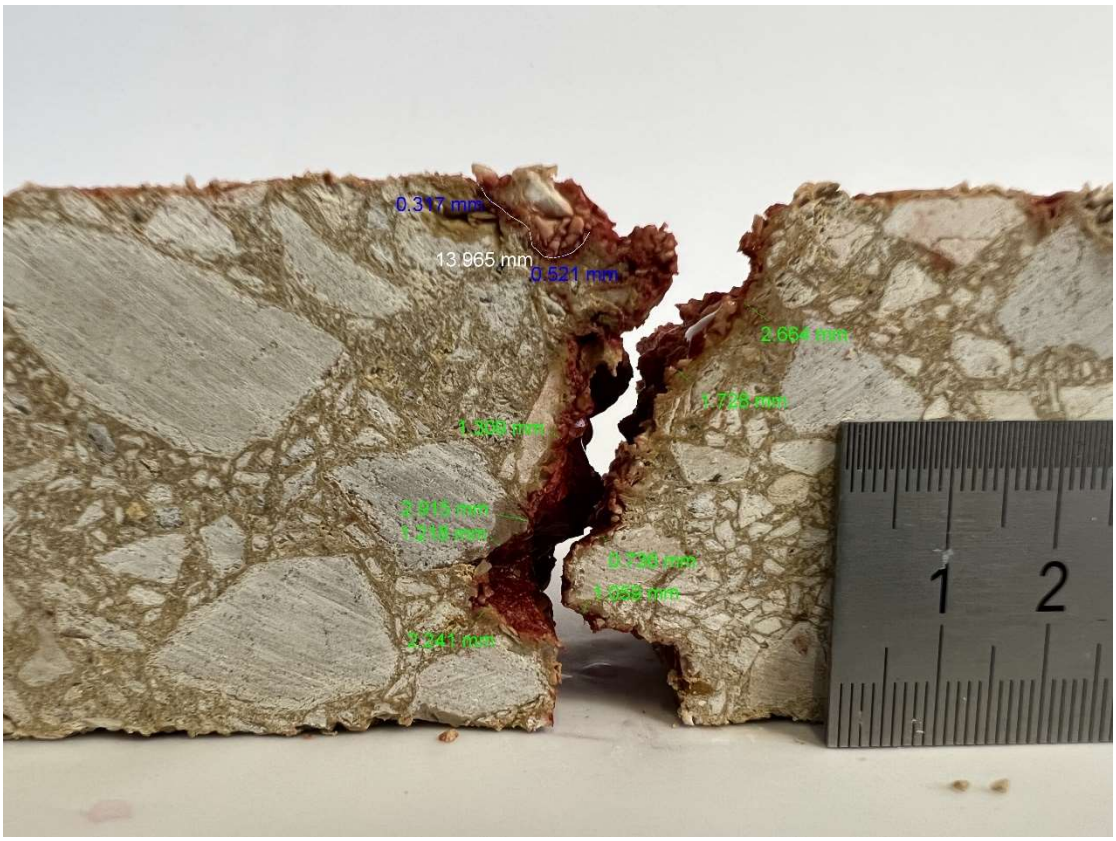
0.317 mm
13.965 mm
0.521 mm
2.654 mm
1.728 mm
1.358 mm
2.915 mm
1.216 mm
0.736 mm
1.058 mm
2.241 mm
1
2

SMA High Damage

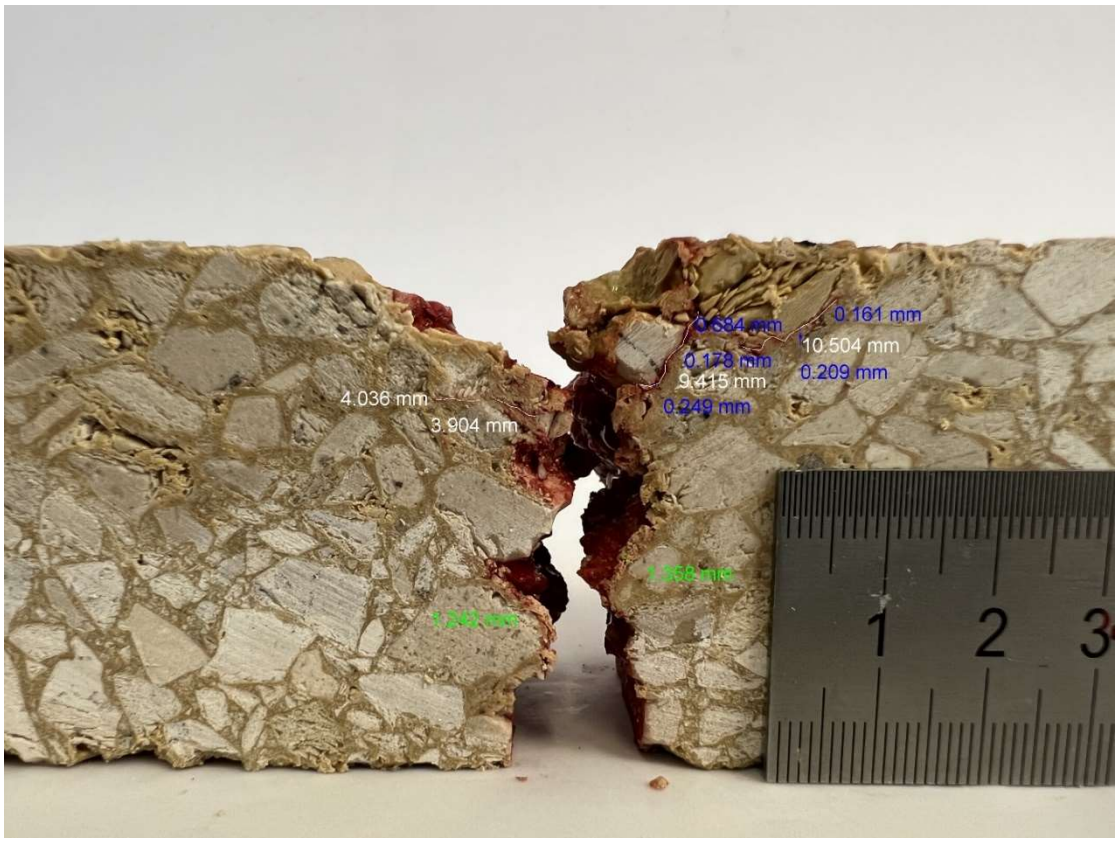

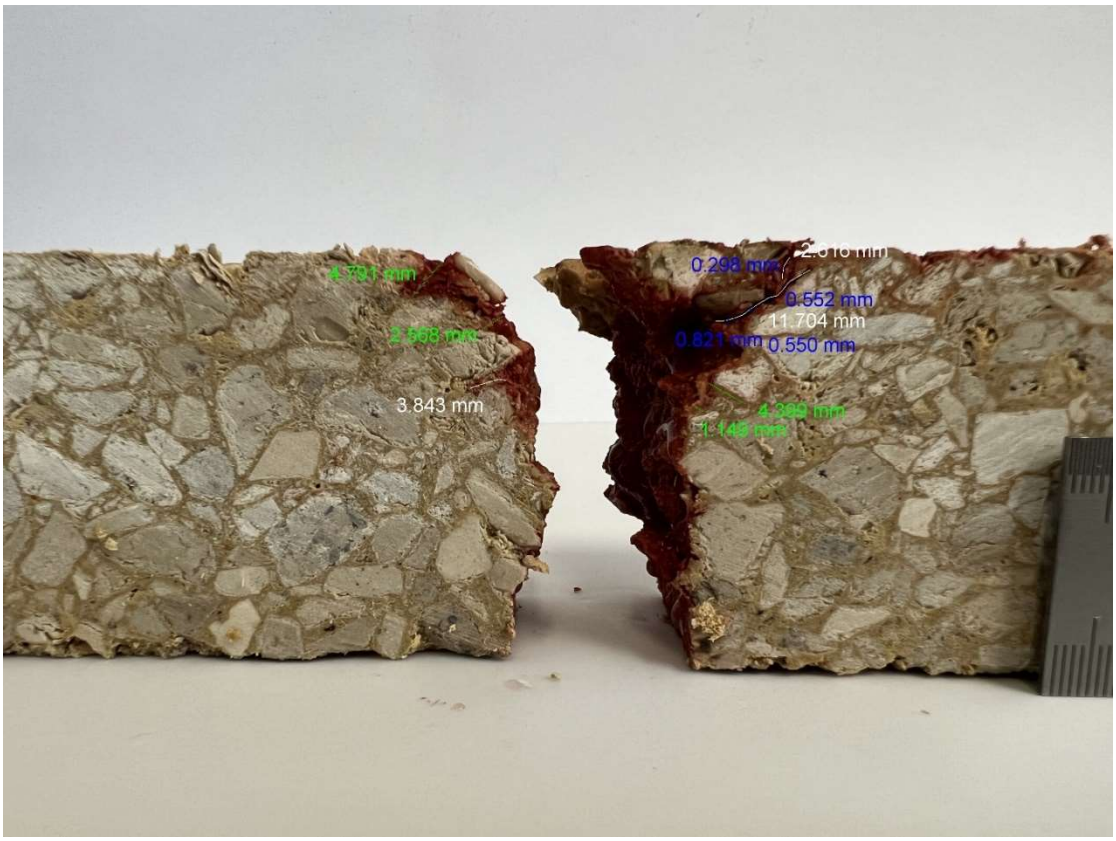
4.791 mm
2.668 mm
3.843 mm
0.298 mm
0.552 mm
11.704 mm
0.821 mm
0.550 mm
4.389 mm
1.149 mm

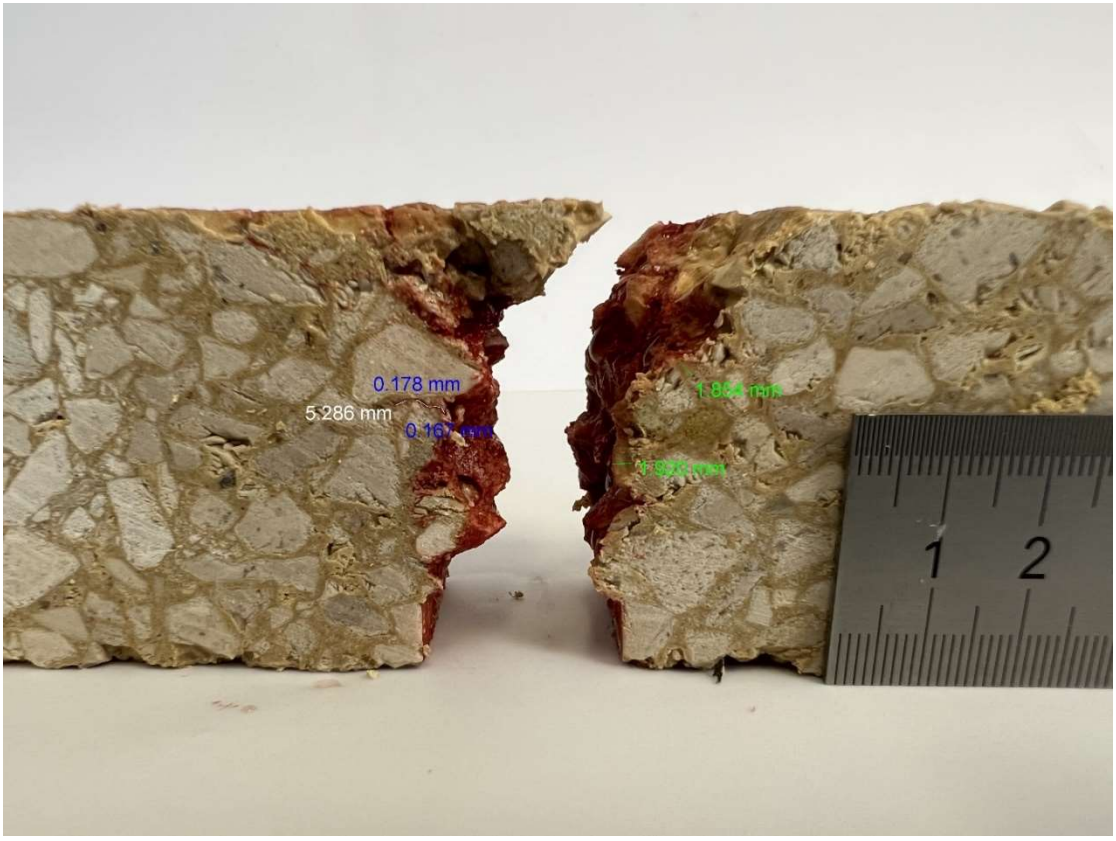
0.178 mm
5.286 mm
1.884 mm
1 2

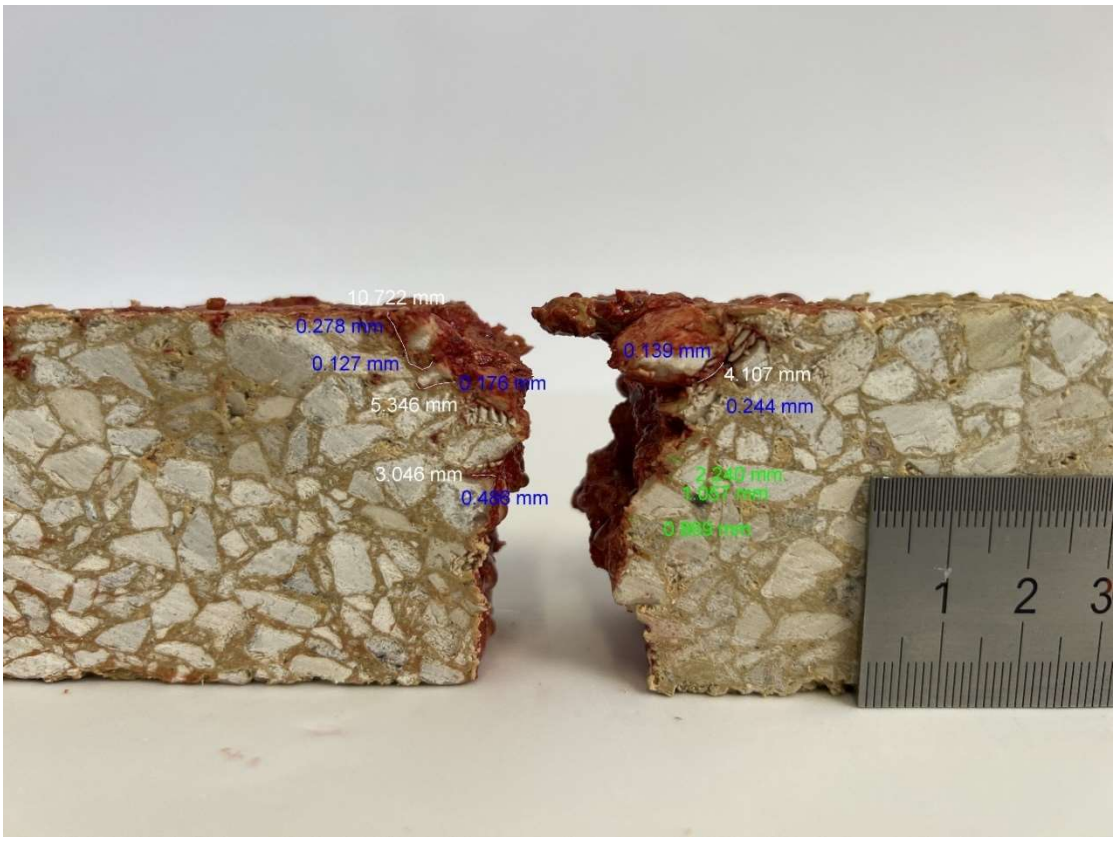

AC Medium Damage

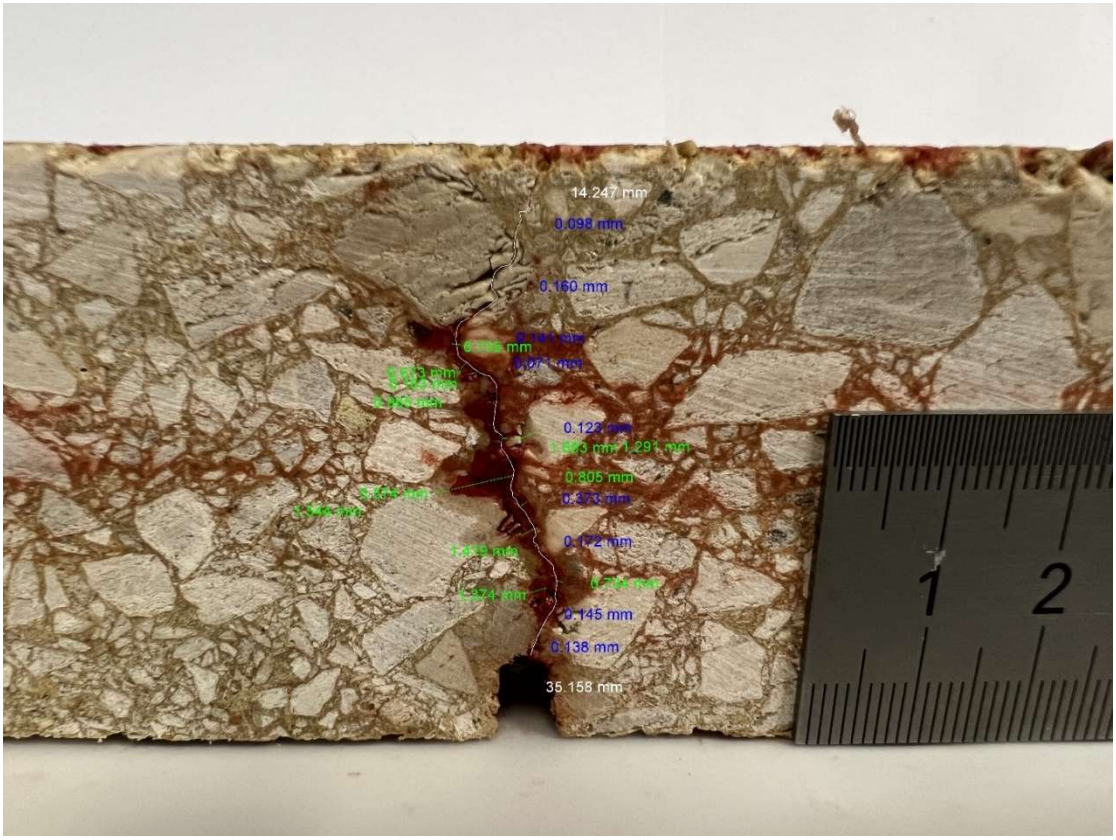

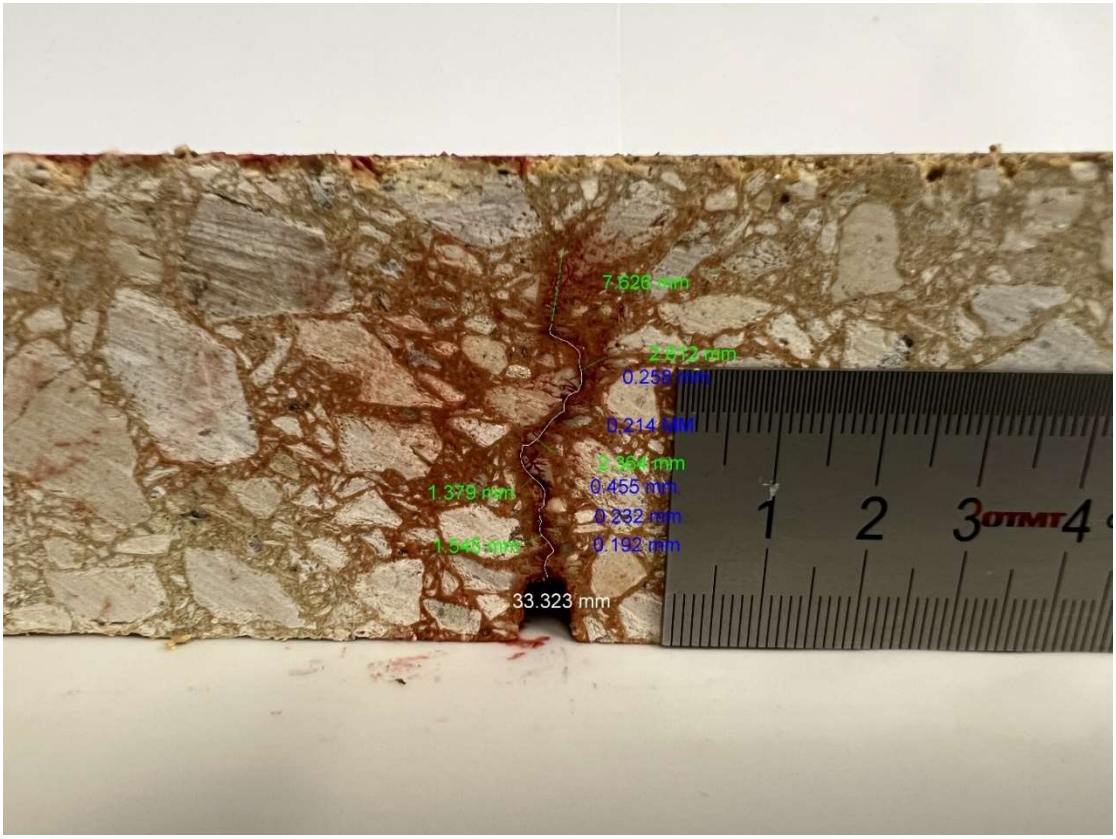
7.626 mm
0.258 mm
0.214 MM
0.455 mm
1.379 mm
0.232 mm
0.192 mm
33.323 mm
1 2 3

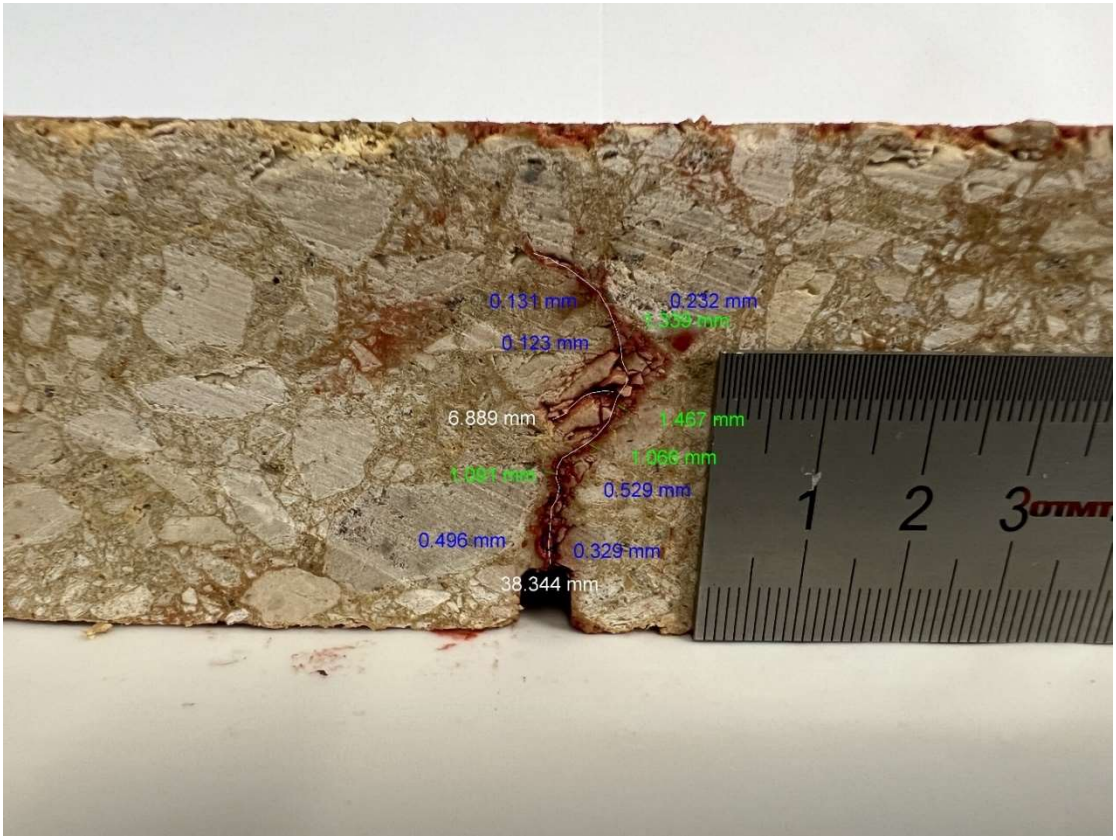
0.131 mm
0.232 mm
0.123 mm
6.889 mm
1.467 mm
0.529 mm
0.496 mm
0.329 mm
38.344 mm
1 2 3

SMA Medium Damage

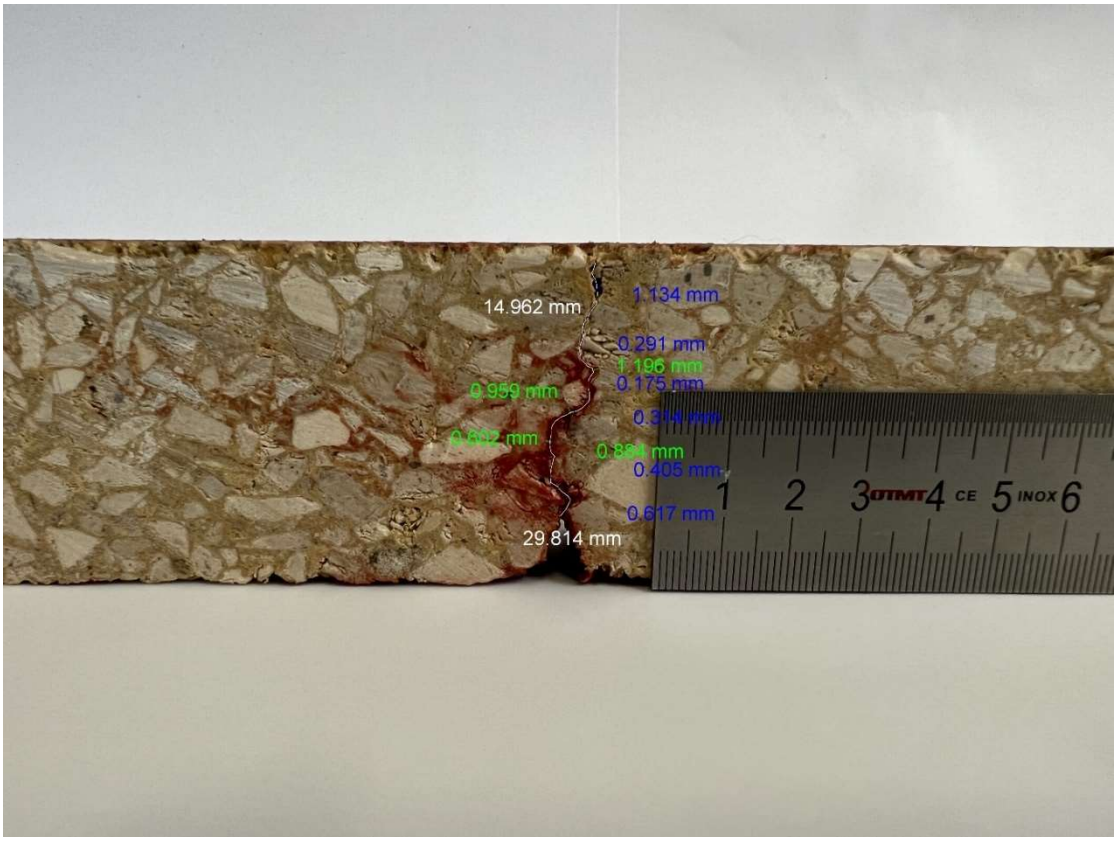

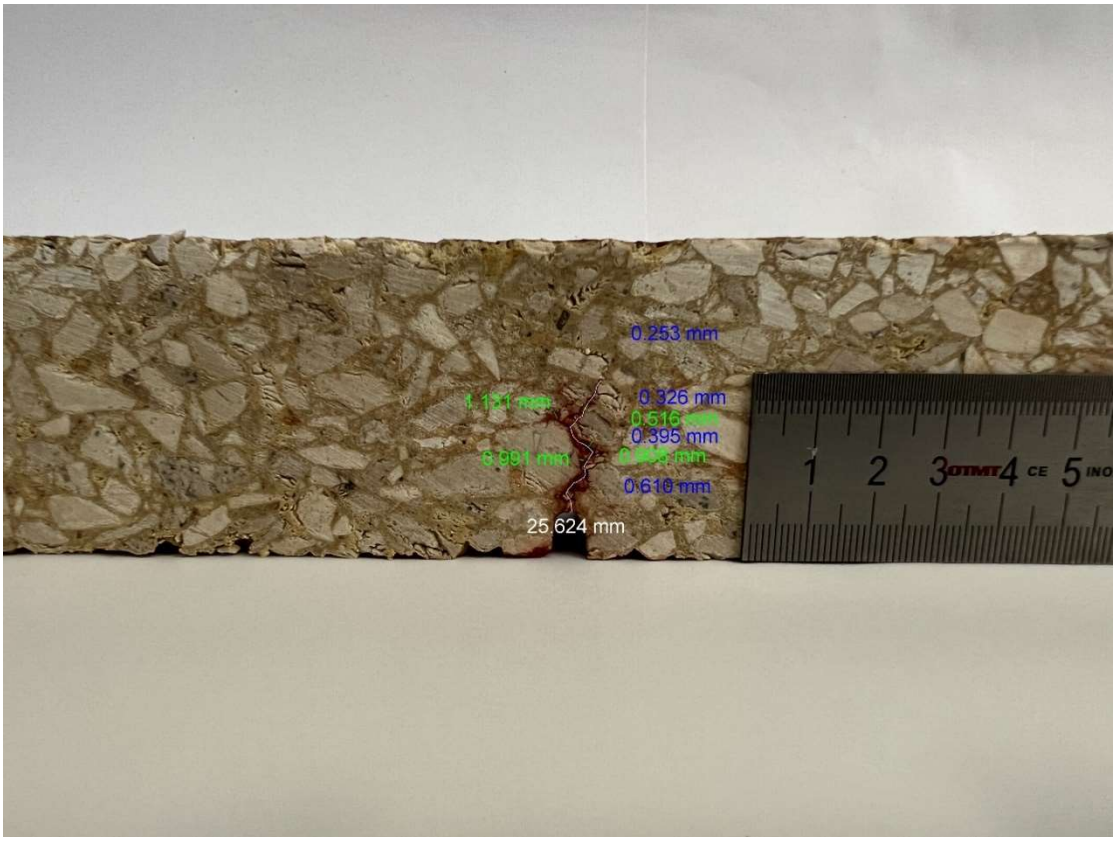

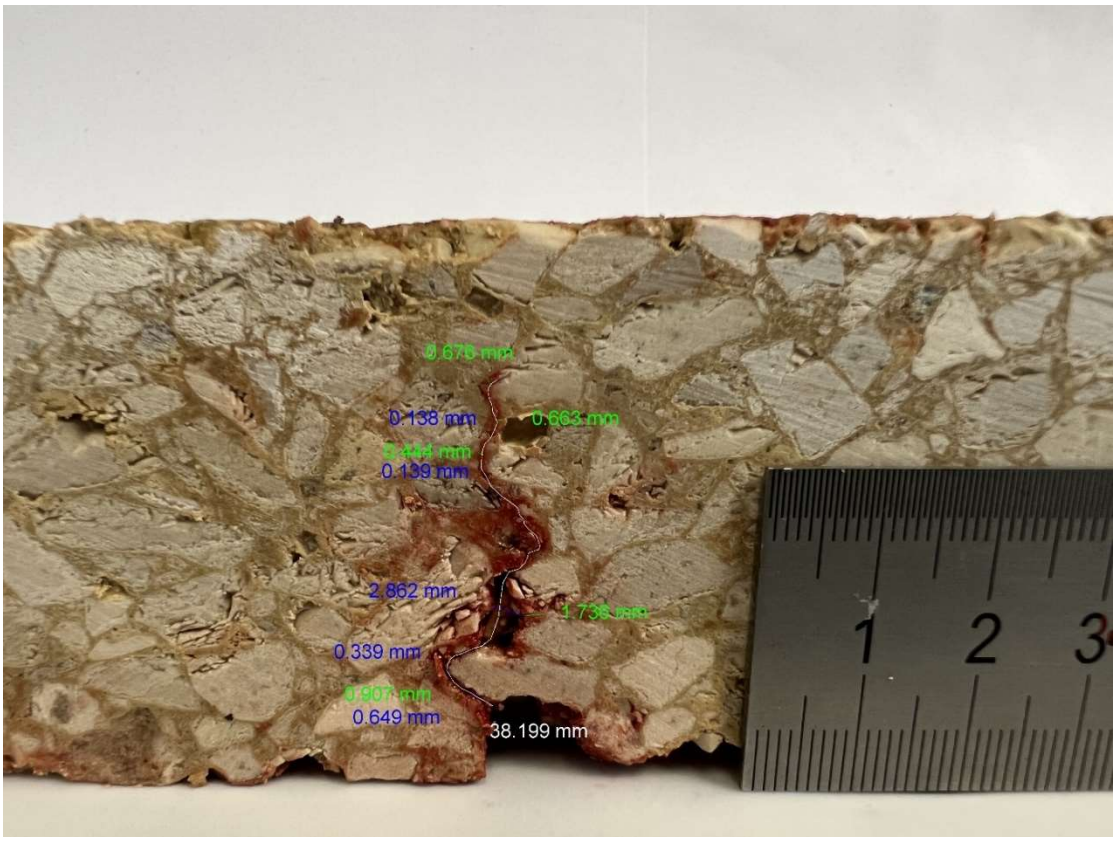

AC Low Damage

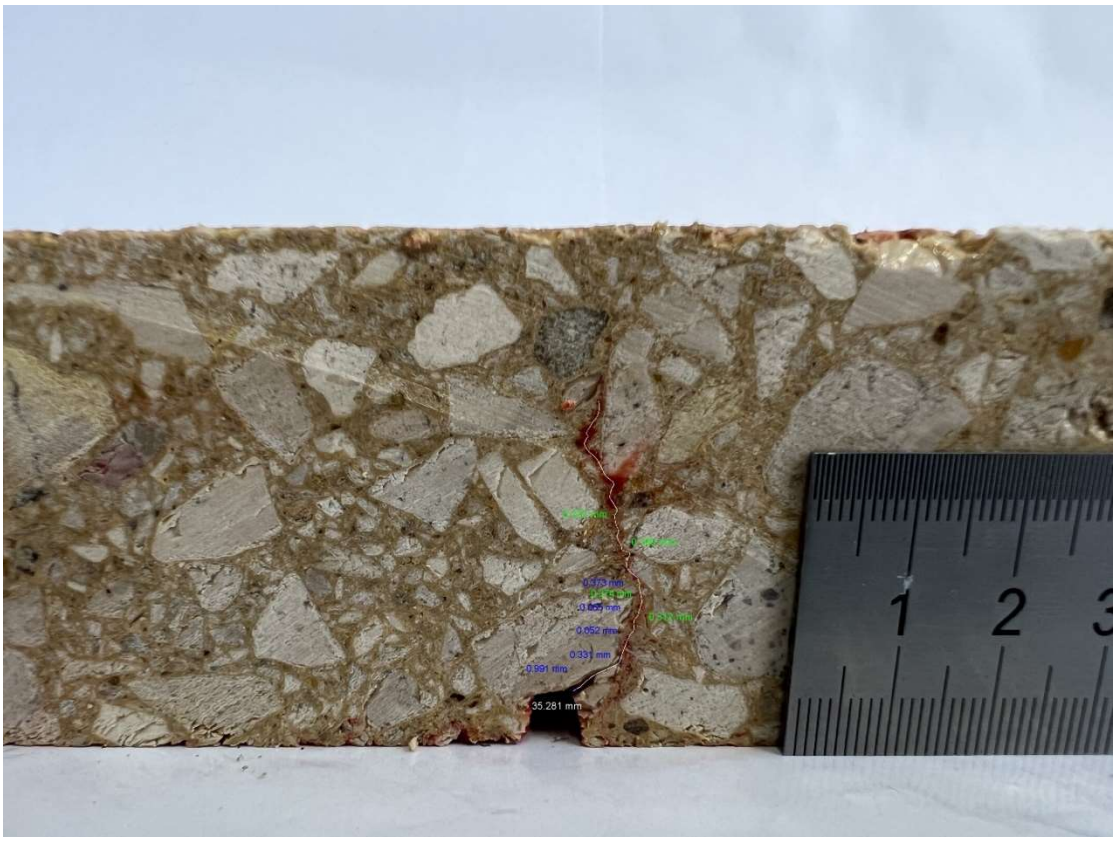
0.373 mm
0.052 mm
0.331 mm
0.991 mm
35.281 mm
1 2 3


38.443 mm
0.309 mm
1 2 3

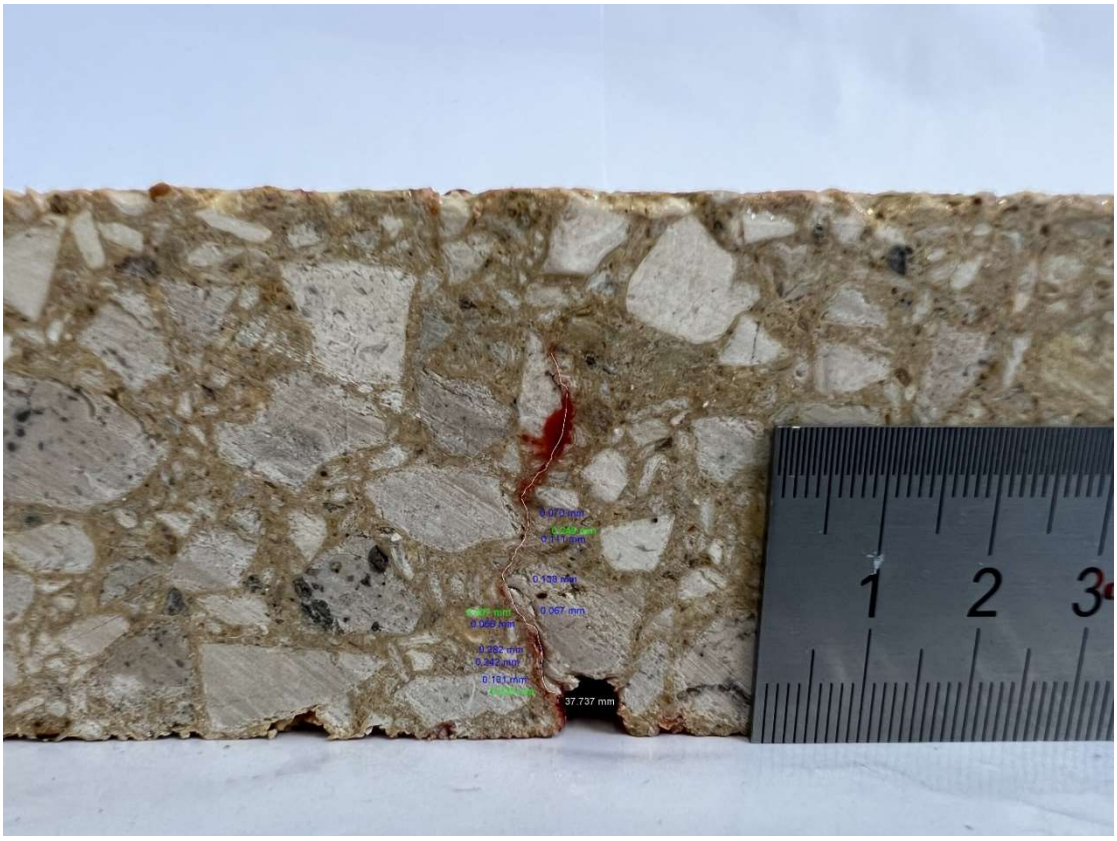

SMA Low Damage

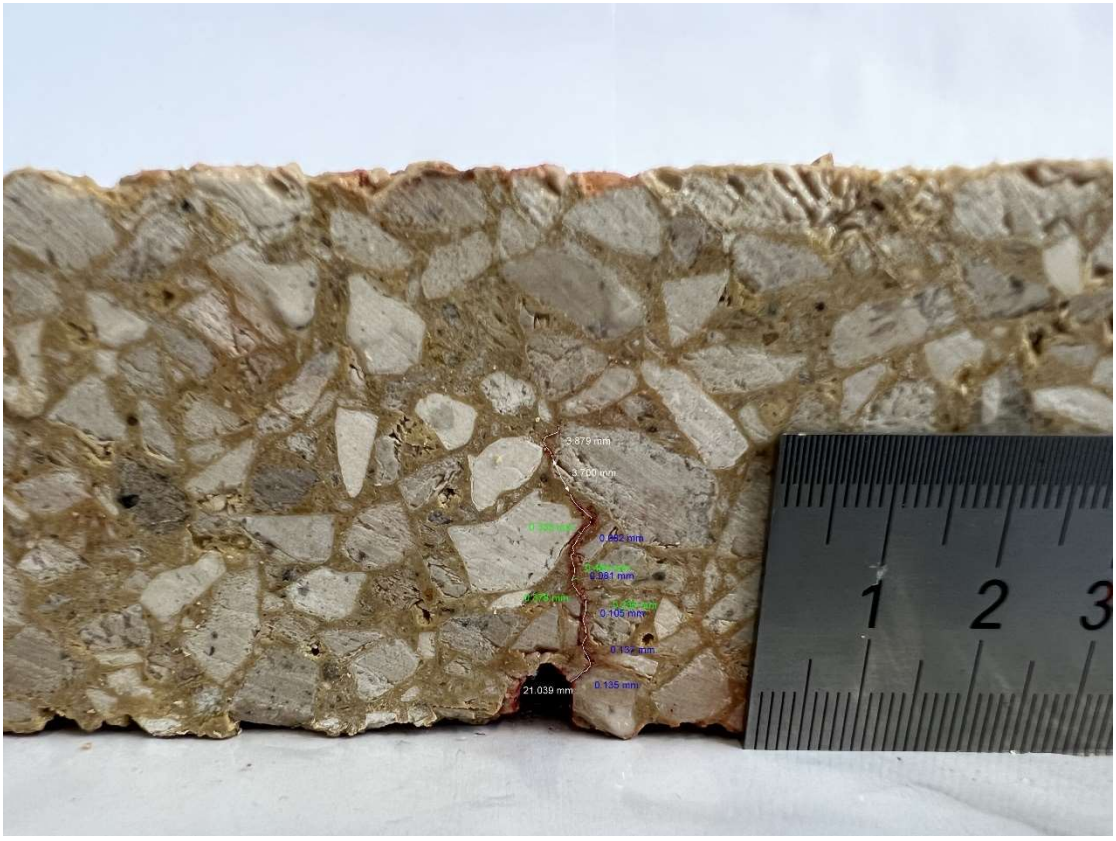

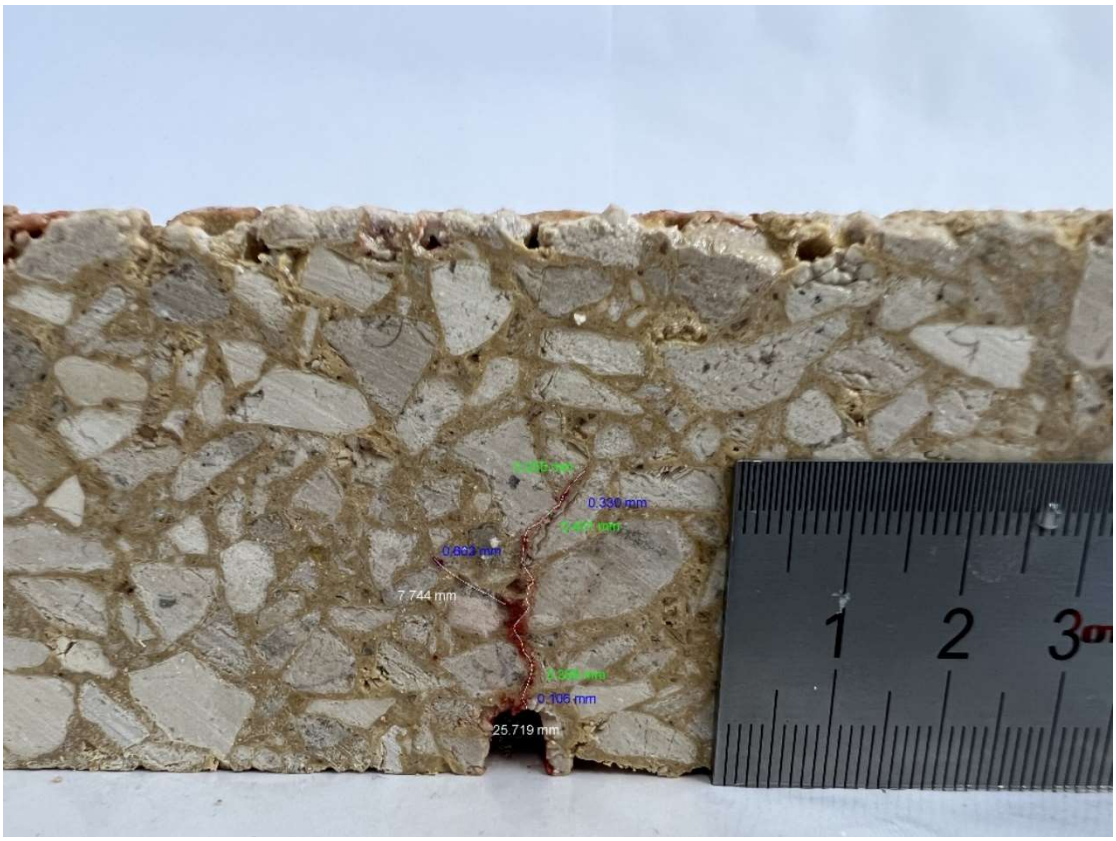
0.330 mm
7.744 mm
0.106 mm
25.719 mm
1 2 3

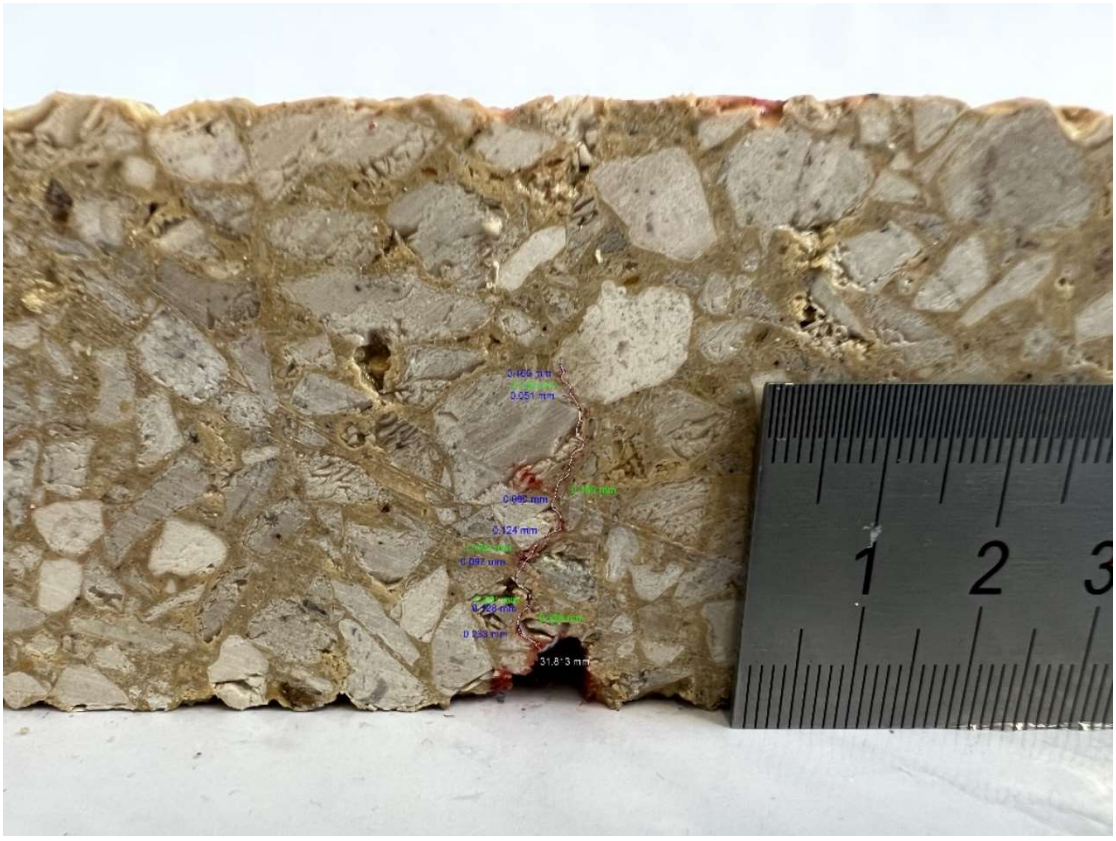
0.051 mm
0.124 mm
1 2 3


13.011 mm
1
2

2022

TIAGO RIBEIRO

STUDY OF ASPHALT SELF-HEALING WITH COLORLESS BINDER AND PIGMENTED OIL

NOVA SCHOOL OF SCIENCE & TECHNOLOGY